Investigating the adaptive mitochondrial shuttles and metabolic reprogramming of transporters in complex I (Ndufs4) knockout mice.

D. Nel

orcid.org/0000-0003-0536-9061

Dissertation accepted in partial fulfilment of the requirements for the degree *Magister Scientiae in Biochemistry* at the North-West University

Supervisor: Prof JZ Lindeque

Co-supervisor: Dr M Pretorius

Graduation July 2022

24159964

I would like to dedicate this dissertation to my dad.

You always encouraged me to be the better version of myself. Thank you for teaching me kindness, integrity and above all else, to never stop believing in my own abilities. I love you and miss you very much every day.

Equipped with his five senses, man explores the universe around him and calls the adventure science.
Edwin Hubble

For since the creation of the world, God's invisible qualities - his eternal power and divine nature - have been clearly seen, being understood from what has been made, so that people are without excuse (Romans 1:20)

PREFACE AND ACKNOWLEGDEMENTS

This study was one of the biggest challenges I had during my academic career at the North-West University, both on a mental and physical level. From understanding new methods to running back and forth to the vivarium for mouse collection, the main goal was to gain more understanding about the mighty mitochondria and a highly prevalent disease caused by their malfunction. Thank you to the mice that gave their lives in the pursuit of science and advancement of our understanding with regard to this disease.

First, I would like to thank my supervisor, **Prof Zander Lindeque** for all his guidance and assistance, not only with this degree but also my honours degree. Also, thank you for having me as a student over the years and passing along knowledge in methods, equipment and techniques. Thank you for your patience and unrestricted supervision during my studies and allowing me to make my own contributions to my project's planning and outcome.

Second, I would like to thank my co-supervisor, **Dr Marianne Pretorius** for her immense help and guidance with both practical and theoretical work regarding the transcriptomics that I was not as familiar with. Her contributions with both the practical work and guidance with unforeseen problems led to the easier completion of this project. Also, thank you for your encouragement and determination during this project.

Thank you to **Dr Maryke Schoonen**, for making the intimidating sequencing equipment seem less of a challenge. Your supervision and guidance during the sequencing and help with any questions and unforeseen problems contributed immensely to the completion of this study.

I would also like to thank **Belinda Fouchè** for being my partner with the practical work and also being a shoulder to cry on when needed. Your help and support with the transcriptomics work is very much appreciated.

A special thank you to **Gunter van der Walt**, for teaching me the ways of genotyping and PCR. Also, for your help and advice with mice collection, metabolomics and data processing. You are a unique soul whose company and encouragement I enjoyed and needed over the years.

Thank you to the **Mito-family**, for all the support and encouragement. Thank you for allowing me to be part of such a unique and fantastic group of people. Also, a special thank you to **Prof Francois van der Westhuizen** and **Prof Roan Louw** for your leadership of the Mitochondrial Research Laboratory into the success it is today. It truly is the most pleasant work and research environment.

Thank you to the **Mitochondria Research Laboratory**, the **Metabolomics Laboratory**, the **Molecular Biology Laboratory,** and the **BOSS Laboratory** for allowing me to use your equipment, reagents and consumables for the execution of the practical work of this study.

A very sincere thank you to the **North-West University** for their financial support and also to the **Preclinical Drug Development Platform (PCDDP)** for the housing of the mice and their staff for their assistance in the care of the mice and collection of the mice tissue.

I would also like to thank the **National Research Foundation** for their financial contribution to the Ion Torrent S5 Semiconductor Sequencer and the Ion Chef Instrument. These instruments are quite revolutionary, and it was a great privilege to be able to work on them.

To my Science-family, **Anandi Rautenbach**, **Tiaan van Zyl**, **Laurene Coetzee** and **Armand Vorster**, for being a friend and a helping hand. Your support, advice and caring during the years was not only a necessity but is much appreciated. Thank you for all the encouragement, especially during this study.

To my home-friends and family, especially my parents, **Danie and Annatjie Nel**, the biggest thank you for your unconditional love and support during the years I attended the North-West University. Thank you for encouraging me to be the best version of myself and believing in me and my abilities. Also, thank you for your genuine interest in my studies and allowing me to pursue my academic interests. Your prayers and encouragements kept me going through all the late nights and tears. I love you very much.

Lastly, I would like to thank my best friend and the love of my life, **Ryno le Roux**, for his unfailing love and continued support throughout my academic career. Thank you for your

patience and enduring my very long ramblings and explanations of things you don’t need to know. I love you very much!

A very special thank you to **Riza Nagel** for taking the time out of her very busy schedule to do the tedious proof reading of this dissertation.

ABSTRACT

Mitochondrial disease is one of the most prevalent inherited paediatric disorders among children, with a prevalence of 1 in 5000 children. Leigh syndrome is the result of a Complex I (CI) deficiency and disrupts the redox balance needed for the function of various dehydrogenase enzymes. Due to the extensive heterogeneity of the disease, it remains a challenge to diagnose and treat mitochondrial diseases. One of the most overlooked areas for possible treatment is the solute carriers of the inner mitochondrial membrane (IMM). These solute carriers function together to form shuttle systems that transport electrons over the impermeable IMM, which can possibly aid in recovery of the disrupted redox balance. Targeted transcriptomic analysis was done on liver, heart and brain tissue collected from a CI deficient (*Ndufs4* knockout) mice model to analyse the gene expression of the selected solute carriers part of the malate-aspartate shuttle and the citrate-pyruvate shuttle. The proteins of the glycerol-3-phosphate shuttle was also included due to its ability to also carry electrons over the IMM. This was done by making use of the Ion GeneStudio™ S5 Semiconductor Sequencer accompanied by the Ion Chef™ Instrument. Targeted metabolomics was also done on the selected tissue on the metabolites transported by the solute carriers, also to deduce if there are any changes in their abundance with diseases like Leigh syndrome. This was done via GC-TOF-MS and LC-MS/MS analysis. Transcriptomic analysis revealed for the liver tissue, *Gpd1* (glycerol-3-phosphate dehydrogenase 1), *Mdh1* (malate dehydrogenase 1), *Me1* (malic enzyme 1) and *Slc25a1* (solute carrier family 25 member 1, citrate carrier) were all down regulated in the knockout group. For the heart tissue, *Slc25a22* (solute carrier family 25 member 22, glutamate carrier) and *Me1* (malic enzyme 1) were also down regulated in the knockout group and for the brain tissue, *Me3* (malic enzyme 3), *Slc25a3* (solute carrier 25 member 3, phosphate carrier) and *Slc25a22* (solute carrier family 25 member 22, glutamate carrier) were all up regulated in the knockout group. Changes in the expression of these genes all seem to be an effect of the redox imbalance due to complex I deficiency or revolve around an attempt to maintain energy production. Metabolomic analysis indicated an increase in abundance in metabolites associated with the down-regulated enzymes and shuttles. These changes all seem to be an effect of the complex I knockout and not an attempt to compensate for the disruption of the cells function. Considering this study involved an unconventional method for gene expression analysis, the overall

success in the outcome of this study can be attributed to the combination of transcriptomics and metabolomics data to give a better understanding of the events at molecular level with abnormalities such as complex I deficiency.

Key terms: Mitochondria, Mitochondrial shuttles, Solute carriers, Transcriptomics, Metabolomics, Gene expression, Adaptive response, Complex I deficiency, OXPHOS system, Ndufs4 mouse model.

ABBRIVIATION LIST

A	-	Absorbance
ADP	-	Adenosine diphosphate
ATP	-	Adenosine triphosphate
BAM	-	Binary alignment/map
BCAA	-	Branched-chain amino acids
bDNA	-	Branched DNA
BSTFA	-	N, O-bis(trimethylsilyl)trifluoroacetamide
°C	-	Degrees Celsius
CI	-	Complex I
CII	-	Complex II
CIII	-	Complex III
CIV	-	Complex IV
cAMP	-	cyclic adenosine monophosphate
cDNA	-	Complementary DNA
CoA	-	Co-enzyme A
CoQ	-	Co-enzyme Q (see Q10 in abbreviation list)
Cu_A	-	Copper binding site A
DNA	-	Deoxyribonucleic acid
dsDNA	-	Double stranded DNA
DPR	-	Distal promotor region

ESI	-	Electron spray ionization
FAD	-	Flavin adenine dinucleotide
$FADH_2$	-	Flavin adenine dinucleotide (reduced form)
FMN	-	Flavin mononucleotide
$FMNH_2$	-	Flavin mononucleotide (reduced form)
GC	-	Gas chromatography
GC1	-	Glutamate carrier 1
GDP	-	Guanine diphosphate
GPD	-	Glycerol-3-phosphate dehydrogenase
gDNA	-	Genomic DNA
GTP	-	Guanine triphosphate
H^+	-	Proton
HET	-	Heterozygous
HEPA	-	High-efficiency particulate absorbing
HPLC	-	High performance liquid chromatography
IMM	-	Inner mitochondrial membrane
IMS	-	Intermembrane space
ISP	-	Ion Sphere™ Particle
IVC	-	Individually ventilated cages
KO	-	Knockout
LC	-	Liquid chromatography

MIA	-	Mitochondrial intermembrane space assembly
miRNA	-	micro-RNA
MOX	-	Methoxamine
MS	-	Mass spectrometry
mtDNA	-	Mitochondrial DNA
nDNA	-	Nuclear DNA
Ndufs4	-	NADH:ubiqinone oxidoreductase iron-sulphur protein 4
Ndufs4+/+	-	Wildtype
Ndufs4+/-	-	Heterozygous
Ndufs4-/-	-	Knockout
NAD+	-	Nicotinamide adenine dinucleotide
NADP	-	Nicotinamide adenine dinucleotide phosphate
NADH	-	Nicotinamide adenine dinucleotide (reduced form)
NADPH	-	Nicotinamide adenine dinucleotide phosphate (reduced form)
NGS	-	Next generation sequencing
KO	-	Knockout
OMM	-	Outer Mitochondrial Membrane
OXPHOS	-	Oxidative Phosphorylation System
PCPPD	-	Preclinical Drug Development Platform
PCR	-	Polymerase chain reaction
PN(#)	-	Post-natal day (#)

ppm	-	parts per million
PPR	-	Proximal promotor region
PUFA	-	Polyunsaturated fatty acids
QC	-	Quality control
qPCR	-	Real-time PCR
Q10	-	Ubiquinone
QH^-	-	Ubisemiquinone
QH_2	-	Ubiquinol
QQQ	-	Triple quadrupole
RNA	-	Ribonucleic acid
ROS	-	Reactive Oxygen Species
RT-qPCR	-	Reverse transcriptase real-time polymerase chain reaction
SAM_1	-	Sorting and Assembly complex
SAM_2	-	Sequence alignment/map
SLC25	-	Solute carrier family 25
SPF	-	Specific Pathogen Free
SRE	-	Sterol regulatory element
SREBP	-	SRE binding protein
ssDNA	-	Single stranded DNA
TAC	-	Transcriptome Analysis Console
TCA	-	Tricarboxylic acid

TIM	-	Translocase of the inner membrane
TOF	-	Time-of-Flight
TOM	-	Translocase of the outer membrane
TMS	-	Trimethylsilyl
UCP	-	Uncoupling protein
UV	-	Ultraviolet
USA	-	United States of America
VDAC	-	Voltage dependent anion-selective channel
WT	-	Wildtype

TABLE OF CONTENTS

LIST OF TABLES

LIST OF FIGURES

CHAPTER 1 – INTRODUCTION

Mitochondria – the powerhouse of the cell. These organelles are present in the cytoplasm of cells (except erythrocytes) where they produce energy in the form of adenosine triphosphate (ATP). Mitochondria are double membrane organelles. The outer mitochondrial membrane (OMM) is permeable to most small molecules. The OMM contains voltage dependent anion-selective channels (VDAC) which is considered as a general diffusion pore. These channels do not have specific substrates and the only specificity of the channel is the size of the molecule being transported (Colombini, 2016). The IMM is rather complex when compared to the OMM. It is highly impermeable to molecules and ions due to the membranes' important function in energy production. The selectivity of this membrane is linked to the specific carriers located in this membrane (Kunji *et al.,* 2020). Most of these carriers are members of the solute carrier 25 (SLC25) gene family. These genes encode carriers that are exclusively located in the IMM (Bender & Martinou, 2016). Most importantly, the IMM plays host to the oxidative phosphorylation (OXPHOS) process and its components.

The SLC25 gene family plays an important role in the homeostasis of metabolites and ions between the mitochondrial matrix and the intermembrane space (IMS) and or cytoplasm. These transporters carry a wide variety of molecules, which include substrates and/or products of various pathways. Other functions and roles include heat production, mitochondrial dynamics, signalling, cellular differentiation, development, and cell death. There are currently 53 members to the SLC25 gene family, and all (except one) are functional monomers. The aspartate-glutamate carrier functions as a dimer, containing an amino-terminal (NH_2) calcium regulatory domain (Tang *et al.,* 2020).

Some members of the SLC25 gene family function together to form shuttle systems. These shuttle systems function together to maintain optimal concentrations of metabolites over the IMM. One important function is to move the electrons of nicotinamide adenine dinucleotide (reduced from) (NADH) over the IMM, considering that the IMM is impermeable to NADH. Malate is an electron carrier in the cytosol and can be moved into the mitochondrial matrix. There, it can be enzymatically converted to other intermediates and donate electrons to nicotinamide adenine dinucleotide (oxidized form) (NAD^+) (Kola *et al*., 2015).

The OXPHOS system is made up of five multi-subunit enzyme complexes. Each of these complexes play a role in the production of ATP. Complexes I and II (CI and CII) transfer electrons from NADH and flavin adenine dinucleotide ($FADH_2$) respectively to complexes III and IV (CIII and CIV) where oxygen (O_2) acts as the final electron acceptor to produce water (H_2O). This series of exergonic redox reactions move protons (H^+) over the IMM via CI, CIII and CIV to maintain a electrochemical gradient over the IMM, that drives the phosphorylation of adenine diphosphate (ADP) to ATP (Tang *et al.,* 2020). Deficiencies in any of these complexes result in mitochondrial disorders.

Leigh syndrome is one of the most common mitochondrial disorders. It has a varying clinical presentation due to the heterogeneity of the disease. One of the causes of Leigh syndrome is complex I deficiency, where a gene associated with complex I (nuclear or mitochondrial DNA) is mutated. This is associated with severely diminished ATP production via the oxidative phosphorylation (OXPHOS) system and leads to serious complications and clinical symptoms with regard to high energy-demand tissues (Finisterer, 2008) (Lake *et al.,* 2015). Disease symptoms are quite extensive; however, neurological manifestations are common because the brain and nervous system are energy demanding systems (Baldo & Vilarinho, 2020). Energy production is impaired when complex I is deficient leading to the above-mentioned clinical presentation. Moreover, complex I deficiency also leads to a redox imbalance (increased NADH:NAD^+ ratio) and it is responsible for the uptake of electrons from NADH, yielding NAD^+. NAD^+ is an important aspect in the functionality of a very large variety of dehydrogenase enzymes, including those of the tricarboxylic acid cycle (TCA), banched-chain amino acid (BCAA) catabolism, glycolysis etc. When a shortage of NAD^+ occurs, such as with the case of Leigh syndrome, various metabolic pathways will have reduced functionality and intermediates of said pathways will accumulate (Terburgh *et al*., 2021).

Considering the role of the SLC25 transporters and metabolite shuttle systems, it is still unclear how a complex I deficiency influences these shuttles. Hence, the focus of this study is to investigate the effect of a complex I deficiency on metabolite shuttles (i.e. specific members of the SLC25 gene family, enzymes and metabolites associated with them). With the availability of a whole-body complex I knockout mice model (presenting with Leigh syndrome), it is possible to investigate the effect of complex I deficiency on the expression of genes associated with these shuttle systems and the concentration of

metabolites involved in their exchange mechanisms. Considering these shuttle systems have the ability to shuttle electrons over the impermeable IMM, overall reprogramming might be possible to ensure that enough ATP is ultimately produced with the complex I deficiency.

This dissertation contains seven chapters. Chapter **one** contains brief background information that led to the design and motivation for this study. Chapter **two** consists of literature regarding the mitochondria, mitochondrial dysfunction, the solute carrier family 25 and the genomic, structural, and functional aspects of the SLC25 gene family, shuttle systems and their functionality, the information of each protein involved in the chosen shuttle systems, the problem statement, the aims, objectives, and the study design. Chapter **three** provides literature of the chosen methods and procedures. Chapter **four** lists all the experimental procedures done to complete the study. Chapter **five** lists the results obtained from the experimental procedures. Chapter **six** gives a discussion and interpretation of the combined transcriptomic and metabolic analysis. Chapter **seven** concludes on the findings of the study, gives the strengths and limitations of the study, and also provides possible future prospects. Annexures at the end of this dissertation lists findings that were not part of the main results.

CHAPTER 2 – LITERATURE REVIEW

2.1 The Mitochondria

The mitochondria are endosymbiotic, double membrane organelles that produce energy for the cell in the form of ATP via oxidative phosphorylation (Bender & Martinou, 2016). Every cell can contain hundreds of copies of mitochondria and maintains aerobic respiration (Ylikallio et al. 2010). Mitochondria are also responsible for various other cell functions such as cell signalling, programmed cell death and biosynthetic reactions. Mitochondria also contain all the enzymes involved in the TCA cycle that produces reducing equivalents utilized by the electron transport chain to reduce molecular oxygen (Roger et al., 2017). The OMM is permeable to small molecules (Giacomello et al., 2020). VDAC is responsible for most of the molecule transport over the OMM. The IMM is impermeable to most molecules, in order to maintain the electrochemical gradient over the membrane, which is used for the phosphorylation of ADP to ATP (Bouillaud et al., 2016). This membrane contains various shuttle systems and specific transporters that allow the selective transport of molecules over the membrane while maintaining the membrane potential (Giacomello et al., 2020).

2.2 The Oxidative Phosphorylation (OXPHOS) System

The IMM contains the OXPHOS system. It is made up of five multi-subunit complexes: complex I (NADH-ubiquinone oxidoreductase), complex II (succinate-ubiquinone oxidoreductase), complex III (cytochrome c reductase), complex IV (cytochrome c oxidase) and complex V (ATP synthase) (Signs & Fernandez-Vizarra, 2018). Complexes I, III and IV have the ability to pump protons over the IMM to the IMS in order to create and maintain an electrochemical gradient over the IMM. This gradient is utilized by ATP synthase to phosphorylate ADP to ATP (Zorova, et al., 2018). Complex I or NADH-ubiquinone oxidoreductase oxidizes NADH to NAD+. NADH is an electron carrier that is formed during the oxidation of fatty acids, amino acids and pyruvate (Schmiedel et al., 2003). Complex I (along with complexes III and IV) have to be able to pump more protons to the IMS from the matrix than ATP synthase pumps from the IMS to the matrix in order to maintain the membrane potential over the inner mitochondrial membrane for the synthesis of ATP from ADP (Bouillaud et al., 2016).

2.2.1 Complex I

Complex I is the largest of the mitochondrial OXPHOS system, consisting of 45 subunits. Of these subunits, seven are encoded by the mitochondrial genome while the other 38 are encoded by the nDNA (two subunits are identical) (Finisterer, 2008). Complex I forms an L-shaped protein divided into two domains namely the membrane arm and the matrix arm. The matrix arm contains a flavin mononucleotide (FMN) that can accept two electrons from NADH to form $FMNH_2$ (flavin mononucleotide – reduced form). The electrons are then transferred through a chain of iron-sulphur clusters. At the junction of the matrix- and membrane arms is the ubiquinone (CoQ) binding site, where the two electrons are transferred to CoQ to form ubiquinol (QH2). The last of the iron-sulphur clusters (subunit N2 of the membrane arm) undergoes a conformational change when the electrons are transferred to ubiquinone. This induces the formation of a proton translocation channel by the four of the remaining five membrane arm subunits. Four protons move through the channel from the mitochondrial matrix to the IMS (IMS), because of the energy release from the electron transfer to ubiquinone (Zhao et al, 2019).

2.2.2 Complex II

Complex II consists of only four subunits, making it the smallest of the five OXPHOS complexes. All four of these subunits are encoded by the nDNA and require transport into the mitochondrial matrix via the translocases of the inner and outer membranes (TIM-TOM) import system. Each of the four subunits have a specific role in complex II as a whole. Subunit A, which is the largest of the four subunits contains a flavin adenine dinucleotide (FAD) co-factor and houses the succinate binding site for the oxidation of succinate into fumarate. Subunit B contains three iron-sulphur clusters that accept electrons from succinate oxidation to pass to CoQ. Complex II does not move protons over the IMM (Fullerton et al. 2020).

2.2.3 Complex III

Complex III is made up of 11 subunits, only one of which is encoded by the mitochondrial DNA (mtDNA) (Fernandez-Vizarra & Zeviani, 2015). It should be noted that complex III has two binding sites for CoQ, both located on each of the ends of cytochrome b. One binding site is for the oxidation of QH_2 and the other for QH^- (Zhao et al, 2019). Complex III receives electrons from QH_2. The first electron is moved to the Reisk iron-sulphur

center protein and then to cytochrome c1, followed by transfer to cytochrome c. The one electron-transfer results in an unstable ubisemiquinone (QH^-) with an unpaired electron, which can create superoxide when combined with oxygen. Although, the unpaired electron is in most instances transferred to two heme units of cytochrome b, Heme bL is the first of the two hemes to receive the electron and transfers it to heme bH resulting in the reduction of another CoQ molecule and the formation of another QH^-. Only one of the electrons from CoQ has been transferred, thus with the second electron transfer, the molecule will be completely reduced. It is important to note that complex III moves four protons over the IMM to the IMS (Chandel, 2010).

2.2.4 Complex IV

Complex IV consists of 13 subunits, three (subunits I, II and III) of which are core subunits encoded by mtDNA and 10 of which are accessory subunits and encoded by nDNA. Reduced cytochrome c will interact with subunit II and transfer electrons to the copper binding site (Cu_A) of subunit II. The electrons move to heme a, followed by the movement to the binuclear center of subunit I. Here, O_2 is reduced to water. In total, eight protons move from the mitochondrial matrix. Four of the eight are used to reduce oxygen to water and four are moved to the IMS (Zhao et al, 2019).

2.2.5 Complex V

Complex V is the last of the five OXPHOS system complexes. This complex is made up of two domains, namely F0 and F1. The F0 domain is imbedded in the IMM and consists of a ring structure made up of subunit c units. The ring structure also includes subunits a, b, d, F6 and oligomycin sensitivity-conferring protein, which forms the stalk of complex V. F0 also has a few accessory subunits linked to the ring structure. F1 is connected to F0 via the stalk with subunits ε, δ and γ. F1 protrudes into the mitochondrial matrix and is made up of three α subunits and three β subunits and is considered the catalytic head of F1. When protons move from the IMS to the mitochondrial matrix, stored energy is transferred to the F1 domain. Complex V undergoes a conformational change which enables ADP to be phosphorylated into ATP (Zhao et al, 2019).

2.3 Mitochondrial Genome

The mitochondrion has its own genome of about 16.5 kb in size. It is a circular genome (plasmid) and encodes for 13 essential subunits of complexes I, III, IV and V. Along with the 13 subunits, the mitochondrial genome also encodes for 22 tRNAs and two ribosomal RNAs (Schmiedel et al., 2003). All the enzymes that are needed for mtDNA replication, transcription and translation, is encoded by the nDNA, thus these enzymes are synthesized in the cytoplasm and transported into the mitochondria (Schmiedel et al., 2003). The mitochondrial genome differs from the nuclear genome in several ways:

- Mitochondrial DNA is only inherited from the mother whereas nuclear DNA is inherited from both parents (Sato & Sato, 2013).
- Each cell only contains one set of the nuclear DNA in chromosome format, whereas every cell can contain hundreds of mitochondria, each with multiple copies of mtDNA (Ylikallio et al. 2010).
- Mitochondrial DNA is continuously replicated, unlike nuclear DNA that is only replicated during cell division (Ylikallio et al. 2010).
- Mitochondrial DNA is not evenly distributed between two daughter cells, whereas each daughter cell would receive one exact copy of the nDNA (Aretz et al. 2019).
- Nuclear DNA is protected by histones and have very strict and active repair mechanisms which prevent mutations. Mitochondrial DNA is circular un-wound chromosomes which lack repair mechanisms and are exposed to reactive oxygen species of the electron transport chain and metabolic pathways. This causes mtDNA to have a higher mutation rate (Gonzales-Hunt et al. 2016).

2.4 Mitochondrial Cytopathies

Mitochondrial cytopathies are disorders characterized by mutations in the genes of mtDNA or the nDNA encoding for enzymes involved in the mitochondrial function (El-Hattab & Scaglia, 2016). This group of heterogeneous disorders affects energy-demanding organs like muscle and the nervous system mainly. Due to the wide and non-uniform distribution of mitochondria throughout the various tissues in the body, mutations causing mitochondrial dysfunction can lead to a wide variety of symptoms.

If all the copies of the mtDNA in a cell are identical, the cell is homoplasmic. If different copies of mtDNA are present in a cell, the cell is heteroplasmic. Heteroplasmy plays an important role in the characteristics of mitochondrial disease in terms of symptoms, onset and severity (Schmiedel et al., 2003). This can be explained via a mutation threshold. Disease-causing mutations in the mitochondrial genome require a certain threshold before any clinical manifestations start to appear (Finsterer, 2008). If the total mutant mtDNA copy number exceeds the normal mtDNA copy number, the OXPHOS system will be impaired, leading to insufficient energy production. Because mtDNA undergoes continuous replication, heteroplasmic cells' mutation load can change over time even if the cells are non-dividing cells such as skeletal muscle and nerve cells (El-Hattab & Scaglia, 2016). Heteroplasmic mother cells that undergo cell division do not partition their mitochondria evenly to the daughter cells. This also leads to cells with different mutation loads. Different tissues have various amounts of mitochondria, and each mitochondrion has its own mutation load, thus mutations that cause mitochondrial dysfunction can lead to different diseases (including symptoms, onsets and severities) (El-Hattab & Scaglia, 2016).

Mitochondrial disorders can involve a single enzyme complex or multiple enzyme complexes. A compensatory mechanism is activated to create more mitochondria when ATP production is diminished below the required threshold (Schmiedel et al., 2003). Currently there is no cure available for mitochondrial disorders. The most effective treatments involve symptomatic treatments of complications due to the disorder such as cardiac dysrhythmia and endocrinopathy (El-Hattab & Scaglia, 2016).

Mutations in the genes encoding for the transporters involved in the shuttle systems can lead to a wide variety of diseases. One example is the glutamate carrier isoform 1 (GC1) deficiency. Symptoms of this deficiency include neonatal epileptic encephalopathy and migrating partial seizures. This transporter is one of the key components of the malate-aspartate shuttle and is encoded by the SLC25A22 gene (Palmieri & Monné, 2016). The mutation in the gene encoding for the carrier occurs on exon 17 of the gene at position 1769 where adenine is exchanged for guanine. This causes a glutamine-to-arginine substitution at position 590 of the carrier (Palmieri & Pierri, 2010). This position is highly conserved throughout the SLC25 gene family and is important for the function of the carrier as this glutamate-aspartate residue protrudes into the cavity of the transporter

where substrate binding takes place. This mutation thus inhibits the function of the carrier (Palmieri & Pierri, 2010). Due to the transporter's high prevalence in neurons, most of the symptoms can be attributed to GC1 not functioning in the neurons. The movement of aspartate from the neuronal mitochondria participates in the production of N-acetyl aspartate, which is the precursor for myelin lipids (Taylor, 2017).

2.4.1 Leigh Syndrome

Leigh Syndrome is an inherited neurodegenerative disease mostly affecting infants, although, some adult onset cases have been reported. It is one of the most common mitochondrial diseases with a prevalence of 1 in 5000 live births (Finisterer, 2008) (Lake *et al*., 2015). Considering clinical symptoms and the genetic origin of the disorder, individuals with Leigh Syndrome have a short life span due to the progressive decline on a neurological level and no cure being available (yet). The clinical symptoms of the disease varies, due to the heterogeneous distribution of the mitochondria throughout the body and the various body systems being affected differently by the mutation (Baldo & Vilarinho, 2020). Most of the clinical manifestations include developmental delay and failure to thrive along with other symptoms which includes perinatal asphyxia, respiratory distress, cranial nerve dysfunction, ataxia, dystonia, muscle weakness, hypotonia and lactic acidosis of the blood, cerebrospinal fluid and urine (Schmiedel et al., 2003) (Finisterer, 2008). Progressive decline of the nervous system can be attributed to the formation of lesions on the basal ganglia, cerebellum and/or brainstem.

Mitochondrial complex I deficiency is the most common cause of Leigh syndrome (Finsterer, 2008). Due to the contributions of both the nuclear and mitochondrial genomes for the subunits of Complex I, there are a few mutations that can contribute to a defective Complex I and lead to Leigh syndrome (Schmiedel et al., 2003). Mutations in the subunits of other enzymes of the respiratory chain, as well as enzymes like pyruvate dehydrogenase can also lead to the presentation of Leigh-like syndrome (Finisterer, 2008). Leigh syndrome can be inherited from the parents via autosomal- or X-linked recessive inheritance or mitochondrial inheritance from the mother's side. Mitochondrial inheritance is the most common way of disease-inheritance. The presentation of the clinical symptoms is dependent on the mutation load of the mutated gene's protein. A mutational load of 70% or less, causes an asymptomatic clinical appearance (Baldo & Vilarinho, 2020). Leigh syndrome has a very large heterogeneity, which makes it hard to

identify the gene with a mutation that can cause the disease, seeing as disease-causing mutations have been identified in all of the core subunits of Complex I (Finisterer, 2008).

2.5 Mitochondrial Solute Carriers (SLC25)

The mitochondrial carriers can transport a large variety of molecules, which includes ATP or ADP, amino acids and organic acids such as malate, ornithine and citrulline (Haitina et al., 2006). These membrane-embedded proteins provide the link between the mitochondria and the cytosol (Gnoni et al., 2009). Metabolites can be utilized for different outcomes due to metabolic pathways not being linear. Metabolic pathways such as glycolysis favour the regeneration of electron carriers such as NADH, which is utilized by the electron transport chain in order to ultimately produce ATP (Bender & Martinou, 2016). These shuttles and transporters move substrates for mitochondrial oxidation over the IMM to the matrix of the mitochondria. The oxidation of the transported substrates (positive charge) causes the movement of protons in the opposite direction over the IMM (Bouillaud et al., 2016).

Macromolecules (such as sugar) are catabolized via glycolysis and lactate oxidation to produce NADH in the cytosol (Lu et al., 2008). Cytosolic NADH cannot be transported over the IMM due to the membrane's impermeability to most metabolic intermediates, which includes NADH (Lu et al., 2008). Various shuttles consisting of carriers from the SLC25 gene family have been described that can shuttle electrons from cytosolic NADH over the IMM via metabolic intermediates (Lu et al., 2008) – of which the malate-aspartate shuttle is the best described (Palmieri & Monné, 2016).

2.5.1 Types of Mitochondrial Carriers

Two types of mitochondrial transporters exist, namely passive and active transporters. A passive transporter moves solutes across membranes down their electrochemical gradient. Active transporters create a gradient over membranes by making use of diverse energy-coupling mechanisms (Hediger et al., 2004). Active transporters can be further divided into primary-active transporters and secondary-active transporters. Primary-active transporters are ATP dependent transporters (ATPases) that includes the ABC transporter family and ion pumps while secondary-active transporters make use of the ion gradients generated by the primary-active ion transporters to move solvents via uphill transport over a biological membrane (Hediger et al., 2004). Channels allow movement

of solutes down their own electrochemical gradients. This is controlled by gating mechanisms and single channel conductance.

The type of transport the carrier catalyses is one of the ways in which it is categorized into one of the SLC25 gene family's subfamilies (Palmieri, 2013). The majority of the mitochondrial carriers mediate transport via exchange of substrates on either side of the membrane (antiport). Other transporters make use of H+-co-transport along with the substrate from one side of the membrane. Very few transporters make use of unidirectional transport (uniport) (Palmieri, 2013). These transport mechanisms can be electrogenic to translocate a net electrical charge over the membrane with the transport reaction. Electroneutral transport is achieved by making use of simultaneous carrier mediated H+ movement, by the exchange of solutes with the same charge or by the uniport of electroneutral solutes (Palmieri, 2013).

2.5.2 Genomic Aspects of Mitochondrial Solute Carriers

The SLC25 gene family is a large group of nuclear genes encoding for transporters that are embedded in the IMM. These genes are distributed uniformly throughout the nuclear genome and can contain one to 18 exons and 1 184 – 65 456 base pairs (Palmieri, 2013), (Palmieri & Monné, 2016). An internal targeting sequence may be present that is recognized by the mitochondrial import machinery to embed the transporters into the mitochondrial membrane (Palmieri & Monné, 2016). These transporters are not restricted to the mitochondria and can be observed in other cell organelles such as peroxisomes, chloroplasts and mitosomes. Because these transporters are encoded by the nuclear genome, they are synthesized in the cytosol and have to be imported into the mitochondria membrane. The expression of mitochondrial carriers can be tissue specific, which indicates their importance in special functions (Palmieri, 2013). Due to enzyme and metabolite compartmentalization in the cytosol and the mitochondrial matrix, there is an intensely diverse flux of solutes into and out of the mitochondrion over the IMM (Lu et al., 2008). The compartmentalization has a role in the regulation of the energy metabolism. Communication between these compartments is vital and is achieved by the mitochondrial carriers (Lu et al., 2008). They are responsible for this flux of metabolites, they are involved in many metabolic pathways, play a role in optimal substrate utilization and maintain the balance between ATP synthesis and utilization (Lu et al., 2008).

2.5.3 Structural Properties of Mitochondrial Solute Carriers

The SCL25 transporters are small proteins with a molecular mass of 30 – 34 kDa (Palmieri & Pierri, 2010) and all have specific and unique sequence features, which makes it possible to recognize the mitochondrial carrier family members. These carriers function as homodimers (Gnoni et al., 2009), and their features include a signature three-fold repeated motif, a tripartite structure of three tandemly repeated homologous domains of about 100 amino acids with a conserved signature motive PX[D/E]XX[K/R]X[K/R]X20-30[D/E]GXXXX[W/Y/F][K/R]G (Palmieri & Monné, 2016). Each repeat contains two hydrophobic stretches, which span the membrane as α-helices with a signature motif. The six α-helices (labelled I-VI in Figure 2-1) are arranged that both terminals of the protein are on the cytosolic side of the membrane. The six α-helices are connected via three short α-helices parallel to the membrane on the matrix side and two loops on the cytosolic side (Figure 2-1). The six spanning α-helices are arranged counter-clockwise in a funnel shape open towards the cytosol (Palmieri, 2013). The N-terminus of the even-numbered α-helices and the C-terminus of the odd-numbered α-helices are located on the matrix side of the carrier. The even-numbered and odd-numbered α-helices have an antiparallel arrangement indicated by the alignment of the conserved glycine and proline residues (Palmieri & Pierri, 2010).

Two possible salt bridges have been identified, one on the matrix side and one on the cytosolic side, that closes the central cavity of the mitochondrial carrier (Palmieri & Pierri, 2010). These salt bridges have been linked to the structural function of mitochondrial carriers by enabling the carriers to switch between the matrix-state (m-state) and cytosol-state (c-state) (Palmieri & Pierri, 2010). The salt bridges are possibly formed by the residues of the symmetrical amino acid triplets localized at the C-terminus of the even-numbered transmembrane α-helices on the cytosolic side of the IMM. These networks functions as gates of the carriers in the m-state on the cytosolic side of the carrier. It has also been proposed that the conserved proline and glycine residues of the α-helices act as hinges to switch between the m-state and c-state (Palmieri & Pierri, 2010). A common substrate-binding site has also been identified for the mitochondrial carriers. It is formed by residues of the three even-numbered transmembrane helices that protrude into the cavity of the carrier. The second contact point (point II) on helix four distinguishes between the different substrates. Changes in the amino acid sequence of this contact

point enables it to discriminate between the substrates it can transport (Palmieri & Pierri, 2010). The residues of the odd-numbered transmembrane α-helices that protrude into the cavity at the same level as the contact points of the even-numbered transmembrane α-helices, may also participate in substrate binding.

The amino acid sequences of the mitochondrial carriers indicate inter-repeat triplet amino acids of the different mitochondrial carriers. These triplets protruding into the carrier cavity can be used to characterize the mitochondrial carrier sub-families as well as predict the function or substrate specificity of unidentified carriers. It is important to note that some of the amino acid triplets used for characterization purposes are shared by more than one of the subfamilies. Some of the subfamilies are also characterized by more than one set of amino acid triplets (Palmieri & Pierri, 2010). The amino acid triplets can be symmetrical (consists of the same three amino acids) or be asymmetrical (consists of three different amino acids). The symmetrical triplets are well conserved throughout the mitochondrial carriers. They contribute to the structural integrity and the mechanism by which the carriers function. The asymmetrical triplets are not as conserved as the symmetrical triplets are. They are important for the recognition and binding of the specific substrates of each mitochondrial carrier, due to the asymmetrical distribution of the functional groups on the substrate (Palmieri & Pierri, 2010). Glycine and proline residues have been well conserved in the transmembrane α-helices. These residues are located between the active site and the gates on both sides of the carrier. Their function has been speculated as hinges for the switch between the m-state and c-state (Palmieri, 2013).

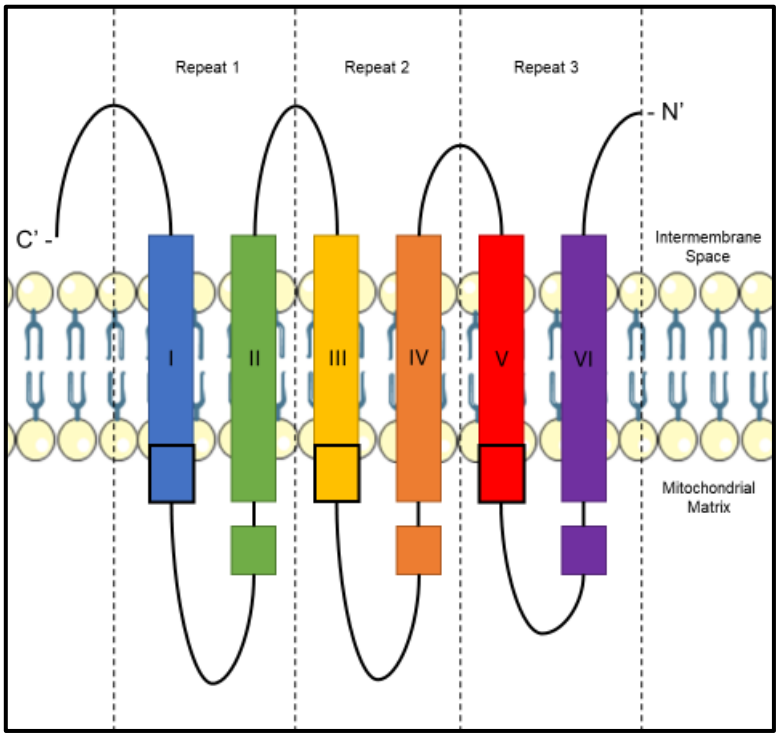

Figure 2-1: General Structure of the SLC25 gene family. Repeats 1, 2 and 3 indicated with dashed lines represent the three tandemly repeated homologous domains of about 100 amino acids. Coloured rectangles represent the six hydrophobic α-helicases that span over the IMM.

2.5.4 SLC25 Import into the Mitochondrion

As mentioned, mitochondrial carriers are nuclear encoded and are synthesized in the cytoplasm, and thus needs to be incorporated into the IMM. This process is called mitochondrial protein import. This process forms part of the intracellular trafficking of proteins (Ferramosca & Zara, 2013). Proteins that are meant to be embedded in the IMM have an extended amino acid sequence at the C-terminal with a conserved sequence PX(D/E)XX(K/R), which contains the information for the protein to be targeted to the mitochondria. This sequence is known as the carrier sequence (Ferramosca & Zara, 2013). The sequence of amino acids is presented as an amphipathic α-helix with a hydrophobic and a hydrophilic side and has a positive charge. This sequence is unique and has a very specific interaction with receptors on the OMM. The recognition α-helix is cleaved off either during or after the import to the mitochondria (Ferramosca & Zara, 2013). Some of the precursor proteins do not contain the α-helix extension, but rather have an internal targeting sequence such as the metabolite carrier family. It has been

suggested that these proteins contain a repetitive structure between the three homologous segments characteristic of the SLC25 family, that may function as the internal targeting sequence (Ferramosca & Zara, 2013).

The import proteins of the mitochondria comprise of three translocation protein complexes called TOM, TIM23 and TIM22. As indicated by their names, TOM is localized on the OMM along with the sorting and assembly machinery (SAM complex) and the TIM complexes are localized to the IMM (Ferramosca & Zara, 2013). The two TIM complexes have the same function but have different substrates. TIM23 imports precursor proteins with a recognition α-helix extension, while TIM22 imports precursor proteins with an internal targeting sequence. This IMS of the mitochondria contains the mitochondrial intermembrane space assembly machinery (MIA) which is responsible for oxidative protein transport and protein folding (Ferramosca & Zara, 2013).

2.5.5 Solute Transport Mechanisms

The mitochondrial carriers make use of various modes of transport to move solutes across the IMM (Palmieri & Monné, 2016). It is important to preserve the proton electrochemical potential gradient over the IMM that is generated by the electron transport chain, as it is important for the phosphorylation of ADP to ATP (Palmieri & Pierri, 2010). The transporters can make use of antiport, uniport or proton compensated anion symport (Figure 2-2). A combination of these modes of transport can also occur (Palmieri & Monné, 2016). The electrical nature of the transporter is also important and can be either electrophoretic or electroneutral. Electrophoretic mitochondrial carriers translocate net electrical charge over the mitochondrial membrane by transporting charged solutes that results in an electrochemical imbalance over the membrane (Palmieri and Pierri, 2010). Electroneutral transport is the simultaneous transport of protons such as anion/H+ co-transport, cation/H+ exchange or proton-compensated exchange of substrates (Palmieri, 2013). For example, the human ornithine carrier can transport ornithine+ against citrulline and H+ and the oxoglutarate carrier that exchanges oxoglutarate^{2-} for malate^{2-} (Palmieri & Pierri, 2010). Antiport entails an obligatory 1:1 exchange of two substrates. Three of the mitochondrial carrier subfamilies make use of this mode of transport due to their electrical nature. The first is the ADP/ATP carrier subfamily that exchanges ADP with a negative three charge (ADP^{3-}) for ATP with a negative four charge (ATP^{4-}) and the second is the aspartate-glutamate carrier subfamily that exchanges glutamate^{-} and H^{+} for

aspartate$^-$. The third is the uncoupling proteins that only transport protons. In all three cases, the exchange of these solutes over the mitochondrial membrane results in a charge imbalance over the mitochondrial membrane (Palmieri & Pierri, 2010). Uniport has a unidirectional substrate transport where one solute is moved over the membrane. Uniport can be electrophoretic or electroneutral, depending on the substrate specificity of the solute carrier. Electrophoretic exchanges using uniport as transport mechanism can cause disruption of the electrochemical gradient, such as that of the IMM, while electroneutral exchanges using uniport transport mechanisms will cause no change in an electrochemical gradient (Palmieri, 2013). An example of electrophoretic exchange using uniport mode of transport is the uncoupling proteins, which only transport protons in one direction over the mitochondrial membrane (Palmieri & Pierri, 2010). Symport uses co-transport and counter transport of solutes with a charge. This mode of transport also maintains an electroneutral balance over the mitochondrial membrane. For example, mitochondrial subfamilies for phosphate mediate the transport of anions with an equal number of protons (Palmieri & Pierri, 2010). For solute transport through the mitochondrial carriers, the carriers undergo reversible conformational changes, which entail switching between the m-state and the c-state (Palmieri & Pierri, 2010).

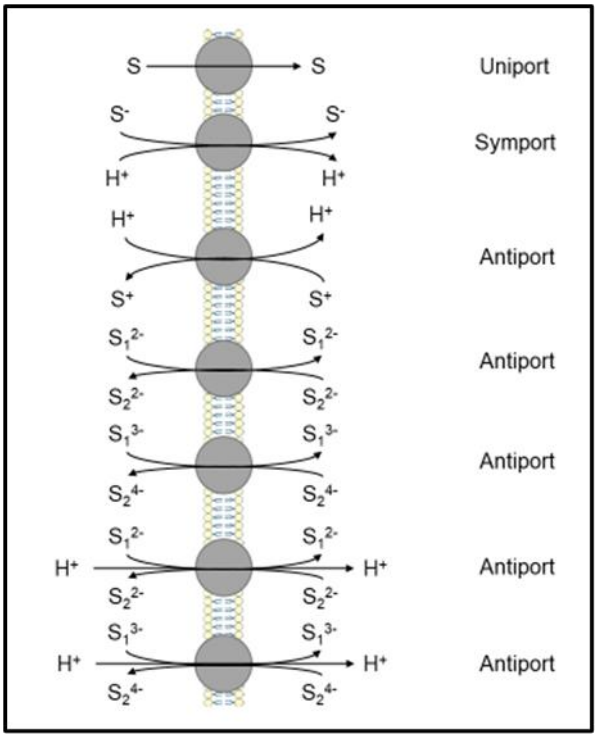

Figure 2-2: Transport mechanisms of the mitochondrial solute carriers as described by Palmieri (2013) (Figure from original depicted in Palmieri, 2013). S: substrate, H^+: protons. Arrows indicate the direction of movement.

2.5.6 Functional Properties of Mitochondrial Solute Carriers

In previous studies, each current member of the SLC25A gene was identified via substrate specificity experiments. This method entails gene expression in yeast, then purifying the products of the genes and reconstituting them into liposomes in which the substrate transport is assayed (Palmieri & Pierri, 2010). The low homology should be taken into consideration with regard to conclusions about a transporter's substrate specificity when substrate specificity analysis is not used to identify a transporter. Previous studies indicated that even isoforms with almost identical amino acid sequences have substantial differences in substrates and/or kinetic parameters (Palmieri, 2013). The SLC25 gene family has a very diverse range of metabolites that can be transported. The metabolites are mostly negatively charged but can also be positively charged or have no charge (zwitterions) if one considers the physiological pH at which the transporters function (Palmieri & Monné, 2016). The mitochondrial carriers are divided according to the specific type of solutes they transport and can be further divided into sub-families according to their substrate specificity and kinetic properties. The subfamilies are also

characterized by specific amino acid triplets (Palmieri, 2013). Thus far, 24 subfamilies have been identified and some subfamilies have the potential to transport additional (untested) substrates.

Mitochondrial carriers utilize different aspects of solutes as their functional driving force. These can include the solutes concentration gradient over the membrane and the electrochemical potential over the IMM that is generated by the respiratory chain. A substrate would enter the carrier from either side of the membrane. The carrier protein then enters the transition state. The substrate is then bound to the active site in the middle of the carrier cavity. The binding of the substrate triggers additional structural changes, which then leads to the conformational change of the carrier. The substrate-induced conformational changes are attributed to the hinged movements of the even and odd numbered transmembrane α-helices (Palmieri, 2013). These transporters contribute directly to various metabolic pathways by ensuring sufficient solute flux to and from the metabolic pathways. The activity of the mitochondrial transporters is regulated by different aspects, which includes inhibitors or activators, changes in the functional parameters of the transporter (driving forces, kinetic parameters, and concentration of the substrate) and alterations in the gene expression of the transporters. Others include epigenetics, certain cell conditions and drugs.

2.6 Mitochondrial Shuttle Systems

Shuttle systems of the mitochondria have a combination of carrier- and exchange proteins that regulate and maintain metabolite concentrations on both sides of the IMM. The concentrations of these metabolites are maintained at the optimal concentrations, which means not necessarily at equal concentrations on either side of the IMM (Korla et al., 2015). Different shuttle systems can transport the same metabolites over the IMM and can be linked to each other and other metabolic pathways, such as the TCA cycle via these shared metabolites. An example of such a metabolite is malate. Malate is transported in both the citrate-pyruvate shuttle and the malate-aspartate shuttles and also plays a key role in the function of the TCA cycle (Korla et al., 2015). Malate in the IMS of the mitochondria acquires the electrons of NADH and can then be exchanged for α-ketoglutarate over the IMM to the mitochondrial matrix, along with the two electrons of NADH. NADH cannot move over the IMM, thus, malate is an effective way to shuttle

electrons of cytosolic NADH to NAD in the mitochondrial matrix when malate is converted to other carbon skeletons, such as oxaloacetate (Korla et al., 2015).

2.6.1 Citrate-Pyruvate Shuttle

The main functions of the citrate-pyruvate shuttle are to move electrons of NADH and carbon skeletons for the TCA cycle, from the IMS to the mitochondrial matrix. The shuttle makes use of two carrier proteins from the mitochondrial solute carrier family (SLC25A1 and SLC25A3) as well as five enzymes. Also included in the shuttle system is a pyruvate pump, which makes use of a symport mechanism to move pyruvate and protons from the IMS to the mitochondrial matrix (Korla et al., 2015). In the mitochondrial matrix, acetyl-CoA is first converted to citrate via citrate synthase. As previously mentioned, the IMM is impermeable to most molecules, including acetyl-CoA. Citrate is then moved from the mitochondrial matrix to the IMS and malate is moved in the opposite direction via the citrate carrier (SCL25A1). In the IMS, the citrate is converted back to acetyl-CoA via ATP-dependent cleavage by ATP-citrate lyase. Oxaloacetate is also formed during this reaction and the acetyl-CoA in the IMS is utilized for fatty acid synthesis (Korla et al., 2015). Oxaloacetate is then converted to malate and NADH is oxidized to NAD+. Malate is then converted to pyruvate via the malic enzyme and NADP is reduced to NADPH. The pyruvate carrier transports pyruvate back into the mitochondrial matrix where it can be utilized in the TCA cycle after being converted back to acetyl-CoA via pyruvate dehydrogenase. NAD+ is also reduced back to NADH for complex I to utilize (Korla et al., 2015). Figure 2-3 gives a visual representation of the above-described process.

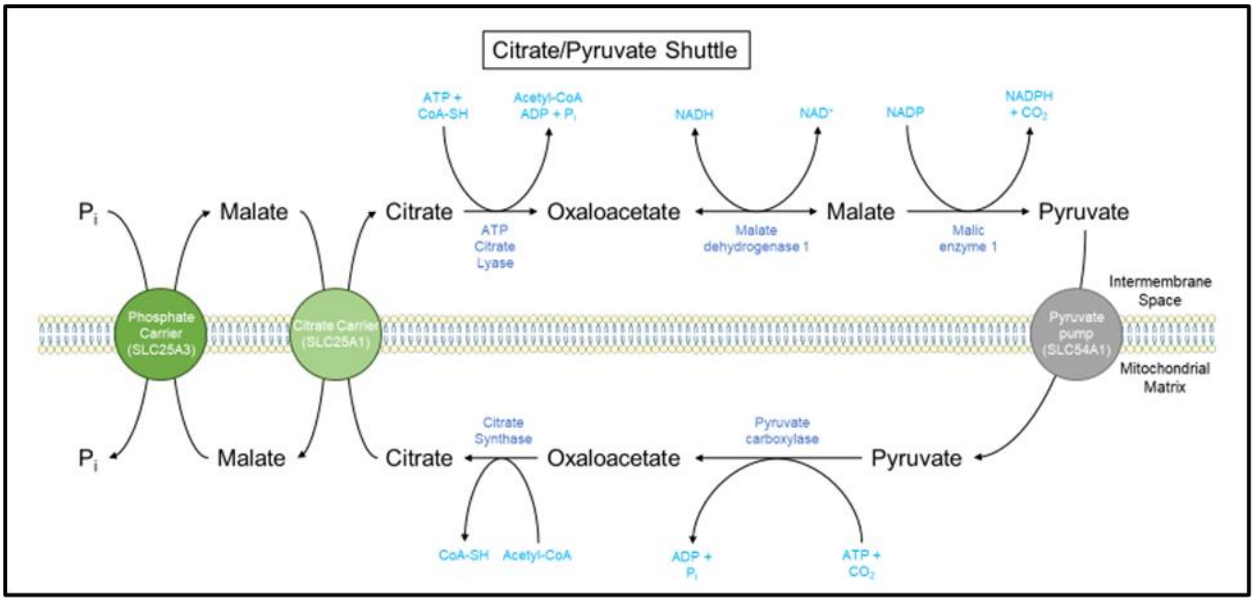

Figure 2-3: The Citrate-Pyruvate Shuttle System with all SCL25 carriers, substrates, intermediates, enzymes, and co-factors

2.6.1.1 SCL25A1 – Citrate Carrier

The citrate carrier is responsible for the transport of citrate over the IMM. This transporter has an important function in various metabolic pathways, which includes fatty acid synthesis and gluconeogenesis. Reducing equivalents are also transported via this carrier. The gene responsible for the citrate carrier (SLC25A1) is located on chromosome 22.q11.2 (Huizing et al., 1998), with seven introns and eight exons (Gnoni et al., 2009). The citrate carrier protein's expression is specific to tissue types where is plays a vital role. An abundance of SLC25A1 mRNA levels have been associated with tissues that host metabolic pathways such as gluconeogenesis and fatty acid synthesis (such as the liver). Tissues that have low activity of said metabolic pathways have low abundances of SLC25A1 mRNA (Huizing et al., 1998). The expression of the citrate carrier in the various tissues of the body is regulated by the metabolic pathways to which it supplies substrates or removes products (Gnoni et al., 2009). The expression is also regulated by insulin and inflammation (Catalina-Rodriguez et al., 2012).

The carrier makes use of electroneutral exchange of citrate (tricarboxylic acid) with one of three compounds: another tricarboxylate/H+, a dicarboxylate (malate or succinate) or phosphoenolpyruvate (citrate-malate antiport). Citrate moves from the mitochondria to the cytosol (Gnoni et al., 2009). This carrier also has an important role in the metabolic

pathway of carbohydrates and lipogenesis. Once acetyl-CoA is formed from the catabolism of carbohydrates, it is transported to the cytosol in the form of citrate. In the cytosol, citrate has many important functions. It participates in cholesterol- and fatty acid synthesis and is a positive allosteric modulator for acetyl-CoA carboxylase. Cytosolic citrate provides NADPH for lipogenesis via malic enzyme and NAD+ (via citrate lyase and malate dehydrogenase) for glycolysis (Gnoni et al., 2009) (Kaplan et al., 1993). The citrate carrier has two substrate binding sites per monomer. As the mitochondrial carriers of the SLC25 gene family consists of two monomers, it totals to 4 substrate binding sites per carrier (Gnoni et al., 2009).

2.6.1.2 SLC25A3 – Phosphate Carrier

The most important role of the phosphate carrier is to transport inorganic phosphate over the IMM for the phosphorylation of ADP to ATP (Huizing et al., 1998). The substrates for the synthesis of ATP are supplied by the phosphate carrier (inorganic phosphate) and ADP/ATP translocase. ADP/ATP translocase moves ADP into the mitochondria to be phosphorylated and synthesized ATP out of the mitochondria to be used by the cell (Runswick et al., 1987). The gene encoding for the phosphate carrier is located on chromosome 12 and consists of nine exons. Alternative splicing leads to two mRNAs for the phosphate carrier protein. The differences in the two resulting phosphate carriers can be attributed to their functional properties and their tissue specificity i.e. ATP production (Huizing et al., 1998). The transport of phosphate into the mitochondrial matrix is achieved by making use of proton co-transport or via the exchange of hydroxyl ions. When proton co-transport is utilized, inorganic phosphate with a negative charge is moved into the mitochondrial matrix and protons that have a positive charge is moved out of the mitochondrial matrix (Runswick et al., 1987). When making use of the hydroxyl exchange, there is no change in the charge over the membrane due to the negative charges carried by both the inorganic phosphate and hydroxyl ions (Runswick et al., 1987).

2.6.2 Uncoupling Proteins

The phosphorylation of ADP to ATP is driven by die proton gradient over the IMM. Protons return to the IMS via ATP synthase while ATP synthase also phosphorylates ADP. Any movement of protons over the IMM other than through ATP synthase causes decoupling of the membrane potential, leading to less ATP being synthesized (Bouillaud et al., 2016).

Uncoupling proteins (UCPs) are located in the IMM and have the ability to move protons over the IMM. There are currently five observed uncoupling proteins. UCP1, UCP2, UCP3, UCP4 and UCP5, which are encoded by the *SLC25A7, SLC25A8, SLC25A9, SLC25A27* and *SLC25A14* genes respectively. These carriers transport protons directly over the IMM to the mitochondrial matrix causing the decoupling of electrochemical gradient over the IMM (Zhao et al., 2019). The energy is thus released as heat, instead of being used to phosphorylate ADP (Haitina et al. 2006). The proton transport to the mitochondrial matrix induces an acid-base exothermic reaction, releasing heat from the reaction. Heat is also generated from the cellular catabolism that is accelerated via UCP1 (Bouillaud et al., 2016). These proteins are mainly observed in brown adipose tissue, which corresponds to their physiological function of heat production (Zhao et al., 2019).

UCP1 transports protons directly, thus the uncoupling mechanism of UCP1 is dependent in the activation and presence of UCP1. High levels of UCP1 are needed (such as for brown adipose tissue) for the uncoupling mechanism to function effectively (Crichton et al., 2017). In addition, the expression levels of uncoupling proteins are strictly regulated, as over-expression of these proteins can cause an increase in the uncoupling mechanism. Other factors such as the temperature of the environment and the type of tissue also regulate the expression of the uncoupling proteins. UCP1 has a half-life of 20 to 70 hours, while other uncoupling proteins have a much shorter half-life (30 – 60 minutes). This indicates that UCP1 can be for long term responses while the other uncoupling proteins are for short term responses (Bouillaud et al., 2016).

UCPs have one binding site for nucleotides (ATP, ADP, GTP, GDP) which can inhibit the transporting mechanisms of the transporter. These nucleotides compete for the binding site (Bouillaud et al., 2016). The functionality of UCPs transport mechanism is dependent on the conformational changes induced by either nucleotides or fatty acids binding to UCP. Fatty acid binding induces a conformation where transport can take place, where nucleotide-binding causes a conformation where transport is inhibited. To prevent uncontrolled uncoupling by UCPs, fatty acids present in the mitochondria (probably from fatty acid oxidation), displace the nucleotides, and activate proton transport (Crichton et al., 2017).

2.6.3 Malate-Aspartate Shuttle

This shuttle system is the most prevalent shuttle system in the heart muscle for transporting electrons from NADH in the IMS to NAD+ on the mitochondrial matrix side to ultimately produce NADH for complex I (Korla et al., 2015). This cyclic pathway is one of the contributors of reducing equivalents to the electron transport chain (Runswick et al., 1990). As mentioned, the IMM is impermeable to most metabolic intermediates, which includes NADH (Lu et al., 2008). This shuttle comprises a transport-transamination-redox cycle and makes use of two antiporter transport proteins, the aspartate-glutamate exchanger that is encoded by the SLC25A12 and SLC25A13 (depending on the tissue type) gene and the α-ketoglutarate-malate exchanger that is encoded by the SLC25A11 gene (Palmieri, 2013) (Lu et al., 2008). One of the most important functions of this shuttle is that it regulates the metabolic activity of the mitochondrial compartment and the cytosolic compartment when reducing equivalents of NADH is moved from the IMS to the mitochondrial matrix (Lu et al., 2008). The aspartate-glutamate exchanger (SLC25A12 or SLC25A13) functions by moving aspartate from the mitochondria matrix. This is accompanied by the entry of glutamate and a proton into the mitochondria matrix. Aspartate and glutamate both have a 1- charge while the proton is positively charged, therefore this exchange is an irreversible, electrogenically driven process that controls the rate of the malate-aspartate shuttle (Indiveri et al., 1987) (Lu et al., 2008). The α-ketoglutarate-malate exchanger (SLC25A11) is a bidirectional transporter that functions by the concentration gradient over the IMM of the substrates it transports (Lu et al., 2008). Figure 2-4 gives a visual description of the above-described process.

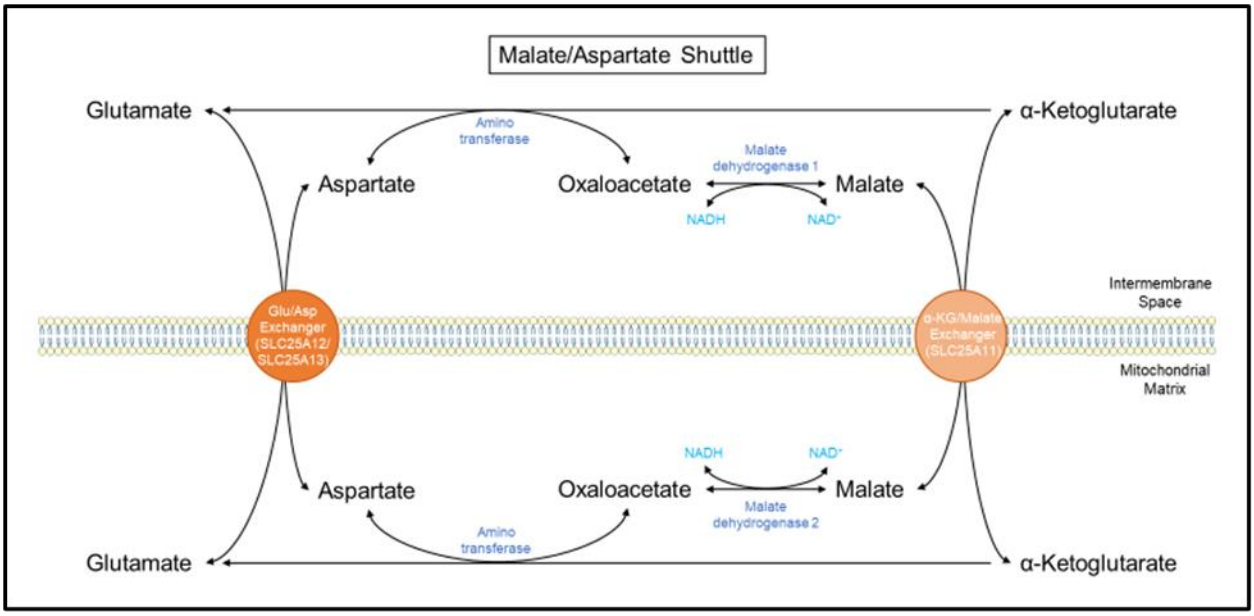

Figure 2-4: Malate-Aspartate shuttle with all SLC25 carriers, substrates, intermediates, enzymes and co-factors

2.6.3.1 SLC25A11 - α-Ketoglutarate-Malate Exchanger

The α-ketoglutarate-malate exchanger transports α-ketoglutarate over the IMM in an electroneutral exchange for malate in the opposite direction (Runswick et al., 1990). Previous studies have also indicated that the protein can also transport various other molecules such as succinate, oxaloacetate, malonate, maleate, D-malate and 2-oxoadipate (Monné et al., 2013). The gene encoding for the protein in located on chromosome 17 in humans and has eight exons and five introns. The protein is expressed mainly in the heart and skeletal muscle, due to the physiological function, that is regulating metabolic function of the mitochondria and the cytosol (Huizing et al., 1998). This carrier also contributes to other pathways aside from the malate-aspartate shuttle, which includes the oxoglutarate-isocitrate shuttle, nitrogen metabolism and gluconeogenesis (via lactate) (Runswick et al., 1990). It also plays a role in mitochondrial fusion/fission, cell death and apoptosis (Monné et al., 2013).

2.6.3.2 SLC25A12 and SCL25A13 - Aspartate-glutamate carriers 1 and 2

The aspartate-glutamate carriers (SLC25A12 – AGC1, SLC25A13 – AGC2) are responsible for the antiport of aspartate and cysteine sulphonate, and glutamate over the IMM (Palmieri, 2013). The gene encoding for SLC25A12 is located on chromosome 2

and contains 18 exons and is predominantly expressed in skeletal muscle, heart muscle and brain tissues (Durdiaková et al. 2014). The gene encoding for SLC25A13 is located on chromosome 7 and is mainly expressed in the liver tissue (Lin et al. 2021). While these carrier isoforms conform to the structural norms of the SLC25 gene family, these carriers contain an EF-hand Ca2+-binding motif at the N-terminal, meaning these carriers' activity is stimulated by Ca2+ in the IMS side of the IMM (Palmieri, 2004). These two isoforms of the aspartate-glutamate carrier play an important role in the malate-aspartate shuttle. The AGCs are essential for the movement of aspartate into the cytosol, where aspartate plays a role in various metabolic pathways such as urea synthesis from ammonia and alanine, purine and pyrimidine synthesis, protein synthesis and gluconeogenesis from lactate (Palmieri, 2004).

2.6.4 SCL25A22 – Glutamate Carrier 1

The glutamate carrier isoform 1 has a wide tissue distribution, which includes the heart, skeletal muscles, lungs, pancreas, liver, kidney and the brain (Palmieri, 2013), (Palmieri & Monné, 2016). The gene encoding for the protein is located on chromosome 37. It also has two main functions: It moves aspartate from the mitochondria to the cytosol and glutamate into the mitochondria from the cytosol and it transfers reducing equivalents of NADH into the mitochondria from the cytosol (Palmieri & Pierri, 2010). The carrier makes use of the antiporter mechanism, seeing as glutamate is moved to the mitochondrial matrix along with a proton. The distribution of the glutamate carrier in the IMM is dependent on the pH of the micro-environment. Entry of glutamate into the mitochondrial matrix is dependent on the energetic state of the mitochondrion. The glutamate carrier can also function in reverse in order to prevent the accumulation of intramitochondrial glutamate (Lunetti et al., 2013). Glutamate dehydrogenase is an enzyme that is exclusively found in the mitochondrial matrix. This suggests that one of the main functions of the glutamate carrier is to provide glutamate for the conversion to α-ketoglutarate and ammonia (NH_3) via glutamate dehydrogenase, but glutamate is transaminated in the mitochondrial matrix to form aspartate and is thus not available for the glutamate dehydrogenase enzyme (Lunetti et al., 2013). The glutamate carrier has also been suggested to play an important role in insulin secretion, as the glucose response is maximized (Lunetti et al., 2013).

2.6.5 The Glycerol-3-phosphate Shuttle

This shuttle moves electrons over the IMM. First, dihydroxyacetone-phosphate is converted to glycerol-3-phosphate by cytosolic glycerol-3-phosphate dehydrogenase (GPD1). During this process, NADH is converted to NAD+. Glycerol-3-phosphate can be converted back to dihydroxyacetone by the IMM imbedded glycerol-3-phosohate dehydrogenase (GPD2), by which two electrons are donated to FAD to form $FADH_2$. This enables the NADH that is produced in the glycolysis pathway to move its two electrons over the impermeable IMM (Shen et al., 2006). Other than transferring the electrons of NADH from the IMS to the mitochondrial matrix, the glycerol-3-phosphate shuttle has other possible functions as well. These include thermogenesis via NADH oxidation by bypassing complex I and regulating cytosolic glycerol 3 phosphate (Mráček et al., 2013). Previous research done indicated that a deficiency in the glycerol-3-phospate dehydrogenase enzyme, leads to an increase in the NADH/NAD+ ratio and an inability to regain the balance under stress conditions (Shen et al., 2006). It should be noted that both enzymes can reverse their reactions (Sato et al., 2016). The shuttle activity is dependent on both GPD1 and GDP2 being present in equimolar proportions (Mráček et al., 2013). Figure 2-5 gives a visual description of the above-described process.

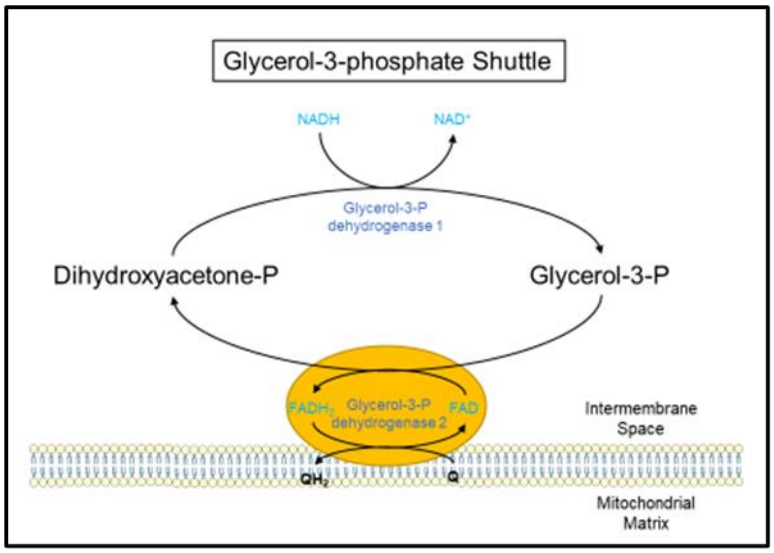

Figure 2-5: Glycerol-3-phosphate shuttle with all substrates, intermediates, enzymes and co-factors.

2.6.5.1 Glycerol-3-phosphate dehydrogenase 1 (soluble/cytoplasm)

GPD1 is present is the cytosol of the mitochondrial IMS. The enzyme is dependent on NADH to reduce dihydroxyacetone phosphate to glycerol-3-phosphate (Sato et al., 2016). GPD1 shares no homology with GPD2 (Mráček et al., 2013). The gene encoding for the protein is mapped to chromosome 12 with eight exons in humans. Three isoenzymes have been identified of this enzyme indicating specific functions in certain tissues (Menya et al., 1995). The enzyme has a molecular weight of 37.5 kDa with 349 amino acids in length (Joshi et al., 2014). The protein is expressed mainly in brown adipose tissue, with other distributions including the brain and the liver.

2.6.5.2 Glycerol-3-phosphate dehydrogenase 2 (mitochondrial)

GPD2 is imbedded in the IMM. This enzyme is dependent on FADH2 and can oxidize glycerol-3-phosphate back to dihydroxyacetone phosphate (Sato et al., 2016). The gene encoding for GPD2 is located on chromosome two in humans and is highly conserved throughout different species (Mráček et al., 2013). The protein is expressed in most tissues to a very high extent, leading to the conclusion of an unknown physiological function (Mráček et al., 2013). The mature protein has a molecular weight of about 74 kDa after the recognition presequence is removed due to import into the IMM (Mráček et al., 2013).

2.7 Problem Statement

Mitochondrial disease can be defined as deficiencies in the mitochondrial oxidative phosphorylation system (Esterhuizen et al., 2017). Complex I of the respiratory chain is the largest of the electron transport chain and dysfunction results in Leigh syndrome. Since Complex I converts NADH to NAD+, a deficiency in complex I units results in a redox imbalance and slowed redox reactions (via dehydrogenases) leading to the build - up of numerous metabolites in different pathways. Complex I is also one of the main contributors of the electrochemical gradient over the IMM, which is needed for the phosphorylation of ADP to ATP (Schmiedel et al., 2003). Defective complex I units diminishes the electrochemical gradient over the IMM, ultimately causing less ATP to be synthesized. Extensive research has been done on Ndufs4-/- (complex I deficient) mice which revealed adaptive mechanisms that compensate for the diminished function of complex I - such as the adapted complex II and CoQ cycle (Terburgh et al., 2019). Since

the mitochondrial shuttles are able to move reducing equivalents over the highly impermeable IMM, it is likely that these shuttles also compensate for the defect. However, this hypothesis remains untested, and the following questions highlight the gap in our knowledge when it comes to the role of these shuttles in complex I deficiency:

1.

1. Which IMM transporters are differently expressed due to a complex I deficiency, and how does this contribute to the observed metabolite levels and the disease state? More importantly, how do these differentially expressed transporter influence the redox state?

2. What enzymes involved in these shuttles are differently expressed in Ndufs4-/- mice tissue, and what is the effect on disease?

3. Are there differences in the levels of metabolites involved in mitochondrial shuttles when Ndufs4-/- knockout mice tissue is compared to control mice?

2.8 Aims and Objectives

The main aim of this study is to investigate the adaptive responses of the above-mentioned shuttle systems in Ndufs4-/- and Control (i.e. wild type) mice brain, liver and heart samples.

The objectives formalized to reach the aim of this study:

1. Breeding, genotyping and acquisition of Ndufs4$^{-/-}$ and control mice samples (brain, liver and heart).
2. Targeted transcriptomic analysis of the selected mitochondrial transporters (SLC25 gene family) and involved enzymes.
3. Metabolomic analysis and comparison of the selected shuttles' involved metabolites in both the Ndufs4 -/- and control mice.
4. Integrative interpretation of transcriptomic and metabolomics data.

2.9 Study design

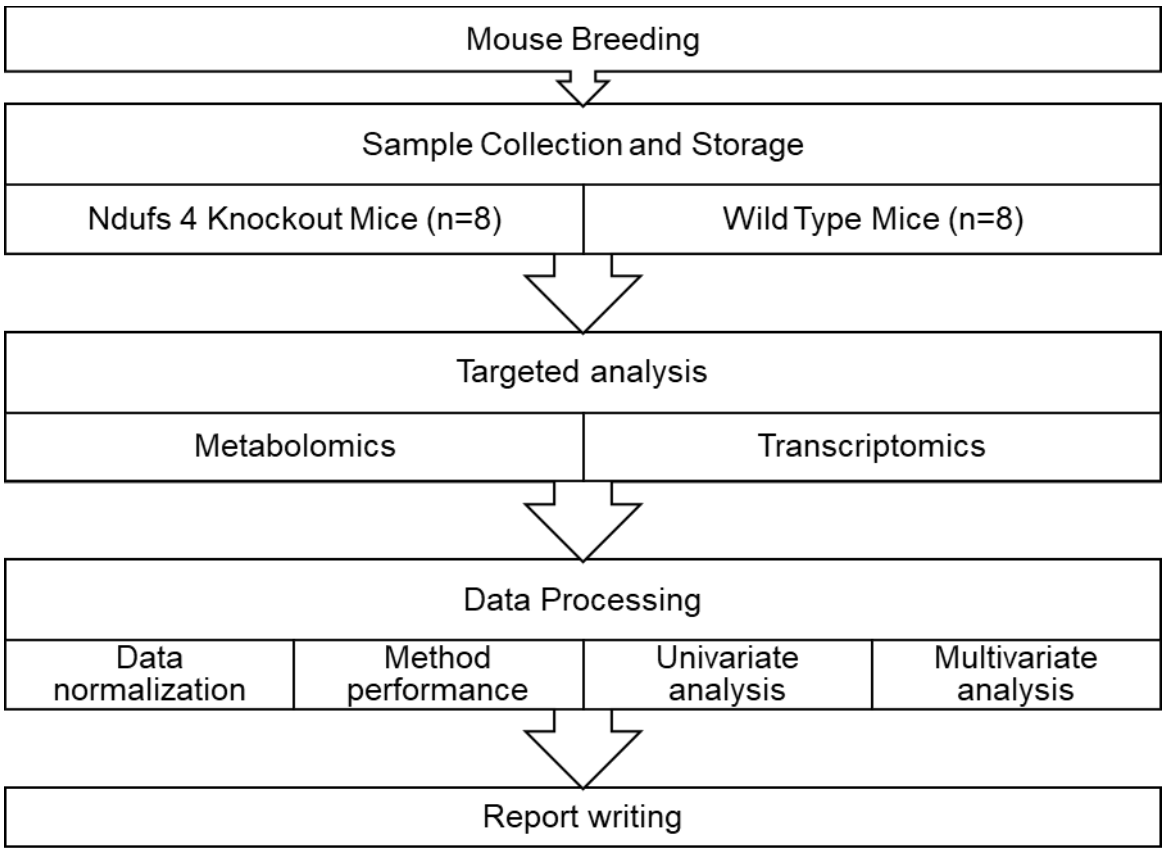

Figure 2-6: General study design for the execution of this study

CHAPTER 3 – PRINCIPLES OF EXPERIMENTAL PROCEDURES

3.1 Ndufs4 Knockout Mice

To understand specific biological roles of genes and/or proteins, gene targeting is used to alter a specific gene. This is achieved by the genetic homologous recombination of a mutated form of a specific gene to a designated genetic locus. This leads to the origin of a mutated version of the original gene (Hall et al., 2009). When considering a suitable host for knockout models, the laboratory mouse (Mus musculus) offered specific advantages when the study of human genetic diseases is concerned. These include similarities between mice and humans such as development, physiology behaviour and diseases. Almost all mice genes also have homologs in humans and the mouse genome supports homologous recombination in embryonic stem cells (Austin et al., 2004).

As described previously, a complex I deficiency is one of the main causes of Leigh syndrome (Finsterer, 2008) and complex I is the largest of the five OXPHOS complexes with 45 subunits (Zhao et al, 2019). The Ndufs4 subunit of complex I is one of the most often mutated genes with complex I deficiency in humans. These mutations lead to the presentation of Leigh syndrome. The C-terminal of the Ndufs4 subunit is phosphorylated in order for the protein to be matured and imported into the mitochondrion (Valsecchi et al. 2012). The knockout genotype of the mice used in this study were created by the excision of exon 2 from the NADH:ubiquinone oxidoreductase iron-sulphur protein 4 (*Ndufs4*) gene. This exon encodes for the first 17 amino acids of the mature Ndufs4 protein. With the excision of exon 2, a frameshift mutation occurs that inhibits the synthesis of mature Ndufs4 proteins. This means the protein is unable to be phosphorylated to mature and be imported into the mitochondrion (Valsecchi et al. 2012).

Excision of exon 2 of the *Ndufs4* gene was done via the Cre-Lox recombination technique (Kruse et al. 2008). This is a powerful gene editing tool combining the cre-enzyme (creates recombination) and lox-P (locus of crossing over (x), P1) sites in nuclear DNA (McLellan et al. 2017). Lox-P sites are 34 base pair sites (13 bp symmetrical sequences flanking an 8 bp non-symmetrical sequence) which the cre-enzyme recognizes and binds to. The orientation of the two lox-P sites determines the type of recombination to take place (Aquila et al., 2018). The Cre-Lox system requires two basic elements for successful genetic recombination. The first is a host that is engineered to have a genetic

locus where the target DNA sequence is flanked by two lox-P sites and the second is the host must be able to express the cre-enzyme specific to that lox-P sites. The expression of cre-enzyme is usually controlled by a specific promotor sequence. If the promotor and enhancer sequences are tissue specific, the recombination will also be tissue specific (McLellan et al., 2017).

3.2 Genotyping of Ndufs4 Mice

The obtained mice were part of an extensive breeding program. The heterozygous mice carried the mutation of the *Ndufs4* gene. Breeding heterozygous mice can ultimately lead to offspring with one of three genotypes. Genotyping the mice entails characterizing the mice according to a specific gene (or genes) result on the phenotype. Genotyping was done by means of polymerase chain reaction (PCR) analysis. PCR entails denaturing the template DNA with heat into single strands of DNA. This is followed by the annealing of oligonucleotide primers to the denatured DNA. These primers create a short double stranded DNA sequence for polymerase to bind and start the extension of the ssDNA into dsDNA. A thermal cycler is used to simplify the whole process due to the differences in temperature needed for denaturing DNA, annealing primers, and extension via DNA polymerase. This cycle is repeated and with each repeat, the gene of interest will be amplified exponentially (Green & Sambrook, 2019). Tail snips were used to isolate template DNA from each of the mice. The *Ndufs4* gene was amplified using primers that was specifically designed for this gene (sequences shown in Table 4-1) (Valsecchi et al., 2012). The amplicons were then separated on an agarose gel containing ethidium bromide. The agarose gel was placed in a buffer and the samples loaded into wells created during the casing of the gel. When current was passed through the buffer and gel, the DNA moved to the cathode, due to the negative charge of DNA. The separation of the DNA is based on the size of the DNA fragments. Small fragments move faster through the gel than the larger DNA fragments. Wild type mice have two alleles with intact *Ndufs4* genes and yield a single amplicon band of about 1229bp. This indicates that the full *Ndufs4* gene is intact and present. Heterozygous mice will be a carrier of both alleles of the gene, where one allele is fully intact, and the other allele is missing exon 2 of the *Ndufs4* gene. This yields two separate amplicon bands on the gel with a size of 1229bp and 429bp, respectively. The knockout mice will have two alleles that both have exon 2 missing. This results in a single amplicon band of 429bp, indicating that the mice have a

completely missing exon 2 of the *Ndufs4* gene. These genotyping results were used to select the mice for this study and breeding pairs for the continuous breeding program of this mice strain.

3.3 Sample Collection

Mice were allowed to reach the age of 45 days post-natal (PN45) but were not allowed to age beyond 50 days post-natal. Endpoint studies were done to determine the life expectancy of the knockout mice and observed rapid decline after PN35. These mice would die at ~PN50 (Kruse et al., 2008). The application for ethical approval entailed that all animals be subjected to humane endpoints and thus required the mice to be euthanized before natural death occurred. Thus, mice were euthanized between PN45 and PN50 via cervical dislocation according to the guidelines set in place by the vivarium of the Preclinical drug development platform (PCDDP). This is the chosen method for the animals used in this study, as other methods such as carbon dioxide overdose or anaesthetic overdose can cause metabolic variance and stress in the animals before death. A study done by Staib-Lasarzik *et al.* in 2014 have shown that gene expression is also influenced by euthanasia methods such as anaesthesia (Staib-Lasarizik *et al.,* 2014). After euthanasia, the animals were dissected, and the organs of interest were harvested (brain, liver and heart). Organs were placed in a microcentrifuge tube (Eppendorf) and snap frozen in liquid nitrogen. Samples were also kept in liquid nitrogen and moved from the vivarium to the ultra-freezer. A second tail snip was collected during sample collection and used for confirmatory genotyping analysis. Samples were kept at -80°C until further analysis was done. In total, tissue samples from 30 mice were collected specifically for this study. Of the 30 mice, ten were wildtype mice, seven were heterozygous and thirteen were knockout mice.

3.4 Gene Expression Analysis

Gene expression of a protein can be influenced by many factors. Many sources can contribute to variation in gene expression. These variations include anatomy (tissue type), disease and environmental factors such as temperature and diet. Diseases can cause the up-regulation of genes that could be advantageous to the situation, such as proteins that contribute to the immune response as well as the down regulation of other proteins (Fassbinder-Orth, 2014). To assess if there was any change induced in the expression of

genes due to a complex I deficiency, gene expression analysis needed to be performed. Various methods exist to assess gene expression, but all start with RNA isolation. The kit used for RNA isolation makes use of a magnetic bead-based purification system to ensure higher and more consistent RNA yield (ThermoFisher, www.thermofisher.com/order/catalog/product/AM1830#/AM1830). Another method that was considered for RNA isolation was TRIzol, which makes use of a phase separation method. This method has been found to cause variation during the RNA extraction step.

DNA is transcribed to RNA and RNA is translated to form a protein. Various processes in the cell regulate this genetic flow of information. Messenger RNA (mRNA) levels of transcribed genes at any given time represent the balance between transcribing certain genes and denaturation of their mRNA's (Dölken et al., 2008). The proteins of interest (Table 3-1) are present in tissue types where they have a physiological function, such as the uncoupling protein that is most abundantly present in brown adipose tissue. The gene encoding for this protein (*SLC25A7*) is actively expressed in brown adipose tissue, while the expression of this gene would be limited in other tissue types (Bouillaud et al., 2016). Quantifying gene expression in tissue types is possible via gene expression analysis. Various methods are available for gene expression analysis such as reverse transcriptase real-time polymerase chain reaction (RT-qPCR), branched DNA (bDNA) assays, microarrays or sequencing approaches such as Next Generation Sequencing (NGS) (Fassbinder-Orth, 2014). Sequenced-based methods are the more preferred methods when factors such as requirements for the analysis, execution of the analysis, possible errors during the analysis, reproducibility and correlations between data and samples is considered (Fassbinder-Orth, 2014).

Table 3-1: List of genes that are of interest for transcriptomic analysis in mouse brain-, heart-, and liver tissues

Gene Code	Protein gene encodes for
Gpd1	Glycerol-3-phosphate dehydrogenase 1
Gpd2	Glycerol-3-phosphate dehydrogenase 2
Mdh1	Malate dehydrogenase 1
Mdh2	Malate dehydrogenase 2
Me1	Malic enzyme 1
Me2	Malic enzyme 2

Me3	Malic enzyme 3
Slc25a1	Citrate carrier
Slc25a3	Phosphate carrier
Slc25a11	α-ketoglutarate-malate exchanger
Slc25a12	Glutamate-aspartate exchanger 1
Slc25a13	Glutamate-aspartate exchanger 2
Slc25a22	Glutamate carrier

RNA is not directly sequenced due the macromolecule's instability. The RNA is first isolated from the starting material, such as tissue, by homogenizing the sample and isolating the RNA. This can be done via various approaches such as phase-separating solutions (these methods depend on the polarity of the RNA) or more specific methods that make use of magnetic beads (MagMAX-96 Total RNA Isolation Kit) where RNA binds to RNA-specific magnetic beads (Fassbinder-Orth, 2014). The RNA needs to be quantified to determine if adequate amounts are available. The purity of the RNA also needs to be determined. The RNA is then converted to complementary circular DNA (cDNA) by making use of an enzyme called reverse transcriptase. It catalyses the reaction of converting RNA to DNA. The resulting double-stranded DNA (dsDNA) can then be used for sequencing. NGS primarily has 3 major check points, which is template preparation, sequencing and imaging. When making use of cDNA, a DNA library first has to be constructed. This method has a reduced error rate and increased efficiency (Li et al., 2015) (Lou et al., 2013). These copies are then sequenced via high-throughput sequencing technology (Li et al., 2015).

One of the more advanced technologies for NGS is the semiconductor-based systems, such as the Ion GeneStudio S5 system. The instrument makes use of an electronic reading board to interface with the chip (Rothberg et al., 2011). A microprocessor is present for signal processing as well as a fluidics system that correlates the reagent flow over the chip containing the samples. During sequencing, the four nucleotides are sequentially washed over the chip containing the template DNA. When one of the nucleotides is complementary to the template strand base, the base is incorporated into the newly forming strand (Rothberg et al., 2011). The hydrolysis of the incorporated nucleotide triphosphate causes the liberation of a single proton that causes a small pH

change in the surrounding buffer. The sensor detects the pH change after each sequential read and the detected signal from the change in pH is correlated back to the base that was incorporated. After each flow of the different nucleotides, the remaining unincorporated nucleotides are washed away to eliminate errors in the sequencing (Rothberg et al., 2011).

3.4.1 RNA Quantification and Quality Check

With regard to gene expression analysis, the quality and quantity of RNA is crucial for reliable results. Due to the instability of RNA, degradation can occur quickly due to various reasons, which include improper sample handling, extended periods in storage, inadequate storage conditions and movement between laboratories. Environmental factors include UV exposure, heat and the presence of RNases. It would thus seem that RNA samples need to undergo extensive testing to assess the quality and quantity of the RNA, especially for downstream applications such a gene expression analysis (Vermeulen et al., 2011). RNA was quantified using two basic biochemical principles, namely, spectrophotometry and fluorescence. RNA quantification on the NanoDrop One spectrophotometer requires minimal sample input and no sample preparation. The NanoDrop One determines the ratios between the absorbance values obtained from three wavelengths. Absorbance at 280nm and 230nm measures the protein background absorption and 260nm gives the absorbance of light by nucleic acids (Both RNA and DNA) (Annexure B). A ratio of 1.8-2.1 for the A260/A280 is usually an indication of pure RNA. The ratio of >2.0 for the A260/A230 is indicative of low contaminants being present (Kuang et al., 2018). RNA quantification via fluorescence is considered the more accurate approach due to the fluorescent dye binding specifically to RNA (Shokere et al., 2009).

To assess the quality of the RNA, a bleach-gel electrophoresis approach is a newer approach when compared to denaturing RNA gel electrophoresis. Denaturing gels require extensive preparation steps, toxic chemicals, multiple washing steps and the use of special running buffers. To avoid tedious experimental procedures, a simpler approach was considered. Bleach gels consist of the well-known 1% agarose gel, containing a small amount of 6% sodium hypochlorite. The main purpose of the bleach in the gel is to denature the RNase enzymes and damage said enzymes via oxidation. There is also possible denaturing of secondary RNA structures (Aranda et al., 2012).

3.4.2 Library Preparation

The synthesized cDNA was ligated with a barcode-, primer- and adapter sequences. Library preparation is the first important step with regard to NGS. Before the library preparation can start, the cDNA needs to be diluted to 0.883 ng/µl in a total volume of 15 µl. The library preparation was done with the Ion AmpliSeq™ Transcriptome Mouse Gene Expression Kit (ThermoFisher Scientific, Catalogue number A36554) on the Ion Chef™ Instrument (ThermoFisher Scientific, Catalogue number 4484177). This core expression panel is a single multiplexed panel targeting ~20 000 genes of the mouse genome. During library preparation, the cDNA is amplified using specific primer pairs. These primer pairs are designed to target ~150 bp fragments of specific genes. After the amplification is done, primers are digested to an extent and then ligated with a primer-, barcode- and adapter sequences. The adapter sequence is used during the sequencing step and is ligated on one side of the cDNA fragment. The Ion AmpliSeq™ Transcriptome Mouse Gene Expression Kit contains 32 unique 10 bp barcode sequences. These barcodes are to identify which cDNA fragment corresponds to which sample. The adapter sequences are short DNA sequences that anneal the cDNA fragments to the Ion Sphere™ Particle (ISP). These are both ligated to the cDNA on opposite side of the primer sequence.

Figure 3-1: Schematic representation of cDNA after ligation. Adapter, Barcode and Primer

3.4.3 Template Preparation

Template preparation follows library preparation. This entailed the prepared libraries to be ligated to Ion Sphere™ Particles (ISP). This was followed with bead enrichment and DNA preparation on the ISP. The ISPs were then loaded onto the sequencing chips. After the chips were loaded, they were ready to be sequenced. After the ligation step, an emulsion PCR was performed. This entailed oil droplets that contain the needed material (one ISP, one ligated cDNA strand, primers and PCR mix) to amplify one strand of cDNA. The end goal of this step was to ligate all the adapters on the ISP with the copies of one the original cDNA strand. This process was very random, thus not all the oil droplets in

the reaction containes all the material needed for the emulsion PCR to be executed. The emulsion PCR began with the denaturing of the cDNA strand into two single strands of DNA.

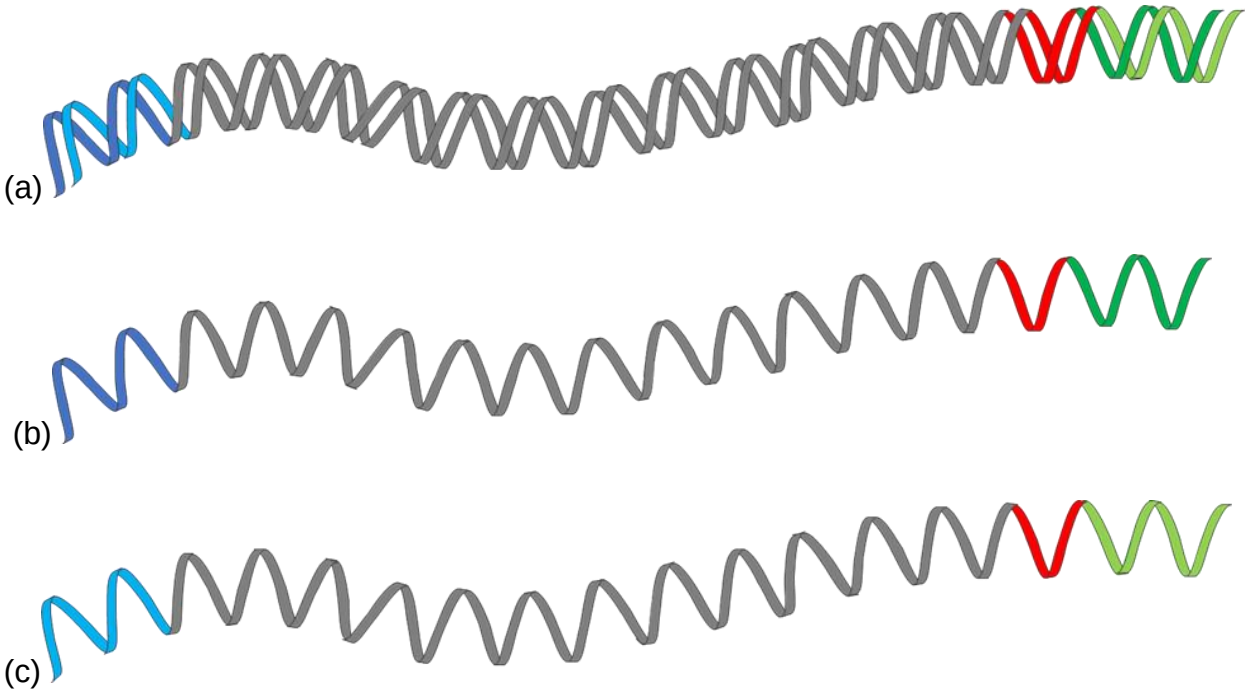

Figure 3-2: Double stranded cDNA is denatured into two single strands of cDNA. (a) Double stranded DNA, (b) Reverse Strand, (c) Forward Stand

After denaturing, the adapter of the reverse strand was ligated to one of the adapters on the ISP. The ISP adapters are complementary to the adapter sequences ligated to the cDNA. The adapter on the ISP functions as a primer for the elongation step that follows. The forward strand was not ligated to the ISP as the adapter's sequence of the forward strand was not complementary to the sequence of the adapter on the bead. The polymerase amplified the forward strand of the reverse strand in the direction of the adapter side to the primer side. Elongation of the forward strand was still possible though. The primers in the oil droplet were bound to the complementary primer sequence of the forward strand, making it possible for the polymerase to amplify the complementary reverse strand of the forward strand in the direction of the primer side to the adapter side.

After extension, both the original reverse strand (on the bead) and the original forward strand (not on the bead) were double stranded again. This was followed by another denaturing step to convert the dsDNA to ssDNA again. The original reverse strand detached from the ISP, leaving the complementary amplified forward strand annealed to

the ISP via the phosphate backbone of DNA. A primer was added to this forward strand on the primer side. The original reverse strand annealed to another adapter on the ISP, to continue the process further. The original forward strand was also denatured. The complementary reverse strand was then free to also anneal to an adapter site on the ISP. Another primer was bounds to the original forward strand on the primer side and amplification continued again. The entire process continued for 13 cycles (as recommended by the manufacturer's manual) until the entire ISP's adapter sites were occupied with double stranded DNA sequences. ISPs were enriched and loaded onto the sequencing chips.

3.4.4 Next Generation Sequencing Data Processing

After the sequencing was completed, the generated data of each run was viewed on the Ion Torrent Suite™ Software (pre-installed on Torrent Server). Data analysis is divided into primary and secondary analysis. Primary analysis is mainly the detection and then analysis of signals generated during the sequencing run. During the sequencing run, bases were incorporated, causing a pH change in the well micro-environment. This generated a signal that was correlated to the sequential flow of the nucleotides during the sequencing run. The server received these signals as raw voltage data and generated a DAT file. During each of the sequential nucleotide flow, an acquisition file was created that contained the raw signal measurement of each well on the chip which was converted to incorporation measures for the nucleotides. These generated WELLS files. Last step for primary data analysis was base calling. This was done via a base calling module. This entailed determining the most likely base sequence via complex mathematical models and algorithms (Pereira et al., 2020).

Next is quality control which entailed filtering the reads and trimming primer and adapter sequences. During the Sequencing run, errors occured and these errors in base calling were given a quality score that indicated the probability of the base call being incorrect (Phred score). Trimming entailed removing the bases at the ends of reads. This raised the read quality but also decreased the read length. Demultiplexing sorted the reads according to the barcode adapters followed by removing the remaining library adapter sequences, as adapter sequences can interfere with the assembly and mapping steps. Each sample was assigned and ligated with a barcode sequence during library preparation (Pereira et al., 2020).

Secondary analysis was simply aligning the reads, either against a reference genome or without a reference genome. This analysis created binary alignment/map (BAM) files and sequence alignment/map (SAM_2) files. These files contained all the read sequences, base quality scores, alignment locations, differences between the reference genome and sequenced genome and mapping quality scores (Pereira et al., 2020). The *.chp files were generated via various plug-ins from the BAM files and contained the expression level data as required. The *.chp files was processed further in the Transcriptome Analysis Console (TAC) from ThermoFisher Scientific. Data was exported from TAC in *.csv file format for further processing in Microsoft Excel.

Before any univariate statistics was performed, normality of the data was determined using the Shapiro-Wilk test. This was done to determine the suitable statistical tests and pre-treatment methods. Variables (genes) that have a non-parametric distribution required non-parametric statistical testing (or appropriate data pre-treatment). This required non-parametric variables and parametric variables to use two different t-tests. This was avoided by transforming that data, so all variables had a more parametric distribution and was achieved via logarithmic transformation and scaling of the data. Univariate statistical analysis aimed to point out if there are marked differences between the two groups (hypothesis testing) and if so, how big of a difference was present (magnitude difference). Hypothesis testing was done via a t-test. This calculation was done in Microsoft Excel. This generated a p-value for every variable, which indicated the probability of an observed difference. A p-value smaller than 0,05 was indicative of statistical significance. It should be noted that the p-values were not false discovery rate (FDR) corrected, due to the targeted nature of this analysis (small set of variables tested). Specific genes were selected for this study, which lead to a minimal contribution and adjustment of the FDR (Frane. 2015). When considering the null-hypothesis of this study, one would assume that if the null-hypothesis is true, all observations made would be completely by chance and not due the complex I dysfunction. Although, previous (Terburgh et al., 2021), (Miller et al, 2021) studies on the specific mouse model used for this study indicated very specific differences and thus rejected the null-hypothesis.

Effect size was also determined in Microsoft Excel and generated a d-value. Effect size takes into consideration the variance of the data and was thus considered rather than fold change. The determined d-value indicated that if a significant difference was present

between the two groups, how big the difference was between these two groups. Variables with a p-value of less than 0,05 and a d-value larger or equal to 0.8 (Lakens. 2013) were considered as important and greatly perturbed in the experimental group. Further analysis was done via the MetaboAnalyst 5.0 platform to identify outliers in the samples and to determine in which direction the notable changes occur (Pang et al., 2021).

3.5 Metabolic Analysis

The previously mentioned mitochondrial shuttles transport organic acids and amino acids over the IMM during their functional cycles. These metabolites are glycerol-3-phosphate and dihydroxyacetone phosphate from the glycerol-3-phosphate shuttle, α-ketoglutarate, aspartate and glutamate from the malate-aspartate shuttle and citrate, pyruvate from the citrate-pyruvate shuttle. Malate and oxaloacetate are both participants in the malate-aspartate and citrate-pyruvate shuttles. Complex I deficiency affects tissues with high energy demands the most, and it is possible that the shuttle systems involved in counter measures against the clinical presentation of the disease will also be affected in these tissues (Gnoni et al., 2009) (Palmieri & Pierri, 2010) (Runswick et al., 1990) (Shen et al., 2006).

Changes in the metabolic activity of the knockout mice was determined using metabolic analysis. To determine the concentration of organic acids and amino acids in various tissues, analysis can be done by making use of, for example, liquid chromatography coupled with tandem mass spectrometry. This combination makes use of the physical separating abilities of liquid chromatography and the identification abilities of mass spectrometry (Kumar et al., 2018). This entailed the extraction of the metabolites from the selected tissues. To extract metabolites, the single phase- and two-phase in-house Bligh-Dyer methods were used, depending on the tissue type. This method involved homogenising the tissue in methanol, water and chloroform with ratios depending on the tissue weight and whether a single-phase extraction or two-phase extraction is performed. Single-phase extraction makes use of a 3:1:1 methanol:water:chloroform ratio, while with a two-phase, the ratios are adjusted so that an organic phase and an inorganic phase is formed. The two-phase extraction is suited for tissue types containing high levels of lipids, such as brain tissue. Lipids can cause difficulties and variance in downstream applications, such as LC-MS analysis, so the two-phase extraction method is used to minimize the lipid content of the sample without causing variance to the remaining

metabolite content of the sample. The use of more than one analytical platform enables the option to integrate the measures of the same metabolites and also identify possible variance between the platforms (De Livera et al. 2013). This is then followed by derivatization.

Ionization of the molecules was needed for down-stream detection via the triple quadrupole analyser. Ionization causes the loss of an electron from the molecule fragments, resulting in fragments with a positive charge. With the separating column having a positive stationary phase, retention times was determined by the charge of the ion-fragments. Cation-fragments had a short retention time, while anion-fragments had a long retention time. When the ion-fragments left the column, they moved through the mass analyser. The mass analyser had a magnetic field, that deflected the ion-fragments according to their mass-to-charge (m/z) ratio. By adjusting the magnetic field, the detector identified the ion-fragments (Wal et al., 2010). When comparing the analysis between healthy and non-healthy tissue samples and types, differences between the concentrations of these organic acids and amino acids arose. In the subject of mitochondrial disease and mitochondrial shuttle systems, this could be an indication of adaptive responses in the shuttle systems to accommodate the clinical symptoms of a complex I deficiency.

3.5.1 GC-TOF-MS

Gas chromatography (GC) is the volatile separation of analytes on a stationary phase using a mobile gas phase. The use of GC is limited to an extent to compounds that are both volatile and thermally stable. Compounds with high volatility usually elute first as the volatility of the compounds are inversely proportional to the partition coefficient. The volatilization of the compounds is facilitated by the temperature of the column and/or stationary phase; thus, the column temperature can reach up to 300°C. The flow rate of the mobile phase or gas needs to be at optimum rate to ensure maximum separation on the stationary phase in the column. When coupled with time of flight (TOF) mass spectrometry (MS), GC becomes a useful and powerful analytical technique to identify compounds (Wilson & Walker, 2010:470-472).

TOF-MS uses the flight time of molecules in a field-free tube to identify the molecules. Compounds are ionized to have a charge and are then accelerated as to have a constant

kinetic energy. They are then injected into the mass analyser by means of pulsed electric field gradiented orthodoxically to the ion beam to enhance the mass resolution of the of the instrument. Mass resolution is further enhanced using an ion mirror, which consists of a series of ring electrodes, each with an increasing voltage which results in a retarding field. Ions with higher energy penetrate deeper into the field, extending their reflection time. Thus, ions with the same m/z value will hit the detector at the same time, even if the ions have different initial energies. The separated ions' flight times inside the field free region are proportional to the square root of the respective m/z values (Cajka & Hajšlová, 2007).

3.5.2 LC-QQQ

Liquid chromatography (LC) is the separation of compounds on a stationary phase using a liquid mobile phase. Separation is achieved via the compounds' interaction with the stationary phase of the column. The stationary phase is usually of a hydrophobic or non-polar nature while the mobile phase is hydrophilic or polar. Compounds that are hydrophobic will have a higher retention due to their interaction with the hydrophobic stationary phase, while hydrophilic compounds will be easier to elute and thus have a lower retention time. Thus, compounds will be separated based on its polarity preference to either the mobile- or stationary phase (Wal et al. 2010). MS consists of an ionization source, a mass analyser, and a detector. The ionization source causes the displacement of an electron on the molecule, resulting in the molecule having a charge. Electron spray ionization (ESI) is usually the choice of ionization source. ESI entails the sample entering a needle with a high voltage charge. The needle transforms the sample into a fine mist of droplets with an electrical charge on the surface. The solvent then starts to evaporate, causing the electrical charge density to increase at the surface of the droplet. The droplets divide into smaller droplets due to the electrostatic repulsion being larger than the surface tension, resulting much smaller droplets. From these smaller droplets, the sample ions are formed and enters the mass analyser (Wal et al. 2010). The formed ions are the focused into a beam of ions that are accelerated through the magnetic field of the quadrupole mass analysers. The magnetic fields then deflect the ions in a circular path with a radius proportional to the m/z ratio of the ions. The ions are then focused to the detector via the adjustment of the magnetic field and recorded by the detector (Wal et al. 2010).

3.5.3 Internal Standards

Internal standards are compounds of similar molecular structure to the molecules of interest being analysed. An important property of internal standards is that they must behave and respond similarly to the compounds of interest. They also provide a way to control time related changes in elution of analytes and the quantification of an analyte's abundance. A known amount and concentration are added to each sample and then analysed along with the other metabolites present in the sample (Wilson & Walker, 2021:35).

3.5.4 Derivatization

Derivatization is an important step in the preparation of the samples for any mass spectrometry analysis. Underivatized metabolites tend to give poor peak shape and -separation. During the derivatization step with methoxamine (MOX), carbonyl groups (C=O) in molecules are replaced by an oxime derivative ($C=NOCH_3$) (Figure 3-3). Derivatization with MOX can create a basic nitrogen site(s) on the molecules of interest at every =O site present on the molecule, which increases the ionization efficiency in positive ESI techniques (Di Donna et al., 2013).

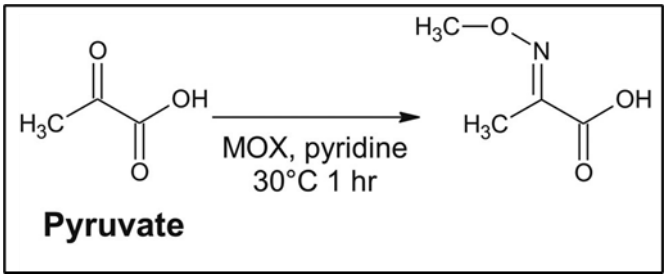

Figure 3-3: MOX reaction - Illustration of the carbonyl group in pyruvate being replaced to form an oxime derivative during the derivatization reaction with methoxamine dissolved in pyridine.

During the derivatization with N,O-Bis(trimethylsilyl)trifluoroacetamide (BSTFA) containing 1% trimethylsilyl (TMS), all the active hydrogens on the hydroxyl- (-OH), thiol/sulfhydryl- (-SH) and -NH groups undergo silylation (Figure 3-4). TMS is a strong silyl donor and will thus react with all the active hydrogens on the metabolites, creating trimethylsilyl derivatives of the molecules (Zhang,& Zuo, 2005).

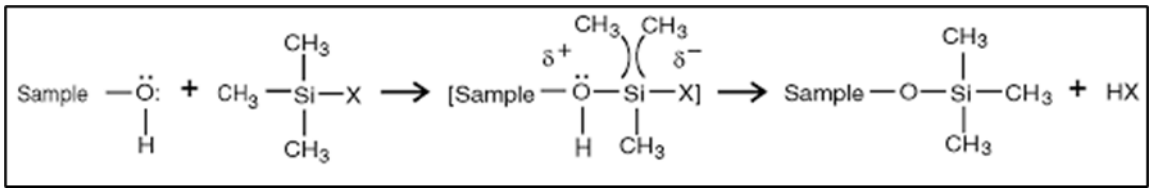

Figure 3-4: General silylation reactions of the active hydrogen on a hydroxyl group. Reaction will occur on all active hydrogens of the -OH, -SH, and -NH groups present on the molecule.

During the derivatization with butanolic-HCl, an esterification reaction takes place, where the hydroxyl groups (-OH) are replaced by an alkyl group (-O-) (Knapp, 1979). The butanol was the substitute for the hydroxyl group as is shown in Figure 3-5.

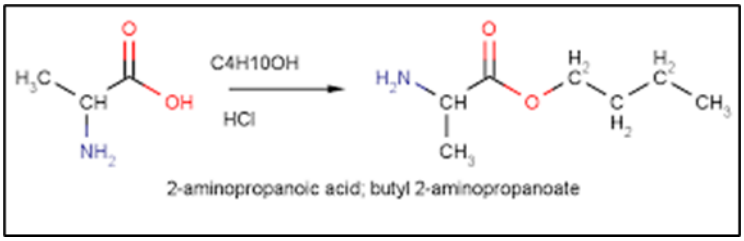

Figure 3-5: Esterification reaction of propionic acid during the derivatization with butanolic-HCl. Hydroxyl groups of the molecule are replaced with an alkyl group.

3.5.5 Quality Control Samples

Quality control (QC) samples needs to represent both the qualitative and quantitative comparison of all the samples assigned to a sample-batch. It should also be noted that because the QC samples are representative of all the samples in the sample-batch and the injection volume of all the samples are equal, all the data from the QC samples, in theory, should to be identical (Dunn et al. 2012). The QC samples were treated and prepared using the same procedures and methods as the normal samples during further preparation steps, as to avoid variance from these samples (Broadhurst et al. 2018).

3.5.6 Metabolomics Data Processing

Large batches of samples can generate large and valuable data sets during metabolomic analysis. These data sets are best interpreted when integrated and comprehended with other ‘omics’ data sets (Cambiaghi et al. 2017). Metabolomics data usually follows a

general transformation process to transform the data into meaningful results. These steps are summarized in Figure 3-6.

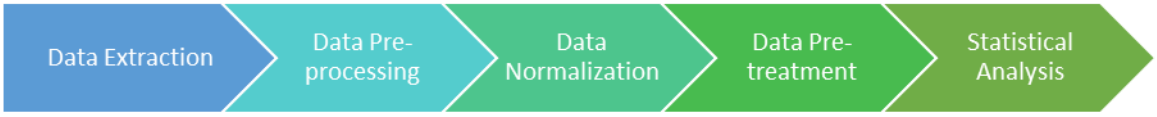

Figure 3-6: Visual representation of the flow of metabolomics data processing

Data extraction was the first step in the process of metabolomics data processing. The raw signals generated by the combined separation and detection technique were pre-processed by ad hoc software tools to facilitate the identification of the detected metabolites. This also involved noise reduction, retention time correction, peak detection and the integration and alignment of chromatograms (Cambiaghi et al. 2017). These software packages were provided along with the chosen machinery.

Data pre-processing entailed checking the integrity of the data and zero-filtering. Specific data matrices are required in specific formats by certain statistical platforms for further data analysis (Cambiaghi et al. 2017). Zero filtering was also preformed where features (variables/metabolites) of the data matrix were removed if the feature was not present in all the samples of the experimental groups participating in the analysis, i.e., the variable did not contain any biological or statistical value (Venter et al. 2015). Missing values, usually present when a compound is not present in a specific sample or the abundance of the compound is below the detection limit of the instrument, were also replaced by 20% of the smallest value recorded for that variable (De Livera et al. 2013). Missing value replacement is an important step for data pre-processing. Missing data reduces the statistical power, thus the testing done might reject the null hypothesis when it is false. It can also cause bias in the estimation of parameters, reduce the representativeness of the sample and can complicate analysis (Kang, 2013). Outliers in the data was also identified and removed. Outliers usually differ from the rest of the data distribution and can be identified by using visual tools such as heatmaps. Data pre-processing was performed automatically by MetaboAnalyst before any univariate analysis was performed (De Livera et al. 2013).

Data normalization was also performed to reduce systemic bias or technical variation and to avoid the misidentification of significant changes between groups (Cambiaghi et al. 2017). The main focus of the metabolomics data was to identify the biological variation of

interest and when normalizing the data set, one eliminates unwanted variation. There were various sources of unwanted variance, which included human error, intra-instrument and inter-instrument variation and different analytical platforms. Various normalization methods can be applied to metabolomics data to reduce/eliminate unwanted variance. These include the use of internal- and/or external calibrators, the addition of QC samples to the sample batches or the use of stable isotopes as an internal- and/or external calibrator (De Livera et al. 2013). Other normalization approaches calculate the concentrations of the metabolites in relation to the area of the internal standard peak or a correction of the variable or compound to the sum of the all the signals of a component that are present in the samples (MSTUS normalization) (Venter, 2017).

Before statistical analysis was performed, data pre-treatment was first performed. This required the correct and appropriate data pre-treatment method as this can affect the metabolites which are identified as significant. The main purpose of data pre-treatment was to convert the data using a logarithmic scale as to focus on the relevant biological information and to minimalize the influence of background noise (Van Den Berg et al. 2006). There were three different types of data pre-treatment processes namely centring, scaling and transformation. Centring involved the conversion of the data to fluctuations around zero instead of the mean metabolite concentration. Scaling divided each variable by the chosen scaling factor. This converted data into differences in concentration relative to the scaling factor. Transformation of data are nonlinear conversions of the data such as logarithmic transformation of power transformation. This reduces the large numbers in the data set relatively more than small numbers and reduces the differences between the large and small numbers, almost to a pseudo scaling effect (Van Den Berg et al. 2006).

After all the data processing steps was completed, ‘clean’ data is the result in the form of normalized peak area that are a true reflection of the intracellular metabolite concentrations (Van Den Berg et al. 2006). Statistical Analysis was performed on the ‘clean’ data set. There are various aims of a statistical analysis on metabolomics data sets (De Livera et al. 2013). For this study, the aim of the statistical analysis of the metabolomics data was to determine if there are any differences in the abundance of the chosen metabolites involved in the mitochondrial shuttles between the mice groups. The most suitable approach for this study entailed a targeted analysis of the chosen metabolites. To conclude on what the data represents on a biological variance level,

univariate and/or multivariate statistical analysis needed to be performed on the data. The univariate analysis approach is usually implemented on targeted metabolomic analysis. This entails one variable, such as metabolite abundance, being used in for statistical analysis. Univariate tests compare the means or medians between two groups, such as knockout mice and wild type mice. Depending on the normality distribution of the data, either parametric or non-parametric tests needed to be executed. Or, depending whether the data is normalized (normal distribution), parametric tests can be performed on the entire data set (Lamichhane et al. 2018). Parametric tests included a t-test, to determine statistically significant differences in metabolite abundance between the groups of interest. This calculated a p-value for every variable (metabolite) which indicated if a difference is present between the groups of interest. A p-value of less than 0,05 was indicative of significant difference between groups. To indicate the magnitude of the difference between the two groups, if a difference is present, effect size is calculated. This generated a d-value which indicated the magnitude of the experimental effect. A d-value equal to or bigger that 0,8 was considered significant (Venter, 2017).

CHAPTER 4 – METHODOLOGY

4.1 Mice Breeding and Animal Housing

This study entailed the investigation of adaptive responses of mitochondrial shuttles and metabolic reprogramming of transporters in complex I deficient mice. Before the commencement of the study, ethical approval was needed. A category 0 application for ethical approval was sent to the North-West University Animal Care, Health and Safety Research Ethics Committee. Ethical approval was received for the execution of this study (NWU-000569-19-S5). To execute this study, we made use of a complex I knock out mouse model. Mice with the Ndufs4 Knockout genotype (Ndufs4-/-), heterozygous mice (Ndufs4-/+, B6.129S4-Ndufs4tm1.1Rpa/J) were obtained from Jackson Laboratories (Bar Harbor, ME, USA).

The mice obtained were part of an extensive breeding program to produce mice with three different genotypes: wildtype mice (WT, Ndufs4+/+), heterozygous mice (HET, Ndufs4-/+) and knockout mice (KO, Ndufs4-/-). Heterozygous mice had to be used for breeding purposes due to the phenotypical nature of the knockout mice. The knockout mice do not reach sexual maturity with live expectancy of only 45 - 55 days post-natal. They also have a smaller body than normal mice and will lose their hair by post-natal day 21 (P21). The knockout genotype may also become lethargic after P30 and often present with blindness and cataracts. After P35, they may develop severe ataxia and my stop gaining weight, cease grooming and die around P50-55 (https://www.jax.org/strain/027058). This Ndufs4 knockout model has a large comparability to patients with Leigh syndrome and is thus a suitable and useful alternative to investigate complex I deficiencies and the disease associated with it.

All mice were housed at the Vivarium of the PCDDP at the North-West University. The area is a specific pathogen free (SPF) environment, ensuring that external pathogens cannot cause infection. Housing conditions were kept constant to limit unexplainable variations in experimental procedures. Litters were kept together in type II long polysulphone cages containing corn cob chips as bedding. Cages were individually ventilated (IVCs – individually ventilated cages) by high efficiency particulate air (HEPA) filtered air (60 air changes/hour). The diet of the mice consisted of a standard laboratory rodent diet (Rodent Breeder, #12RM1845, Lab Chef, Nutrition Hub Pty Ltd, Western

Cape, South-Africa). New mice born from heterozygous breeding pairs were weaned at approximately 3 weeks after birth. They were then assigned a unique identification number using an ear-punch method (Figure 4-1).

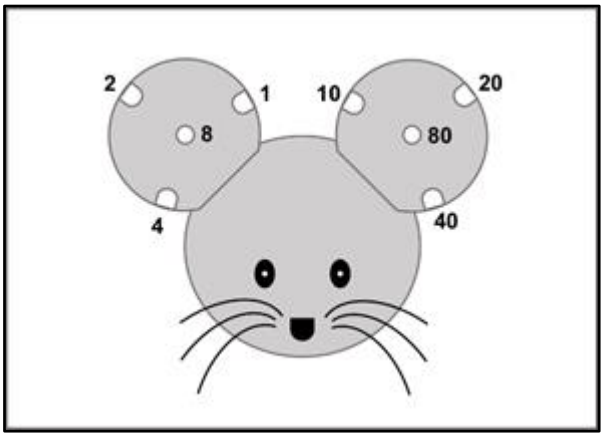

Figure 4-1: Schematics of the ear-punch identification system used to number and identify mice

4.2 Genotyping of Mice

After mice were weaned and identified using the ear-punch method depicted in Figure 4-1, tail snips were collected and kept frozen at -4°C for collection. Tail snips were used to isolate DNA for PCR. DNA was isolated with the ZYMO RESEARCH Quick-DNA Miniprep Plus Kit (Inqaba Biotech, Cat #: D4068) and the solid tissue protocol provided with the kit. The kit makes use of spin columns and a DNA binding matrix with a 25 µg binding capacity (Konstantinidis et al. 2020). After DNA isolation, the DNA was quantified using the NanoDrop spectrophotometer. The NanoDrop gives the concentration in the unit ng/µl, along with the A260/A280 and A260/A230 ratios. These ratios were used to determine the purity and possible contaminants of the DNA. After DNA quantification, the DNA of each isolated tail snip was diluted to 25 ng/µl. After dilution, conventional PCR amplification was performed on each sample. A master mix was prepared for the total amount of samples, using the 2X Phire Tissue Direct PCR master mix, forward and reverse primers specific to introns on either side of exon 2 of the Ndufs4 gene and nuclease-free water. For each diluted DNA sample, 1 µl of sample was added to 9 µl of the prepared master mix in UV-sterilized PCR tubes. The PCR reaction was executed using the ThermoCycler T100 (BioRad) with the conditions of the Phire protocol described in Table 4-2.

Table 4-1: The sequences of the Ndufs4 primers. These primers were purchased from Inqaba Biotech and were used for the genotyping of the mice used in this study. These primers were originally designed by Valsecchi et al. 2012.

Primer	Cat No.	Sequence of the Primer (5' – 3')	Size (bp)	T_m (°C)
Forward (NDUFS4 1060)	S32E6 (Inqaba Biotec)	AGC CTG TTC TCA TAC CTC GG	20	62.45
Reverse (NDUFS4 Rev)	S3424 (Inqaba Biotec)	TTG TGC TTA CAG GTT CAA AGT GA	23	59.2

After PCR amplification of the DNA, the amplicons were separated on a 1% agarose gel containing ethidium bromide, to determine the genotype of each mouse. The agarose was dissolved in 1x Bionic buffer. A ladder (GeneRuler 100 bp DNA Ladder, ThermoFisher Scientific) and three control samples were also added on the gel. The solidified gel was placed in a 1x Bionic buffer. An electric current was passed through the buffer, first at 40 V to concentrate the amplified DNA in the gel and then at 75 V to separate the amplified DNA. Results for all genotyping carried out for this study are shown is annexure A.

Table 4-2: Phire protocol used for PCR reaction during genotyping of mice

Step	Temp (°C)	Time (min) / Rep
1. Initial Denaturing	98	05:00
2. Denaturing	98	00:05
3. Primer Annealing	57.3	00:05
4. Extension	72	00:20
5. Repeat steps 2 – 4	-	X34 (step 2 – 4)
6.	72	01:00
7. Infinite Hold	4	∞

4.3 Sample Collection

Mice were allowed to reach the age of 45 days post-natal (PN45) but were not allowed to age beyond 50 days post-natal. All mice for this study were euthanized between PN45 and PN50 via cervical dislocation according to the guidelines set in place by the vivarium of the PCDDP. After euthanasia, the animals were dissected, and the organs of interest were harvested (brain, liver and heart). Organs were placed in a microcentrifuge tube (Eppendorf) and snap frozen in liquid nitrogen. Samples were also kept in liquid nitrogen and moved from the vivarium to the ultra-freezer. A second tail snip was collected during sample collection and used for a confirmatory genotyping analysis. Samples were kept at -80°C until further analysis was done. In total, tissue samples from 30 mice were collected specifically for this study. Of the 30 mice, ten were wildtype mice, seven were heterozygous and thirteen were knockout mice. The number of mice attributed to each sample group is given in Table 4-3. Aliquots of the same tissue samples were used for both transcriptomic and metabolomic analysis.

Table 4-3: Mice allocation per group for each analysis done on every tissue type.

Transcriptomic Analysis		
	Control Group (WT)	Experimental Group (KO)
Liver	8	8
Heart	4	4
Brain	4	4
Metabolomic Analysis (GC-TOF-MS)		
	Control Group (WT/HT)	Experimental Group (KO)
Liver	18	12
Heart	17	12
Brain	18	11
Metabolomics Analysis (LC-QQQ)		
	Control Group (WT/HT)	Experimental Group (KO)
Liver	18	11
Heart	16	12
Brain	18	11

4.4 Transcriptomic Analysis

Transcriptomic analysis entails the qualitative and quantitative investigation of the entire transcriptome in a cell or tissue type under specific conditions. This entails RNA isolation,

determination of RNA quality and quantity, the conversion of RNA to complementary DNA and then sequencing the cDNA.

4.4.1 RNA Isolation

RNA isolation was done from the liver, heart, and brain tissues by making use of the MagMAX™-96 Total RNA Isolation Kit (ThermoFisher Scientific, Catalogue number: AM1830). The RNA aliquots were stored in 5 different sets of pre-marked tubes. One set of tubes was to determine the RNA concentration using the NanoDrop One spectrophotometer. A second set of tubes was used to store the RNA for the determination of the RNA concentration and genomic DNA contamination. A third set of tubes was used to store the RNA for a gel electrophoresis to determine the RNA integrity of each sample. The fourth set of tubes stored the RNA for the transcriptomic analysis of the samples and the last set of tubes was used to store the remainder of the RNA. The last set was considered a backup for when re-evaluation was needed for any of the above-mentioned analysis.

4.4.2 Determining RNA Integrity, Purity and Concentration

The isolated RNA was quantified twice using two different methods. The first method made use of the NanoDrop One spectrophotometer and a 1% agarose-bleach gel. The Nanodrop One requires little sample input and does not require any sample preparation. The data from the Nanodrop One was used for sample loading of a 1% agarose bleach gel. Between 200ng and 500ng of RNA per sample was loaded into the wells of the gel. After the RNA was separated on the gel, two distinct bands (28S and 18S) were visible on the gel after imaging on the ChemiDoc™ MP System. The top band (28S) had an intensity of 1.5X to 2X of that of the bottom band (18S), which indicated that the RNA was still intact. Presence of genomic DNA was confirmed by a distinct band at the top of the gel, in the well. RNA degradation can be detected if a smear is visible below the 18S band.

The RNA concentration and the concentration of gDNA contamination were quantified using the Qubit 2.0 Fluorometer (ThermoFisher Scientific, Catalogue number Q32866) along with the Quibit® RNA HS Assay Kit (ThermoFisher Scientific, Catalogue number Q32852) and the Qubit® dsDNA HS Assay Kit (ThermoFisher Scientific, Catalogue number Q32851), to verify the qualitative gel results were. This method makes

use of fluorescence to determine the concentration of nucleic acids or proteins. The fluorescent dye binds specifically to the molecule of interest. The fluorescence is then measured by the Qubit 2.0 Fluorometer. The concentration was determined by the Qubit 2.0 Fluorometer with the help of reference standards measured before the samples.

4.4.3 RNA Conversion to Complementary DNA (cDNA)

Parameters were set in place for the quality and quantity of the isolated RNA. The samples were chosen for conversion to cDNA if they met the criteria. The criteria included a 28S:18S ratio of 1.5 to 2.0 from the agarose bleach gel as well as minimum degradation of the RNA (no smear under the 18S band). The samples that indicated gDNA contamination on the agarose-bleach gel, were also analysed using probes specific to DNA and then quantified using the Qubit 2.0 fluorometer. Genomic DNA contamination of less than 10% than the total RNA concentration was still acceptable. Some of the samples was reisolated if the RNA was not of sufficient quality. The concentration of the RNA was also considered before the conversion to cDNA.

For the conversion of RNA to cDNA, SuperScript™ IV VILO™ Master Mix (ThermoFisher Scientific, Catalogue number 11756050) was used. The kit requires between 1 pg and 2.5 µg of RNA. The RNA was first diluted to 3.33 ng/µl in a MicroAmp Optical 8-tube Strip (ThermoFisher Scientific, Catalogue number 4323032). The total reaction volume used for the conversion was 15 µl. The T100 Thermal Cycler (BioRad, Catalogue number 1861096) was used to execute the protocol of the SuperScript™ IV VILO™ Master Mix. The protocol is listed in Table 4-4. The concentration of the synthesized cDNA is supposed to be equal to the concentration of the input RNA, thus it was assumed that the concentration of the synthesized cDNA was 3.33 ng/µl.

Table 4-4: Protocol of SuperScript™ IV VILO Master Mix to convert RNA into complementary DNA (cDNA)

Step and Action	Temperature and Duration
1. Anneal the Primers	25 °C for 10 minutes
2. Reverse Transcribe RNA	65 °C for 10 minutes
3. Inactivate enzyme	85 °C for 5 minutes

4.4.4 Library Preparation

The prepared cDNA was diluted to 0.833 ng/µl in a total volume of 15 µl. The synthesized cDNA was fragmented, ligated with a barcode-, primer- and adapter sequences. This was followed by removing the caps of the four tubes on the Ion AmpliSeq™ Chef Reagents DL8 cartridge. The primer panels needed to be added to the cartridge. Primer panels were first vortexed to mix the contents and then centrifuged according to the provided guidelines. Tubes A and B of the cartridge was removed and replaced with the Ion AmpliSeq™ Transcriptome Mouse Gene Expression Core Panel (ThermoFisher Scientific, Catalogue number A36554). Next, the synthesized and diluted cDNA was added to the Ion Code™ 96 Well PCR Plate. cDNA was added to wells A1 to H1 on the plate. Wells A6 to H6 contained the dried down Ion Code™ barcodes. The wells that contained the cDNA was inspected for the presence of bubbles. Bubbles were removed by very gently pipetting the well of the PCR plate that contained any bubbles. Next, all the reagents and consumables were loaded into the Ion Chef™ Instrument (ThermoFisher Scientific, Catalogue number 4484177). The door was opened and latched. Loading started with the Ion AmpliSeq™ Chef Solutions DL8 Cartridge, which was loaded into the solutions station. This was followed by loading the Ion AmpliSeq™ Chef Reagents DL8 Cartridge into the reagents station. The empty Tip Cartridge from the previous run was moved to the used pipette station and a new Ion AmpliSeq™ Tip Cartridge L8 was loaded into the new pipette station on the left side of the deck. Next, the Ion Code™ 96 Well PCR Plate containing the cDNA was loaded and a new PCR Frame Seal was slid into the automated heated cover. This was followed by the loading of the Enrichment Cartridge into the Enrichment station and then carefully closing the door of the Ion Chef™ Instrument. The Ion Chef™ run was started. This entailed a step-by-step process involving a check to ensure all the reagents and consumables were loaded correctly and properly, a deck scan and the selection of the appropriate number of primer pools, target amplification cycles and the anneal/extension time for the run. After the run was complete, all the expended consumables and reagents needed to be removed according to the programmed instructions indicated by the Ion Chef™ Instrument.

4.4.5 Template Preparation and Chip Loading

Template preparation followed library preparation. This is done on the Ion Chef™ Instrument, making use of the Ion 540™ Kit (ThermoFisher Scientific, Catalogue number

A30011) and the Ion 540™ Chip Kit (ThermoFisher Scientific, Catalogue number A27765). Template preparation required the prepared library to be diluted to 70pM in a total volume of 25 µl. First, the consumables needed to be prepared. This entailed the unboxing of the Ion 540™ Chef Reagents cartridge 45 minutes before the run, to allow the cartridge to reach room temperature. All other cartridges and consumables were also removed from their packaging and placed on the bench next to the Ion Chef™ Instrument. Next, the diluted libraries were loaded into the Ion Chef™ Library Samples Tubes (barcoded). Libraries were kept on ice while preparations were done. This was followed by the loading of the consumables and reagents according to the Ion Chef™ Instrument's protocol and order. The Ion 540™ Chips were also loaded into the Chip-loading centrifuge. The centrifuge contained small buckets to house the chips and each chip would receive a Chip adapter. After loading all consumables and reagents into the Ion Chef™ Instrument, a thorough check was done to confirm everything was correctly loaded and placed into the correct positions. The template preparation run was started according to the Ion Chef™ Instrument's step-by-step instructions. This included a deck scan where the Ion Chef™ Instrument scanned all the barcodes of the loaded consumables and reagents. When the library preparation and chip loading was done, the loaded chips could be removed and sequenced immediately.

4.4.6 Sequencing

After the chips were loaded, they were ready to be sequenced on the Ion GeneStudio™ S5 Semiconductor Sequencer (ThermoFisher Scientific, Catalogue number A38194). Chips were unloaded from the adapter/chip/bucket assembly of the Ion Chef™ Instrument. One of the chips were loaded into the sequencer and the other was kept safe in a chip storage container at 4°C while the first chip was sequenced. The stored chip was allowed 20 minutes to reach room temperature before being loaded into the sequencer. This was followed by the removal of the expended solutions and reagents from the Ion GeneStudio™ S5 Semiconductor Sequencer and replaced with new solutions and reagents. The chip from the previous run needed to remain in the Ion GeneStudio™ S5 Semiconductor Sequencer while initialization took place. This old chip was replaced by the new chip after the initialization was completed. After the planned run was confirmed in the Ion GeneStudio™ S5 Semiconductor Sequencer, the sequencing run was started. When prompted, the first chip was replaced by the second chip in storage

to continue the sequencing of both chips. After sequencing of the second chip was completed, a post-run clean-up was performed to avoid contamination on the next sequencing run.

4.4.7 Next Generation Sequencing Data Processing

After the sequencing was completed, the generated data of each run was viewed on the Ion Torrent Suite™ Software (pre-installed on Torrent Server). Signal detection during the run was correlated to base calling which in turn, generated the sequence data of the template strands on the ISP. One of the main features of the Ion Torrent Suite™ software is the automatic filtering of the sequencing data. This includes various features such as removing the adapter, primer and barcode sequences annealed during the library preparation, as well as removing reads of poor quality. Poor quality reads are the result of more than one template present on one ISP. Data from each sequencing run was downloaded from the server in *.chp file format. These files contain the gene-level information and the gene expression values obtained from the sequencing run. Data was processed via the TAC software (provided by ThermoFisher Scientific). The values obtained were normalized to the reads per million to make the samples comparable (also across chips). The obtained data of the genes of interest were exported from TAC as a *.csv file, which was processed further in Microsoft Excel.

Before any univariate statistics was performed, normality of the data was determined using the Shapiro-Wilk test. This was done to determine the suitable statistical tests and pre-treatment methods. Data was transformed using logarithmic transformation (log transformed to base 2) to achieve a more parametric distribution. Hypothesis testing was done via a two-tailed t-test (unequal variance). This calculation was done in Microsoft Excel. This generated a p-value for every variable, which indicated the probability of an observed difference. Effect size was also determined in Microsoft Excel and generated a d-value. Further analysis was done via the MetaboAnalyst 5.0 platform to identify outliers in the samples and to determine in which direction the notable changes occur.

4.5 Metabolomic Analysis

Metabolomic analysis started with the extraction of the metabolites from the selected tissues using the single phase- and two-phase in-house Bligh-Dyer methods. This was followed by drying the extracted metabolites and then derivatizing with a suitable

derivatizing agent(s). Samples of the LC-QQQ were then dried again and resuspended the mobile phase of the LC-QQQ, while samples of the GC-TOF-MS were transferred to inserts. Samples were then analysed on the GC-TOF-MS and LC-QQQ platforms.

4.5.1 Gas Chromatography Time-of-Flight Mass Spectrometer (GC-TOF-MS)

One of the platforms used for metabolic analysis was gas chromatography combined with a time-of-flight mass spectrometer (GC-TOF-MS). The GC-TOF-MS system used for metabolic analysis consisted of a LECO Pegasus HT mass analyser coupled to an Agilent 7890A GC. The fitted column responsible for chromatographic separation was an Agilent DB-1 (20 m × 0.180 mm × 0.18 µm) column. Samples were injected at a 1 µl volume using a split/splitless injector at a 1:10 split ratio. The injection needle was washed throughout analysis with a 50:50 ratio acetone and isopropanol mixture. The front inlet temperature was kept constant at 250 °C. The oven temperature remained at 50 °C for 1.0 min after injection, where after it was increased 5 °C/min to 100 °C. It then increased 10 °C/min to 160 °C, 13 °C/min to 230 °C and 20 °C/min to 300°C where it remained for 2 min. This added up to a total run time of ~30 min per sample. Helium was used as carrier gas at a constant flow of 1.4 ml/min. The ion source temperature was maintained at 200 °C while the transfer line temperature was kept at 225 °C for the entire duration of the run. An acquisition delay of 350 sec was used as a solvent delay. Data was captured with an acquisition rate of 20 spectra (50–950 m/z) per second, with a detector voltage of 50 V over the daily tune voltage and electron energy of −70 V (Venter et al., 2018).

4.5.2 Liquid Chromatography Tandem Mass Spectrometry (LC-QQQ)

The other platform used for metabolic analysis was liquid chromatography combined with a triple quadrupole mass spectrometer (LC-QQQ). The LC-QQQ used for analysis was an Agilent 1200 series LC system, coupled to an Agilent 6410 QQQ mass analyser using ESI. Samples were loaded into the auto-sampler that was kept at 4°C to maintain sample integrity during analysis. The auto sampler injected 2µl sample into the column, while the column temperature remained constant at 30°C. Chromatographic separation was achieved using an Agilent Eclipse plus C18 column (2.1 x 100 mm x 1.8µm) fitted to Thermostatted Column Compartment SL. Mobile phases consisted of (A) HPLC grade water with 0.1% formic acid and (B) acetonitrile with 0.1% formic acid. Reverse phase

conditions were achieved with the gradient settings for the two mobile phases stipulated in Table 4-5.

Table 4-5: Gradient of the Mobile phase B during sample analysis on LC-QQQ

Time interval (min)	Mobile Phase B (%)	Flow Rate (ml/min)
0	40	0.2
1	40	0.2
10	100	0.2
10.2	100	0.3
15	100	0.3
16	40	0.2

4.5.3 Internal Standard Preparation

The internal standards prepared for the metabolomic analysis were 3-phenylbutyric acid (3-PBA), nonadecanoic acid (C19), 2-acetaminophen (2-AAP) and an isotope mixture containing various amino acid isotopes (listed in Table 4-6). All internal standards were weighed off in separate tubes and dissolved in 99% pure, HPLC grade methanol to create stock solutions of each internal standard. For GC-TOF-MS analysis, internal standards were required to have a final concentration of 50ppm while the required internal standard concentration for LC-MS/MS analysis was 10ppm. The stock solutions of the internal standard were used to create the internal standard solution of required concentration by diluting a determined volume of the stock solution with 99% pure, HPLC grade methanol. The internal standard solutions along with the stock solutions were kept at -20°C when not in use and were kept on ice during the addition of the internal standards to the samples. The isotope mixture consisted of various isotopes (listed in Table 4-6) with a final concentration of 1ppm. This mixture was used, along with 2-AAP for the preparation of the samples for LC-MS/MS analysis.

Table 4-6: List of amino acid isotopes contained in the mixture of isotopes

Amino Acid
Arginine
Glycine
Lysine
Citruline

Valine
Methionine
Isoleucine
Phenylalanine
C0 – Free carnitine
C2 – Acetyl carnitine
Glutamic acid

4.5.4 Sample Preparation for Metabolite Extraction

Before metabolite extraction from the samples could take place, the samples needed to be prepared specifically for the extraction method used to simplify the downstream steps. First, the samples of interest were collected from -80°C storage and placed in liquid nitrogen to avoid thawing while sample preparation took place. A 2ml microcentrifuge tube (Eppendrof, Cat# 30120.094) for each sample was marked and weighed beforehand. From each sample, a small piece was cut using a scalpel blade. Cutting was done by making use of a dissection plate on dry ice, also to avoid the sample defrosting while cutting was taking place. The cut piece was placed in its allocated microcentrifuge tube and weighed again. The weight of the microcentrifuge tube was subtracted from the combined weight of the sample and microcentrifuge tube to calculate the weight of the cut piece of sample. The weight of the sample was used to determine the volume of methanol, water and chloroform to be added during the extraction. After weighing, both the remaining sample (unused) and the cut piece of sample was flash frozen again in liquid nitrogen to limit possible defrosting during the weighing process and was kept at -80°C until the extraction step.

4.5.5 Metabolite Extraction from Tissue for GC and LC Analysis

Metabolite extraction started by adding a steel bead to each of the prepared samples. The size of the bead was dependent on the size of the microcentrifuge tube used. Since 2ml microcentrifuge tubes (Eppendorf, Cat# 30120.094) were a 5mm Ø steel bead was added. This was followed by adding methanol, water and internal standards according to the weight of the sample. The weight of the sample was calculated as described during sample preparation. The methanol, water and internal standard is then added according to the determined sample weight and the extraction method used (see Table 4-7). Sample weight is usually measured in mg, meaning that if a sample had a weight of 50 mg, the

volume (in µl) of added solvents would be calculated by multiplying the sample weight with the ratios explained in Table 4-7. It is important to note the solution in which the internal standard (methanol or water) is dissolved. The volumes of the methanol and/or water were adjusted accordingly as to maintain the ratios of each reagent in the extraction protocol used, whether it was the single-phase or the two-phase protocol being used. The samples were then homogenized using the vibration mill at 20 Hz for two minutes if soft tissue was homogenized or 30Hz for three minutes if the tissue was though like muscle tissue. After homogenization, chloroform was added to each sample according to the sample weight. Chloroform was only added after the homogenization step as it causes the tissue to harden and can cause difficulty and variance if it is present in the sample during the homogenization step. The samples were the vortexed for 30 seconds to ensure proper homogenization and then left to incubate on ice for 10 minutes. The incubation step is important for optimal pellet formation during the centrifugation step. The samples were then centrifuged at 2000xg for five minutes at a temperature of 5°C. The microcentrifuge tubes were then carefully removed from the centrifuge as to not disturb the pellet that had formed. The supernatant was transferred to pre-marked glass vials using pasteur glass pipettes and then completely dried under a gentle stream of inert nitrogen gas at 37°C and stored afterward at -80°C until mass spectrometry analysis.

Table 4-7: Sample weight to reagent volume to be added to each sample during metabolite extraction.

	Methanol	Water	Internal Standard	Chloroform	Water
Single-phase	mg X 12	mg X 4	mg X 1	mg X 4	-
Two-phase	mg X 8	mg X 2,5	mg X 1	mg X 8	mg X 4
Two-phase example (50 mg)	50 mg X 8 = 400 µl	50 mg X 2,5 = 125 µl	50 mg X 1 = 50 µl	50 mg X 8 = 400 µl	50 mg X 4 = 200 µl

4.5.6 Sample Preparation for GC-TOF-MS Analysis

Dried extracts were collected from storage, they were defrosted and dried again under a gentle stream of nitrogen gas at 37°C. The drying step was repeated to ensure no moisture remains present in the sample after storage. Moisture, specifically water, can cause hinderance or completely inhibit the derivatization steps that follow (Knapp, 1979)

(Jones & Stenerson, 2021). During the thawing and drying step, the derivatization reagents were prepared. First, MOX is weighed off in a 20ml glass vial. It was then dissolved in pyridine to achieve a final concentration of 20mg/ml. It is important to note that this preparation was done in a laminar flow cabinet as pyridine is highly toxic. After the samples were completely thawed and dried, 50µl of the prepared MOX was added to each sample, followed by a 30 second vortex step. The samples were then incubated at 60°C for an hour.

After the samples were derivatized with MOX, the samples were vortexed to allow them to reach room temperature. This was followed by another derivatization step with BSTFA containing 1% TMS. After the samples reached room temperature, 50µl of the BSTFA containing 1% TMS was added to each sample. The samples were then incubated at 40°C for another hour. After the derivatization steps were completed, the contents of the vials were transferred to a flat-bottom insert. This raised the level of the contents in the vial so the injection needle of the GC-TOF-MS could reach the sample. The original vials were reused as the flat-bottom inserts can be inserted into these vials. The caps of the vials were screwed onto the vials and the samples were then loaded into the sample tray of the GC-TOF-MS so analysis could begin.

4.5.7 Sample Preparation for LC-MS/MS Analysis

The sample preparation for LC-MS/MS analysis differs somewhat from the sample preparation for GC-TOF-MS analysis. The initial steps of thawing and drying the samples were similar. The derivatization agent was again prepared during the thawing and drying step of the samples. First, butanolic-HCl was prepared. This was done by combining butanol and acetylchloride in a 3:1 (v:v) ratio. Thus, butanol needed to be 75% of the total volume of needed butanolic-HCl and the acetylchloride needed to be 25% of the total volume. Butanol was put on ice to lower the temperature to ~4°C. The preparation of butanolic-HCL is a highly exothermic reaction, thus, by lowering the temperature of the butanol and the reaction environment serious incidents was prevented. Acetylchloride was added very slowly can carefully to the butanol on ice using a disposable dropper until the entire volume of acetylchloride was added to the butanol. The butanolic-HCl was left on ice for a further ten minutes to ensure the entire reaction was completed at the lower temperature.

When the samples were completely dried, 200µl of the prepared butanolic-HCL was added to each of the samples/vials using disposable pasteur glass pipettes. This was done in a laminar flow cabinet as the butanolic-HCl is toxic. The caps of the vials were screwed back on and the samples were incubated for 30 minutes at 50°C. When derivatization was completed, the samples were dried again under a gentle stream of nitrogen gas at 37°C. The samples were then resuspended in a 50:50 (v:v) mixture of acetonitrile and HPLC grade water. The resuspended samples were then transferred to a flatbottom insert with a polymer foot and reinserted into the original vial. The flatbottom inserts with the polymer foot is used to ensure that the insert is completely centred in the vial, so the injection needle of the LC-MS/MS does not break the insert. The samples were then loaded into the sample tray of the autosampler and was kept at a temperature of 4°C during the analysis.

4.5.8 Preparation of Quality Control Samples

To ensure the QC samples met the criteria, five quality control samples were created during the metabolite extraction process, for each batch from all the samples allocated to the batch. After chloroform was added to each sample, the samples were vortexed. Then, before the samples were centrifuged, 10µl of each sample was added to each of the QC sample tubes (50µl in total of each sample was used).

4.5.9 Sample Run-sequences and Batch Preparation

Samples were run on both GC-TOF-MS and LC-MS/MS platforms according to the tissue type; thus, each tissue type (liver, heart, and brain) were considered to be a batch. The sample preparation for metabolite extraction for each tissue was done simultaneously for both platforms and then stored at -80°C until the sample preparation for analysis was done. The method for sample preparation for analysis on the two different platforms differ, thus these preparation steps were performed separately to preserve sample integrity and to minimalize errors. The samples for GC-TOF-MS were randomized using a formula provided in Microsoft Excel. The LC-QQQ samples in each batch was placed in order of their mouse numbers. The five QC samples prepared for each batch were placed within the batch with equal number of samples between each QC sample as for both the GC-TOF-MS- and LC-QQQ batches (Table 4-8). Randomization of samples are important to ensure there is no correlation between the results and the preparation- or run order of the

samples. Correlation between the run order, sample preparation order and results cause bias in the study (Dunn et al. 2012).

Table 4-8: Run order of samples in each batch for both GC-TOF-MS and LC-MS/MS analysis.

Run Order	Liver GC-TOF-MS	Heart GC-TOF-MS	Brain GC-TOF-MS	Liver LC-QQQ	Heart LC-QQQ	Brain LC-QQQ
1	**FAMES**	**FAMES**	**FAMES**	1 WT	1 WT	1 WT
2	**QC 1**	62 KO	62 KO	2 HT	2 HT	2 HT
3	21 WT	91 HT	91 HT	3 KO	3 KO	3 KO
4	62 KO	58 HT	58 HT	4 WT	4 WT	4 WT
5	91 HT	4 WT	4 WT	8 KO	8 KO	8 KO
6	58 HT	45 KO	45 KO	21 WT	31 KO	21 WT
7	4 WT	76 KO	76 KO	31 KO	**QC 1**	**QC 1**
8	**QC 2**	**QC 1**	**QC 1**	32 KO	32 KO	32 KO
9	45 KO	2 HT	2 HT	36 KO	36 KO	36 KO
10	76 KO	1 WT	1 WT	39 WT	39 WT	39 WT
11	2 HT	69 KO	69 KO	**QC 1**	40 KO	40 KO
12	1 WT	75 HT	75 HT	40 KO	44 WT	44 WT
13	69 KO	8 KO	8 KO	44 WT	45 KO	45 KO
14	**QC 3**	39 WT	39 WT	45 KO	**QC 2**	**QC 2**
15	75 HT	**QC 2**	**QC 2**	57 HT	57 HT	57 HT
16	8 KO	57 HT	57 HT	58 HT	58 HT	58 HT
17	39 WT	89 HT	89 HT	61 WT	61 WT	61 WT
18	57 HT	86 KO	86 KO	64 WT	62 KO	62 KO
19	89 HT	3 KO	3 KO	65 HT	64 WT	64 WT
20	**QC 4**	77 WT	77 WT	69 KO	65 HT	65 HT
21	86 KO	40 KO	40 KO	**QC 2**	**QC 3**	**QC 3**
22	3 KO	**QC 3**	**QC 3**	75 HT	69 KO	69 KO
23	40 KO	31 KO	21 WT	76 KO	76 KO	75 HT
24	77 WT	90 KO	90 KO	77 WT	77 WT	76 KO
25	31 KO	87 WT	87 WT	78 HT	78 HT	77 WT
26	**QC 5**	78 HT	78 HT	86 KO	86 KO	78 HT
27	90 KO	32 KO	32 KO	87 WT	**QC 4**	**QC 4**
28	36 KO	44 WT	44 WT	88 WT	87 WT	86 KO
29	87 WT	**QC 4**	**QC 4**	89 HT	88 WT	87 WT
30	78 HT	64 WT	64 WT	90 KO	89 HT	88 WT
31	32 KO	36 KO	36 KO	91 HT	90 KO	89 HT
32	**QC 6**	65 HT	65 HT	**QC 3**	91 HT	90 KO
33	44 WT	88 WT	88 WT		**QC 5**	91 HT
34	64 WT	61 WT	61 WT			**QC5**
35	65 HT	**QC 5**	**QC 5**			
36	88 WT	**FAMES**	**FAMES**			
37	61 WT	-	-			
38	**QC 7**	-	-			
39	**FAMES**	-	-			

4.5.10 Metabolomics Data Processing

Data was extracted for the GC-TOF-MS analysis via LECO® ChromaTOF® (v 4.72.0.0), while for LC-MS/MS, Agilent MassHunter Qualitative and Quantitative softwarewas used. Data was extracted as *.csv files and further processed in Microsoft Excel. Data was normalised using the internal standards added to the samples during sample preparation. Abundances for each metabolite in each sample was divided by the abundance of the internal standard and the multiplying with the concentration of the internal standard. The normalised data was then log transformed to achieve more uniform distribution of the data. The p-value and effect sizes were then calculated to indicate which metabolites had differences in abundance when the knockout group was compared to the wildtype group. The logarithmic transformed data was exported again into a *.csv file and loaded on to MetaboAnalyst. Here, data did not undergo and normalization, transformation or scaling as these steps were already done. Boxplots were available to determine in which direction the indicated changes took place with reference to the knockout group.

CHAPTER 5 – RESULTS

5.1 Mice Genotyping and Sample Collection

During this study, a total of 148 new-born mice were genotyped to acquire the appropriate number of samples of each genotype for the different analysis to be done. Genotyping started with the isolation of DNA, followed by the PCR amplification of the *Ndufs4* gene in the isolated DNA and then separating the amplicons on a 1% agarose gel. The isolated DNA concentrations of the selected mice are listed in annexure A and the separated amplicons are displayed in Figure 5-1. Wildtype mice have one amplicon band of 1229 base pairs, heterozygous mice have two amplicon bands of 1229 base pairs, and 429 base pairs and knockout mice have one amplicon band with 429 base pairs. A ladder was added to wells on the side as ‘n reference guide to estimate the amplicon size. The ladder contained DNA fragments of 100 -1000 base pairs in length.

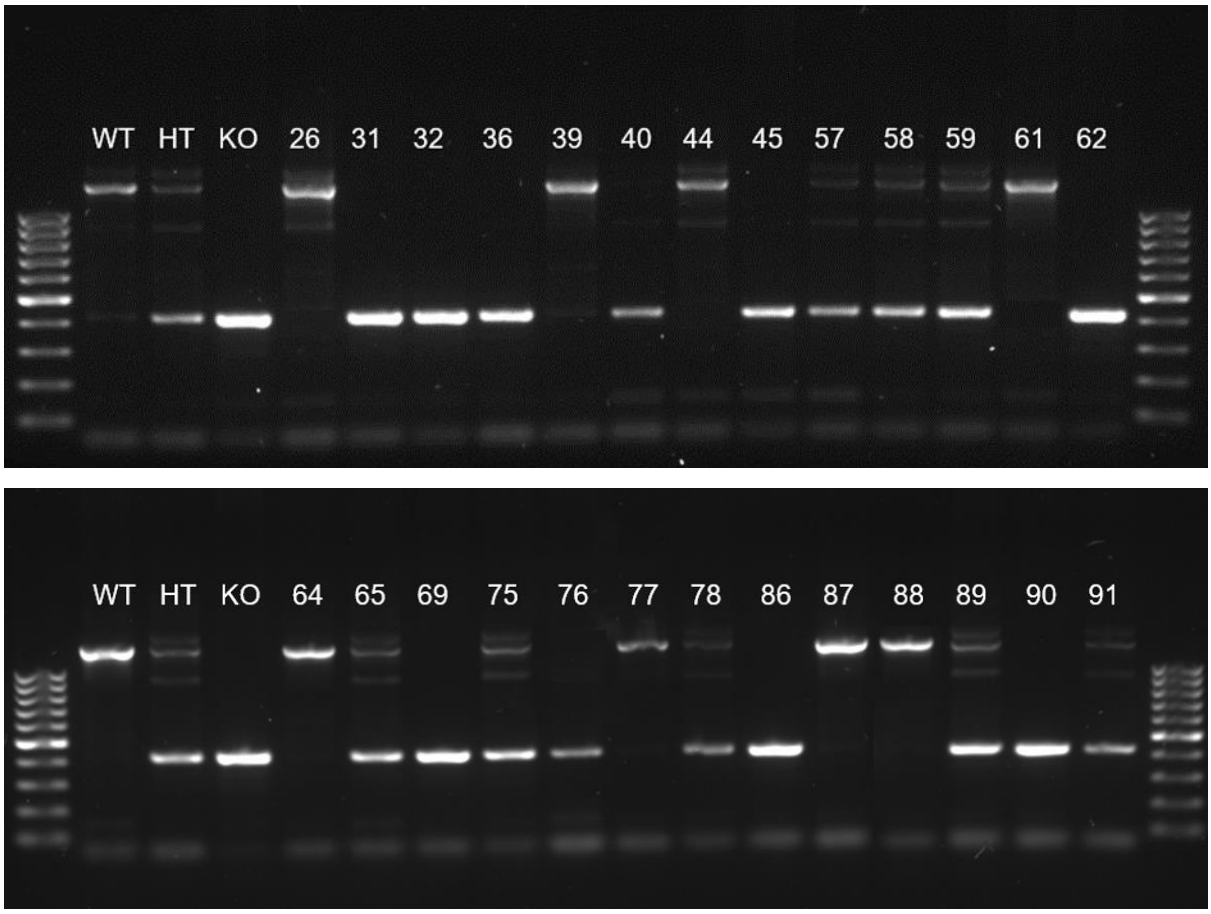

Figure 5-1: Representation of the genotyping results from the genotyping analysis done. The first 3 wells of the gel contained the control samples in the order wildtype (WT),

heterozygous (HT) and knockout (KO) genotype to which the rest of the samples were compared to determine their genotype. The number at the top of the well indicate which mouse each sample represents.

For sample collection, mice were selected based on gender. Male mice were preferred to the female mice as the estrogen of the female mice cause variance during metabolomic analysis. Mice were euthanized between P45 and P50 and tissues were collected. These tissues were immediately snap-frozen and transported in liquid nitrogen. Samples were stored at -80 °C until further analysis was done.

5.2 RNA Quantification, Integrity Confirmation and gDNA Contamination

RNA quantification was first done using the NanoDrop One spectrophotometer. Each sample was measured twice from the RNA sample allocated for the quantification. Results obtained from the NanoDrop One is shown in Annexure (B). The RNA concentration values obtained from the NanoDrop One were used to determine how much RNA (in µl) is needed to determine the integrity of the RNA. RNA integrity was determined using an agarose gel, containing bleach, to separate the RNA into two distinct bands as shown in Figure 5-2. A total amount of ~500 ng RNA was loaded into the agarose gel for each sample. Electrophoresis of the RNA took place at 20 volts for ten minutes to concentrate the RNA, followed by 50 volts for 70 minutes to allow for sufficient separation.

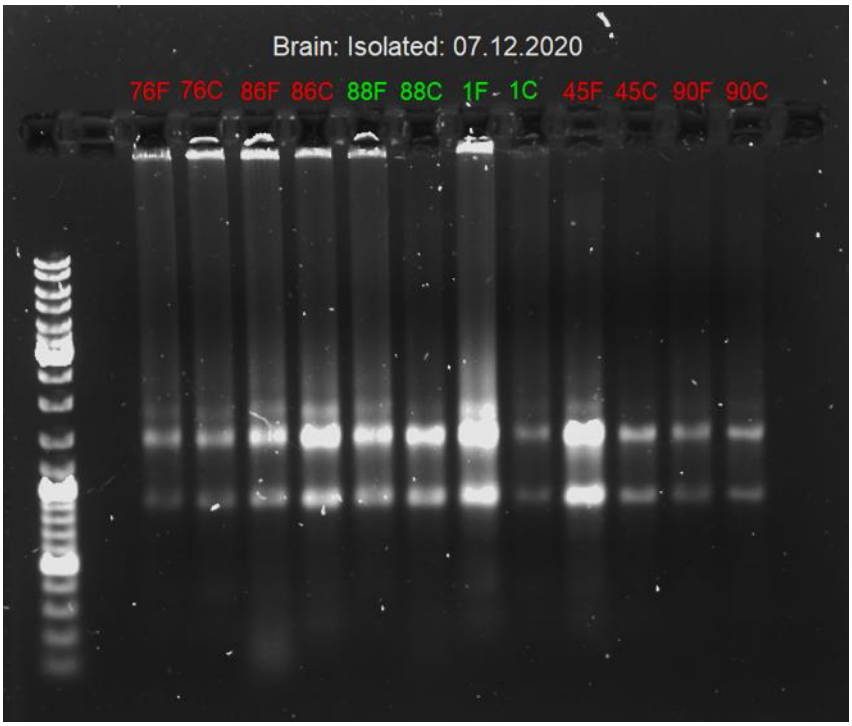

Figure 5-2: Results from separation of isolated RNA on a 1% agarose gel containing bleach via electrophoresis. Numbers at the top of each well represent the sample numbers of the mice from which the RNA was isolated. Red numbers indicate knockout mice while green numbers indicate wildtype mice. The letters accompanying the numbers indicate which area of the brain was used to isolate RNA (F=frontal lobe, C=cerebellum). Two distinct bands are visible on the gel, the top band is the 28S band and the bottom band is the 18S band. The top 28S band usually show at an intensity of 1,5 – 2 time that of the bottom 18S band. Possible genomic DNA contamination can be visualized as a distinct band at the well (such as with sample 1F) and possible RNA degradation can be visualized by a smear below the 18S band (such as with sample 45F)

Additional methods were also performed to determine the RNA concentration of the samples, along with possible DNA contamination. This was performed on the Qubit 2.0 fluorometer using the Quibit® RNA HS Assay Kit and the Qubit® dsDNA HS Assay Kit. Results were given in µg/ml and needed to be converted to ng/µl to be comparable to the results obtained from the Nanodrop One spectrophotometer. This was done using a simple conversion calculation. Qubit results are shown in annexure C. The average RNA isolated from the liver, heart and brain according to the Qubit 2.0 Fluorometer was, 84.78 ng/µl, 18.68 ng/µl and 11.77 ng/µl respectively.

5.3 Sequencing

Sequencing was done on an Ion GeneStudio™ S5 Semiconductor Sequencer. An Ion 540™ chip loaded with ISPs would be loaded into the sequencer along with all consumables and reagents. Results on whether the sequencing run was successful, chip loading and library preparation was visualized on the Ion Torrent Suite™ software after the run was completed. Results for each run is shown in Table 5-1. Chip loading was visualized on the software, where a red chip was an indication of successful/sufficient loading, and a blue chip was indicative of unsuccessful chip loading. Examples of each case is shown in Figure 5-3. It should be noted that the 4th chip loading run resulted in a blue chip, indicative of a failed sequencing run. This Ion 540™ chip was not suitable for data processing after sequencing was completed. This library and template preparation was redone and was successful (see chip 5 in Table 5-1). Each sample was assigned an Ion Code™ during library preparation with which the sequencer could correlate which fragment of DNA belongs to which sample. Results obtained from the Ion Torrent Suite™ also indicated the statistics of each sample with regard to incorporated bases, amount of reads and the mean read length of DNA fragments. Sequencing generated large amounts of data during each sequencing run. Specific data files containing gene level information and gene expression values were downloaded in *.chp file format which was used for data analysis.

Table 5-1: Results obtained from Ion Torrent Suite™ software for the sequencing run, chip loading and library preparation. ISP Loading is indicative of the percentage of chip wells that contained ISPs. The average read length indicated the average length of the called reads in base pair length. Empty wells show the percentage of empty wells on the chip. Enrichment shows the percentage of loaded ISPs that generated a signal during sequencing, while no-template did not generate a signal. Clonal ISPs only contained one template strand of DNA while polyclonal ISPs had more than one template strand of DNA. The final library is the percentage of reads that pass all filters and are recorded in the BAM output file.

Chip Number	Average Read Length	ISP Loading	Empty Wells	Enrichment	No Template	Clonal	Polyclonal	Final Library
1 (Liver)	102 bp	92%	8%	100%	0%	66%	34%	88%
2 (Liver)	102 bp	89%	11%	100%	0%	74%	26%	85%

3 (Heart)	106 bp	92%	8%	100%	0%	65%	35%	87%
4 (Brain)	42 bp	24 %	76%	43%	57%	96%	4%	0%
5 (Brain)	107 bp	92 %	8%	100%	0%	54%	46%	93%

(a) 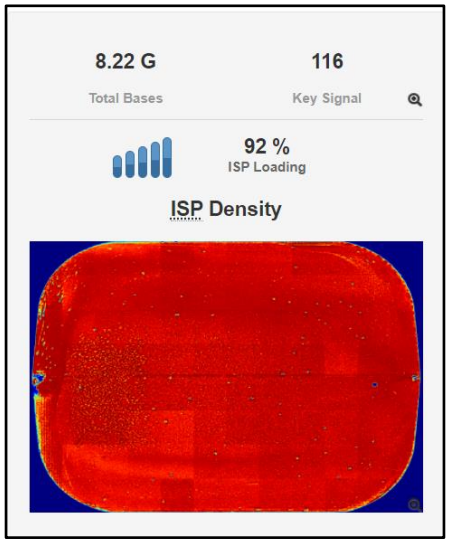

(b) 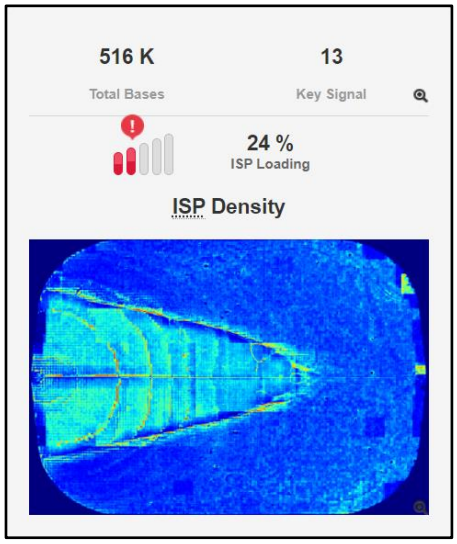

Figure 5-3: Visualization of chip loading on the Ion Torrent Suite software. (a) Red chip indicative of successful chip loading. (b) Blue chip indicative of unsuccessful chip loading. In total, 32 prepared libraries were sequenced using the Ion 540™ chips. Eight libraries were sequenced on one chip, leading to a total of four sequencing runs. An average ISP loading of 91% was achieved for the four sequencing runs and 99% of the loaded ISP contained libraries. A total average of 32% of the ISPs were polyclonal, with 10% being low quality and 1% having adapter dimers. Final library ISPs totalled at 60% on average (Table 4-5). These results are indicative of successful sequencing runs of all 32 prepared libraries. The selected Ion AmpliSeq™ Transcriptome Mouse Gene Expression Kit is a panel specifically designed to target the ~20 000 genes of the mouse transcriptome.

5.4 Transcriptomic Analysis

Data of each sequencing run was downloaded from the Ion Torrent Suite™ software in *.chp file format. These files contain the gene-level information, and the gene expression values. Data was visualized using the Transcriptome Analysis Console (TAC) provided by ThermoFisher Scientific. Data was extracted in *.csv file format and further processed using Microsoft Excel (data not shown). These values were normalized to reads per million. The Shapiro-Wilk normality test was done on untransformed data to determine data distribution. Most importantly, the expression values of each gene in every sample are also given. These expression values were used to calculate the two-tailed t-test

(unequal variance) and effect size. The t-test generates a p-value, which is indicative of the probability of the observed difference. Effect size generates a d-value, which is used to determine the magnitude of an observed difference. A p-value smaller than 0.05 was considered to indicate a statistically significant difference between two groups and a d-value bigger or equal to 0.8 indicates a large difference between the observed variable for two groups. Data of the variables that met the criteria were further examined using MetaboAnalyst 5.0 to determine the direction of the observed changes between the two groups.

Table 5-2: Shapiro-Wilk normality test, t-test and effect size of all the genes of interest of liver tissue sequencing

Liver (Chips 1 and 2)			
ID	Shapiro-Wilk Test	T-test	Effect Size
Gpd1	Not Normal	**0,039**	**1,150**
Gpd2	Not Normal	0,638	0,236
Mdh1	Normal	**0,019**	**1,395**
Mdh2	Normal	0,155	0,800
Me1	Normal	**0,034**	**1,184**
Me2	Not Normal	0,555	0,262
Me3	Not Normal	0,383	0,510
Slc25a1	Normal	**0,009**	**1,596**
Slc25a3	Not Normal	0,160	0,717
Slc25a11	Normal	0,306	0,539
Slc25a12	Normal	0,850	0,087
Slc25a13	Normal	0,289	0,486
Slc25a22	Not Normal	0,284	0,494

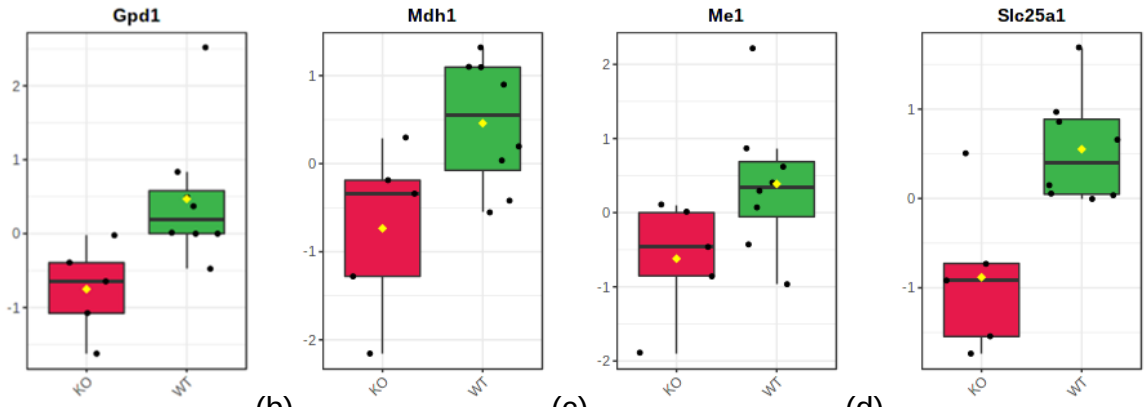

(a) (b) (c) (d)

Figure 5-4: Genes with indicated significant differences between the two experimental groups in the liver tissue. *Gpd1*(a), *Mdh1*(b), *Me1*(c) and *Slc25a1*(d) all had reduced expression in the knockout group. x-axis = Group, y-axis = log2RPM. Red represents the KO group and green represents the WT group as is noticed in figures (a) to (d), the normalized log2 reads per million values were less for all four genes in the KO group when compared to the WT group.

For the liver data, four genes of interest showed significant differences between the wildtype and knock out groups. Significant genes have a p-value of less than 0,05 and an effect size of more than 0.8 (Table 5-2). These genes are *Gpd1*, *Mdh1*, *Me1* and *Slc25a1*. All four of these genes had significantly reduced expression in the knockout group (Figure 5-4).

Table 5-3: Shapiro-Wilk normality test, t-test and effect size of all the genes of interest of heart tissue sequencing

Heart (Chip 3)			
ID	Shapiro-Wilk Test	T-Test	Effect Size
Gpd1	Not Normal	0,593	0,311
Gpd2	Not Normal	0,568	0,340
Mdh1	Normal	0,938	0,047
Mdh2	Not Normal	0,761	0,213
Me1	Normal	**0,036**	**1,675**
Me2	Not Normal	0,710	0,208
Me3	Normal	0,651	0,325
Slc25a1	Not Normal	0,917	0,058
Slc25a3	Normal	0,309	0,661

Slc25a11	Not Normal	0,475	0,413
Slc25a12	Normal	0,426	0,539
Slc25a13	Normal	0,375	0,537
Slc25a22	Normal	**0,007**	**2,801**

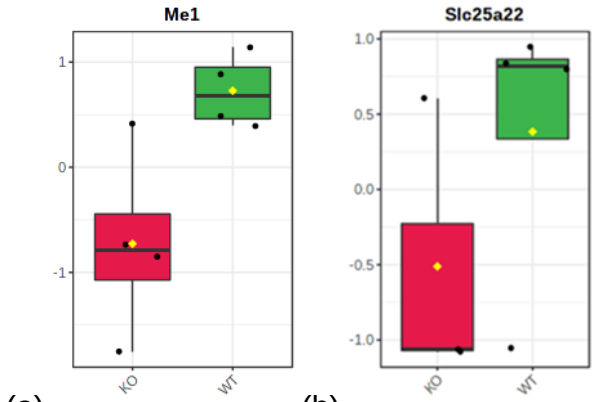

(a) (b)

Figure 5-5: Genes with indicated differences between the two experimental groups in the heart tissue. ME1(a), SLC25A22(b) both had significantly reduced expression in the knockout group. x-axis = Group, y-axis = log2RPM. Red represents the KO group and green represents the WT group. As is noticed in figures (a) and (b), the normalized log2 reads per million were less for both genes in the KO group when compared to the WT group.

For the heart data, two genes of interest showed significant difference between the two experimental groups. Significant genes have a p-value of less than 0,05 and an effect size of more than 0.8 (Table 5-3). Both genes, the glutamate carrier 1 encoded by the *Slc25a22* gene and *Me1*, was down regulated in the knockout group (Figure 5-5).

Table 5-4: Shapiro-Wilk normality test, t-test and effect size of all the genes of interest of brain tissue sequencing

Brain (Chip 5)			
ID	Shapiro-Wilk Test	T-Test	Effect Size
Gpd1	Normal	0,936	0,049
Gpd2	Normal	0,734	0,195

Mdh1	Not Normal	0,514	0,418
Mdh2	Not Normal	0,191	0,852
Me1	Normal	0,364	0,608
Me2	Normal	0,338	0,610
Me3	Normal	**0,025**	**1,861**
Slc25a1	Normal	0,790	0,183
Slc25a3	Normal	**0,006**	**2,754**
Slc25a11	Not Normal	0,932	0,051
Slc25a12	Normal	0,426	0,471
Slc25a13	Normal	0,280	0,892
Slc25a22	Normal	**0,075**	**1,312**

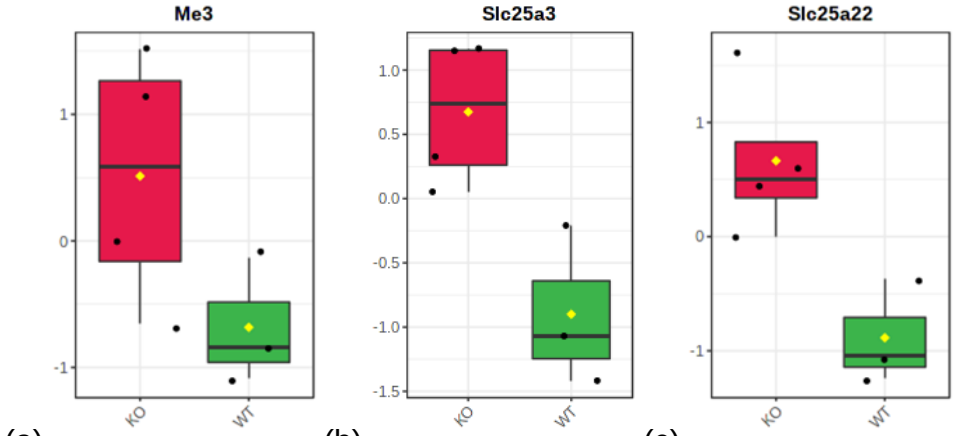

Figure 5-6: Genes with indicated differences between the two experimental groups in the brain tissue. *Me3*(a), *Slc25a3*(b) and *Slc25a22*(c) all had increased expression in the knockout group. x-axis = Group, y-axis = log2RPM. Red represents the KO group and green represents the WT group. As is noticed in figures (a) to (c), the normalized log2 reads per million values were more for all three genes in the KO group when compared to the WT group.

For the brain data, three of the genes of interest were up regulated in the KO group (Figure 5-6). These genes were *Me3*, *Slc25a3* and Slc25a22.

5.5 Metabolomics Analysis

Data from the metabolomic analysis was extracted using software packages that accompanied the platform the analysis was done on. The extracted files were exported into *.csv file format that is compatible with Microsoft Excel™ to be further processed.

Zero filtering and data integrity was completed, followed by the replacement of missing values. Missing values were replaced with 20% of the smallest recorded value for each specific variable. Outliers were identified via heatmaps to be removed if present. No outliers were identified and thus no samples were removed. Each peak intensity was first normalized to the internal standard, and this removed variation of a technical aspect and avoided the misidentification of significant changes between the two groups. For each analyte detected, a p-value and effect size were determined to indicate the analytes with the most significant changes in the data set. Analytes with a p-value of less or equal to 0,05 was considered significant and an effect size of more than 0,8 is considered to indicate a significant difference. A *.csv file was generated from the normalised and log transformed data set to be loaded onto MetaboAnalyst. MetaboAnalyst starts with data pre-treatment where the data was log transformed to minimize the influence of the background noise of the data set. Scaling and centring were not performed along with transformation and normalization as this was done before MetaboAnalyst processing.

5.5.1 Metabolic Analysis – Liver

Targeted analysis of the liver tissue on the GC-TOF-MS was performed on the specific metabolites involved in the shuttle systems. Analysis indicated that malic acid, α-ketoglutaric acid, glycerol-3-phosphate, and glutamic acid displayed significant differences when the wild type and knockout groups were compared (Table 5-5).

Table 5-5: Significant metabolites found in liver tissue via GC-TOF-MS analysis

Metabolite	p-value (< 0,05)	Effect size (> 0,8)
Pyruvate	0,207	0,389
Malic acid	**0,003**	**1,098**
Aspartic acid	0,183	0,413
α-Ketoglutaric acid	**0,044**	**0,679**
Glutamic acid	**0,008**	**0,924**
Glycerol-3-P	**0,048**	**0,643**
Fumarate	0.002	1.146
Niacinamide	0.001	1.223
Arabinofuranose	0.006	0.987
Ribitol	0.007	0.955
Ribonic acid	0.004	1.045
Linoleic acid	0.002	1.205
Linolenic acid	0.003	1.078
Oleic acid	0.0007	1.260
10-Undecanoic acid	0.001	1.208
Arachidonic acid	0.002	1.162

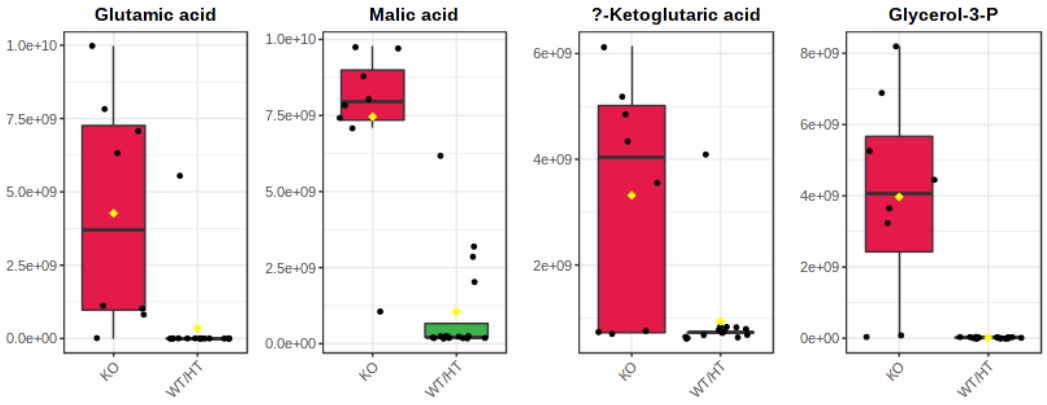

Figure 5-7: Abundances of significant metabolites from targeted analysis. x- axis = group, y axis = normalized log concentrations. Red represents the KO group and green represents the WT group. As is noticed in the figures, the normalized log concentrations were more for all four compounds in the KO group when compared to the WT group.

Another semi-targeted approach was performed on the liver tissue making use of the LC-MS/MS technology. This approach targeted the amino acids in the liver tissue and indicated glutamine as significant (Table 5-5) and to be less abundant in the knockout group (Figure 5-7).

Table 5-6: Significant metabolites found in liver tissue via LC-QQQ analysis

Metabolite	p-value (< 0,05)	Effect size (> 0,8)
Asparagine	0,099	0,545
Ornithine	0,129	0,501
Glycine	0,845	0,048
Serine	0,280	0,274
Glutamine	**0,0000000685**	**2,253**
Alanine	0,453	0,237
Arginine	0,904	0,038
Citrulline	0,667	0,136
Arginine	0,660	0,139
Proline	0,062	0,716
Cystathionine	0,719	0,137
Valine	0,415	0,303
Methionine	0,747	0,115
Cystine	0,070	0,710
Tyrosine	0,156	0,531
Isoleucine	0,967	0,016
Leucine	0,088	0,661

Phenylalanine	0,775	0,110
Homocystine	0,610	0,169
Aspartic acid	0,974	0,0103
Tryptophan	0,571	0,202
Glutamic acid	0,549	0,214

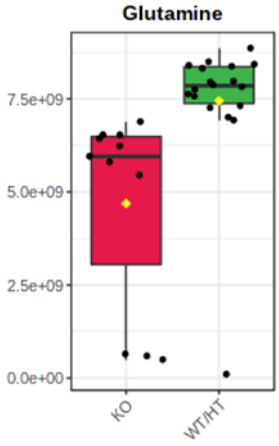

Figure 5-8: Glutamine abundance in liver tissue as was found via LC-QQQ analysis. x-axis = group, y axis = normalized log concentrations. Red represents the KO group and green represents the WT group. As is noticed in the figure, the normalized log concentrations were less abundant for in the KO group when compared to the WT group.

5.5.2 Metabolic Analysis – Heart

The metabolic analysis of the selected shuttle systems on the GC-TOF-MS did not indicate significant changes according to the t-test (p-value) and effect size (d-value). A semi-targeted approach using LC-MS/MS analysis for amino acids, indicated five amino acids that had significant changes between the knockout and wildtype groups. The abundances of leucine, isoleucine, valine, methionine,and phenylalanine were all more abundant in the knockout group when compared to the wildtype group (Figure 5-8).

Table 5-7: Significant metabolites found in heart tissue via LC-QQQ analysis

Metabolite	p-value (< 0,05)	Effect size (> 0,8)
Arginine	0,475	0,248
Glycine	0,813	0,068
Serine	0,366	0,250
Glutamine	0,513	0,192
Asparagine	0,445	0,273
Ornithine	0,489	0,250

Alanine	0,502	0,231
Citrulline	0,790	0,094
Proline	0,089	0,515
Cystathionine	0,551	0,200
Valine	**0,044**	**0,607**
Methionine	**0,021**	**0,720**
Tyrosine	0,611	0,144
Cystine	0,698	0,128
Isoleucine	**0,008**	**0,817**
Leucine	**0,009**	**0,808**
Phenylalanine	**0,009**	**0,854**
Homocystine	0,400	0,270
Aspartic acid	0,801	0,098
Tryptophan	0,874	0,061
Glutamic acid	0,874	0,061

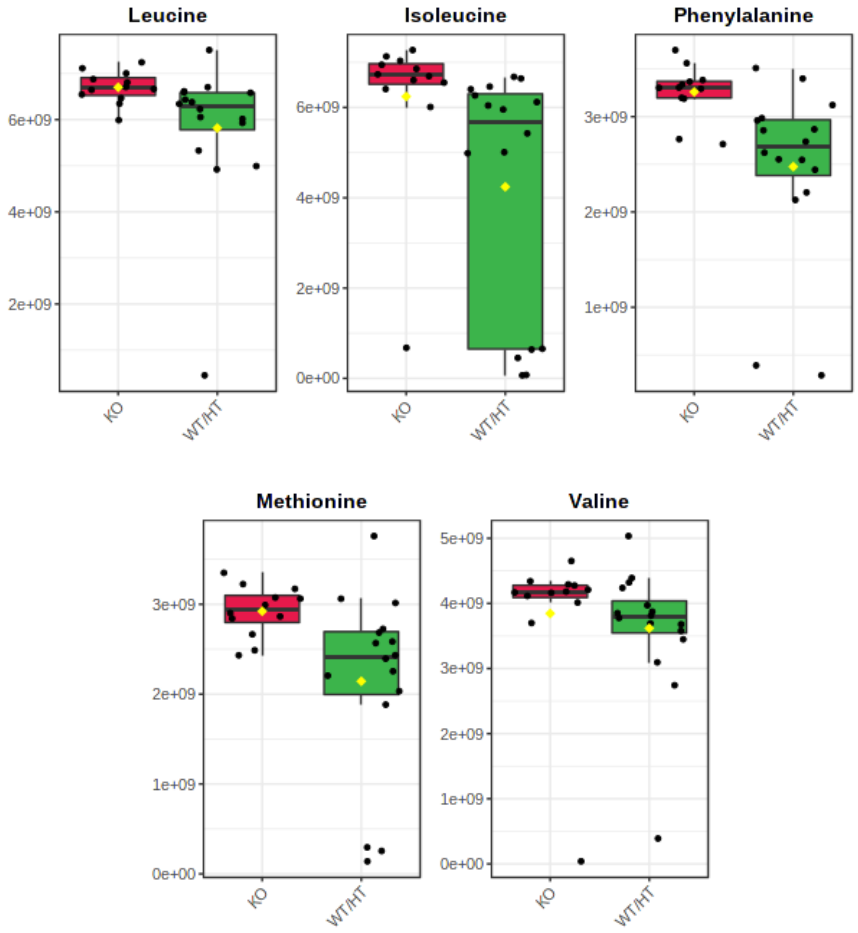

Figure 5-9: Abundances of significant metabolites found in Heart tissue via LC-QQQ analysis. x- axis = group, y axis = normalized log concentrations. Red represents the KO group and green represents the WT group. As is noticed in the figures, the normalized

log concentrations were more for all five compounds in the KO group when compared to the WT group.

5.5.3 Metabolic Analysis – Brain

Table 5-8: Significant metabolites found in brain tissue via GC-TOF-MS analysis

Metabolite	p-value (p < 0,05)	Effect size (d > 0,8)	
Glycerol-3-phosphate	**0,035**	0,634	
Pyruvate	0,252	0,531	
Malic acid	0,276	0,414	
Citric acid	0,283	0,089	
Dihydroxyacetone-P	0,747	0,173	
L-Glutamic acid	0,765	0,322	
Oxalic acid	**0,001**	**0,775**	

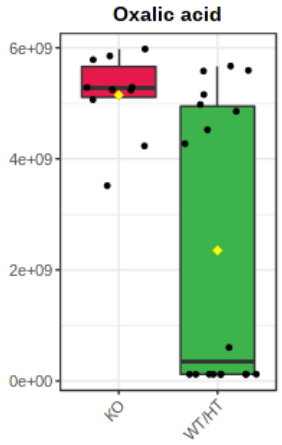

Figure 5-10: Oxalic acid abundance as was found via GC-TOF-MS analysis. x- axis = group, y axis = normalized log concentrations. Red represents the KO group and green represents the WT group. As is noticed in the figure, the normalized log concentrations were less in the KO group when compared to the WT group.

Metabolomic analysis of the brain tissues did indicate differences to an extent in the abundance of the detected metabolites when the knockout and wildtype groups were compared, such as is the case with oxalic acid. Unfortunately, most of the differences were not significant when the p-value and effect sizes are considered as can be observed with glycerol-3-phosphate. A p-value of smaller or equal to 0,05 was significant, indicating that the results had a 5% probability of occurring by chance. The effect size was also determined and indicates the magnitude of the experimental effect or the magnitude of the difference between the two groups. An effect size that is equal to or bigger than 0,8 indicates a large difference between the two experimental groups (Sullivan & Feinn, 2012).

CHAPTER 6 – DISCUSSION

6.1 Mice Genotyping and Sample Collection

Genotyping of the mice lead to the genotype identification of 148 mice during the course of this study. Genotyping the mice is a necessity as this is the primary criteria for the selection of the mice that will be suitable for the study. According to reviewed literature, the KO mice die of natural causes around post-natal day 50. This leads to rigor mortis, resulting in unusable tissues. Thus, it was decided to euthanize the selected mice between P45-50. Visual inspection of the selected mice was used as an unofficial confirmation of the mice genotype. WT mice seemed to have no symptoms associated with Leigh syndrome on the day of tissue collection. The KO mice, however, were much smaller in body size compared to the mice of the control group. They were also blind to an extent and unable to open their eyes fully (Kruse et al 2008). In total, 30 male mice were identified and euthanized for this study. For the metabolomics analysis, 18 were part of the control group and 12 were part of the knockout group. Transcriptomic analysis required the selection of samples that met certain criteria during sample preparation, but these samples were all selected from the above-mentioned 30 mice (see Table in annexure A). It should be noted that the knockout female mice were also euthanized on P50 as to avoid the mice dying due to natural causes. Female wild type mice were euthanized for other studies being conducted while heterozygous female mice were incorporated into the breeding program of the mice. The female mice were not incorporated into this study. It has been shown in previous studies that metabolism in female mammals is directly correlated to the reproduction mechanisms. This can cause variance with metabolomics studies (Fortana & Torre, 2015). Collected samples were stored at -80 °C to preserve sample integrity for a limited period especially for transcriptomic analysis. It is still possible for RNases to be active at -20 °C and in some isolated cases, the activity of ribozymes can be enhanced with freezing (Fabre et al. 2014).

6.2 RNA Isolation

The RNA isolation kit chosen for this study seem to have a limit of the effectiveness when used on small sample numbers. Although this kit was more suited for RNA isolation during this study due to the limited amount of tissue available for analysis. Other methods such

as TRIzol, require large amounts of sample input for the technique to be effective for RNA isolation. The MagMAX™-96 Total RNA Isolation Kit also required preparation steps before RNA isolation could begin, such as cleaning all surfaces and equipment from RNases to preserve RNA integrity and also preparing all the wash solutions and buffers. Sample homogenization also required a transfer step which can lead to sample loss and also cross contamination between samples causing variance and inaccurate results.

6.3 RNA Quantification, Integrity Confirmation and gDNA Contamination

After RNA isolation, it needed to be determined if the RNA is usable for further analysis. This was done by checking the concentration of the isolated RNA, determining the integrity of said RNA and then determining if there was any genomic DNA contamination present in the RNA samples. RNA was isolated from almost all the collected samples. In some cases, one sample was isolated more than once. This was due to insufficient amounts of RNA isolated or when contamination with gDNA was too extensive. Various analysis was done to confirm these criteria of the RNA.

Firstly, RNA was quantified twice using the NanoDrop One spectrophotometer. The replicate readings from the NanoDrop One showed some variance. These values were also used for the integrity check analysis. The average amount of RNA isolated from the liver was ~91 ng/µl, while from the heart and brain tissues less RNA was isolated, with an average of 43 ng/µl and 15 ng/µl respectively. It is possible that more RNA is isolated from the liver due the specific physiological function of the liver, i.e., detoxification (Annexure B) (Ralston & Shaw, 2008). Complex I deficiency causes considerable amounts of physiological stress, which can lead to the alteration of the normal physiological ranges of the body. The liver is the main equalizer of biochemical burdens during long periods of stress. Previous studies have indicated that prolonged physiological stress led to the increased expression of metallothioneins in the liver (Ha et al., 2003). It is possible when one considers the physiological stress caused by complex I deficiency, that more detoxifying enzymes will be needed, leading to an increase in their expression and RNA production.

RNA integrity was determined by making use of an agarose gel containing bleach. Bleach was added to the gel as a precautionary measure against RNases during electrophoresis. The values obtained from the NanoDrop One indicated how much RNA (ng) is in one

microliter of elution buffer. A total of ~500 ng RNA was needed from each sample to be loaded onto the bleach gel. Two bands were visible on the gel after gel electrophoresis was completed. The top band (28S) had an intensity of 1.5X to 2X of that of the bottom band (18S), which indicated that the RNA was still intact (Figure 5-2) (Romero et al. 2014). RNA degradation would have been be detected if a smear is visible below the 18S band (Aranda et al. 2012). If genomic DNA was present in the sample, it would also be indicated on the gel with a distinct band at the top of the gel, in the well. This is due to the DNA moving much slower through the gel than the RNA, especially with the low voltage at which the gel electrophoresis took place. The RNA moving through the gel is in much smaller fragments than the gDNA and thus had a much lower molecular weight (Wieczorek et al. 2021).

RNA was quantified using the Qubit 2.0 Fluorometer, along with the possible genomic DNA contamination. RNA was quantified with the Qubit due to RNA-specific probes of the Quibit RNA HS Assay Kit (ThermoFisher Scientific, Catalogue number Q32852). As was observed with the results obtained from the NanoDrop One spectrophotometer, more RNA was isolated from the liver than was isolated from the heart and the brain. As was mentioned above, this could be due to the specific physiological function of the liver. Genomic DNA contamination was also determined using the Qubit 2.0 fluorometer. Genomic DNA contamination leads to variance and overestimation during gene expression analysis, thus, RNA samples with minimum (gDNA contamination <10% of total RNA concentration) or undetectable DNA contamination were considered to be acceptable for the next step of converting the RNA to complementary DNA (cDNA) (Hashemipetroudi et al. 2018).

After all these analyses was completed, the RNA samples that met all the criteria were used for the conversion to cDNA. Criteria included a ratio of 1,5 – 2.0 for the S28 and S18 bands on the agarose bleach gel and minimum or no genomic DNA contamination needed to be present in each sample.

Table 6-1: Number of participants in transcriptomic analysis of each tissue

Tissue type	Number of KO participants	Number of WT participants
Liver	8	8
Heart	4	4

Brain	4	4

6.4 RNA Conversion to Complementary DNA (cDNA)

Conversion took place in less than half an hour. RNA samples were diluted to 3,33 ng/µl in a total volume of 15 µl. The cDNA samples could not be quantified due to free nucleotides causing possible variance, and it was thus assumed that the synthesized cDNA would have the same output concentration after the conversion. This process had another step to verify the absence of gDNA contamination called the no RT control step. Each sample was prepared twice, where one sample was reverse transcribed to cDNA via reverse transcriptase, while the control samples' master mix did not contain reverse transcriptase, thus no cDNA should be present. The no RT control samples should not have any cDNA present; thus, any detected DNA was considered to be genomic DNA contamination (Fu & Allen, 2019).

6.5 Indicated Differences from Statistical Analysis of Liver Data

The combined metabolomics- and transcriptomic data indicated significant differences in the liver tissue. The first observation is a high concentration of malic acid (see Table 5-5). Malic acid is one of the TCA cycle intermediates and is converted to oxaloacetate via malate dehydrogenase. This conversion is highly dependent on NAD+ as a co-factor. NAD+ is reduced to NADH during this conversion and this step of the TCA cycle is considered one of the rate-limiting steps, meaning that if there is a shortage of the co-factor or substrate, the rate of the entire cycle will slow down (McKenna et al. 1995). There are a few factors that contributed to the high concentration of malic acid (as summarised in Figure 6-1).

Firstly, malate dehydrogenase 1 (Mdh1) has reduced expression in the knockout group (Table 5-1). This enzyme is located in the cytoplasm and is responsible for the reversible conversion of oxaloacetate to malate. This enzyme is co-factor dependent. The direction of the reaction is dependent on the co-factor. When oxaloacetate is converted to malate, NADH is oxidized to NAD+ and donates electrons to malate which carries it over the IMM and donates it to mitochondrial NAD+ (Hanse et al. 2017). This reaction is reversible when conditions require, such as in the case where NADH levels are low and an abundance of NAD+ is present. This reversible reaction is an important step in various

pathways, such as the malate-aspartate shuttle (Broeks et al. 2019). The accumulation of malate can be due to the low abundance of NAD+ (and elevated NADH level) in the mitochondrial matrix. The conversion of malate into oxaloacetate requires NAD+ as a co-factor for MDH1. With NAD+ already in shortage due to complex I dysfunction, it is possible that this enzyme is down regulated to prevent further depletion of NAD+.

Secondly, malic enzyme 1 (Me1) also has reduced expression in the knockout group (Table 5-1). Me1 is also located in the cytoplasm and is dependent on NADP+ as a co-factor. Two other isoforms are also present, both within the mitochondrial matrix. One is dependent of NAD+ as a co-factor (Me2), while the other is dependent on NADP+ (Me3) (Hsieh et al. 2019). Malic enzymes convert malate from the TCA cycle back to pyruvate, which is one of the main fuel sources for the TCA cycle. The reduced expression of Me1 contributes to the accumulating malate as malate cannot be converted to pyruvate. Gene expression of malic enzymes are regulated by various factors which include glucagon and norepinephrine via cAMP, insulin, and thyroid hormones (Hernandez et al., 1993). Insulin increases the expression of malic enzymes while norepinephrine increases the degradation of the malic enzymes (Lorenzo et al., 1989). Mitochondrial dysfunction leads to the inhibition of glucose-stimulated insulin secretion (Mattman et al., 2011), which in turn can reduce the expression of the malic enzymes.

Lastly, Slc25a1 has lower expression in the knockout group (Table 5-2). Slc25a1 is imbedded in the IMM. It is responsible for the co-transport of malate and citrate over the IMM. Citrate is exported from the mitochondrial matrix into the cytoplasm, while malate is transported into the mitochondrial matrix. The expression of this solute carrier is regulated by the metabolic pathways to which it supplies substrates or removes products for (Gnoni et al., 2009), thus it can be concluded that if there is metabolic reprogramming due to disease (such as with mitochondrial dysfunction), it is possible that the expression of the protein can change. The down regulation of Slc25a1 corresponds to malate accumulating in the IMS, while citrate remains in the mitochondrial matrix. The Slc25a1 gene's promotor site contains a sterol regulatory element (SRE) to which SRE binding proteins (SREBPs) can bind. The SRE and its binding protein regulate the expression of the Slc25a1 gene. It has been shown in previous studies (Infantino et al., 2007) that insulin activates the gene reported activity of the SRE-containing promotor of Slc25a1 while polyunsaturated fatty acids (PUFA) inhibit the said activity. As noted in Table 5-4, PUFAs was found to be

more abundant in the knockout group which can be indicative of the possible gene down regulating mechanism of the Slc25a1 gene (Infantino et al., 2007).

When considering complex I deficiency, some of the most prevalent effects are the increase in reactive oxygen species (ROS) and altered redox status (De Haas et al., 2017). ROS causes base modifications in DNA where DNA is oxidized and more prone to mutations (Mikhed et al.,2015). This effect is further enhanced by ROS inhibiting the DNA repair mechanisms. Redox signalling and oxidative stress also cause changes in gene transcription and translation and can affect the repair of DNA. It should also be noted that transcription factors are regulated by the redox balance (zinc-finger motifs and transition metal centres). ROS also destabilizes mRNA via the modifications of the proteins that bind to the AU-rich regions of mRNA. Redox signalling also contributes to the epigenetic regulation of genes via changes in histone function and DNA modification (Mikhed et al., 2015). It is possible that the accumulating effects of ROS and altered redox status from complex I dysfunction is affecting the expression of genes and inducing DNA modifications.

With the reduced expression of Slc25a1, not only will there be reduced movement of malate (and thus electrons) into the mitochondrial matrix, but there will also be reduced movement of citrate into the IMS. Citrate is a vital substrate for cytosolic fatty acid synthesis. Citrate is broken down into acetyl-CoA and oxaloacetate via ATP-citrate lyase. Acetyl-CoA is converted to malonyl-CoA via acetyl-CoA carboxylase. Malonyl-CoA donates a two-carbon skeleton to fatty acids. Statistical analysis indicated that long-chain fatty acids have a higher abundance in the knock-out group (See Table 5-5). Fatty acids are converted to an acyl-CoA in order to enter the mitochondrial matrix. This reaction requires energy in the form of ATP (Williams and O'Neill, 2018). The production of ATP does slow down with a complex I deficiency and thus, fatty acids will possibly accumulate in the cytoplasm due to the inability to move into the mitochondrial matrix.

All the above indicated enzymes with reduced expression in the knockout group is indicative of malate accumulating in the cytoplasm, rather than in the mitochondrial matrix. In the TCA cycle, malic acid is again converted to oxaloacetate via malate dehydrogenase 2 (Mdh2). Mdh2 is also dependent on NAD+ as a co-factor, thus malate would also start to accumulate in the mitochondrial matrix, but it is possible that malate is transported over the IMM via Slc25a3 into the cytoplasm in exchange for organic

phosphate into the mitochondrial matrix. Phosphate is required in the mitochondrial matrix for the phosphorylation of ADP to form ATP.

One of the most recognizable effects of diseases like Leigh syndrome is the disturbed NAD+/NADH ratio, where NADH accumulates due to the dysfunction of complex I, causing a general shortage of NAD+ (Legault et al. 2015). Recent studies on neural cultures have shown changes in the expression of certain enzymes dependent on the NAD+/NADH ratio and NAD+ and NADP metabolism (Inak et al. 2021). NADH and/or NAD+ catabolism, along with the pathways' products and intermediates have also been observed to be more abundant. These include niacinamide, arabinofurnose, ribitol and ribonic acid (See Table 5-4). First, the electron carrier undergoes a hydrolase reaction and is spilt into two products: niacinamide and ADP-ribose. ADP-ribose is split into two molecules where each is left with a phosphate group, leading to AMP and ribose-5-phosphate (Sauve, 2008). Ribose-5-P is considered a pentose sugar due to its 5-carbon structure. Ribose-5-P is further catabolised into D-Ribulose-5-P via an isomerase reaction. D-Ribulose-5-P is either converted to D-Arabinose-5-P or undergoes a dehydrogenase reaction to form D-Ribulose where the phosphate group is removed. D-Ribulose is then either converted to D-Arabinose or Ribitol, which can then be converted into ribonic acid (Kolisek et al. 2005). These reactions are mostly part of incomplete metabolism due to the accumulation of NADH. NADH is supposed to be reduced to NAD+ via complex I, but with complex I being dysfunctional NADH will accumulate. It is possible that these metabolites are being detected due to this accumulation of NADH.

One other enzyme also influenced by the disturbed NADH/NAD+ ratio is the glycerol-3-phosphate dehydrogenase enzyme (Gpd1) (Table 5-2). Gpd1 is present in the cytosol of the mitochondrial IMS. The main function of this enzyme is the reversible conversion of G-3-P to DHA-P. This enzyme is co-factor dependent, and the direction of the reaction is dependent on the co-factor of the reaction. When DHA-P is converted to G-3-P, NADH is oxidized to NAD+ and two electrons are donated to G-3-P. Glycerol-3-phasphate can be converted back to dihydroxyacetone-phosphate via the membrane imbedded glycerol-3-phosphate dehydrogenase 2 (Gpd2) and the two received electrons from NADH is used to reduce FAD to FADH2 inside the mitochondrial matrix where it is utilized by complex II in the ETC (Shen et al., 2006). GPD1 is down regulated in the knockout group, which could be correlated to the disturbed redox balance. Gpd1 has a promotor region with

three domains, the distal promotor region 2 (DPR2), the distal promotor region (DRP) and the proximal promotor region (PPR). The expression of Gpd1 is regulated by tissue-specific trans-acting factors binding to the three promotor domains and there by controls the levels of Gpd1 mRNA expression (Birkenmeier et al., 1992). Glycerol-3-phosphate (G3P) was found to be more abundant in the knockout group (Table 5-5, Figure 5-7). Given the impaired electron entry via complex I, electrons would be shuttled to the ETC via this shuttle. It is possible that these metabolites are utilized in other metabolic pathways in order to maintain the normal function of the mitochondrion. For example, the liver plays an important function in gluconeogenesis which would rather use DHA-P and glyceraldehyde-3-phosphate (GAD-P) as substrate for glucose. With complex I not functioning, the cell will rely on metabolism that bypasses the OXPHOS system in order to maintain ATP production. Glycolysis does not rely on NAD+ as much as the TCA cycle, while gluconeogenesis can utilize the accumulating NADH to ultimately produce glucose.

Glutamine was found to be less abundant in the knockout group (Table 5-6). Glutamine contributes to many cell functions. One of the main functions in liver is its role as substrate for ureagenesis to maintain ammonia homeostasis as well as gluconeogenesis (Xiao et al. 2016) (Curthoys & Watford, 1995). Glutamine is very easily converted to glutamic acid via the phosphate dependent glutaminase enzyme. Glutamic acid is then converted to α-ketoglutarate, while aspartic acid is converted to oxaloacetate. Oxaloacetate is converted to phosphoenolpyruvate, which is one of the first steps in the gluconeogenesis pathway. Gluconeogenesis is an important process when a disease such as Leigh's syndrome is considered. Complex I deficiency is known to cause serious energy shortage. Gluconeogenesis leads to the production of glucose which can be utilized for energy production while an energy shortage is present (Gstraunthaler et al. 1999).

Glutamic acid and α-ketoglutarate were also indicated as more abundant in the knockout group (Table 5-5, Figure 5-7). There seem to be various reasons for the accumulation when the abovementioned data is taken into consideration. Glutamic acid can be converted to α-ketoglutarate via two reversible reactions. The first is via the glutamate dehydrogenase enzyme which requires NAD+ as a co-factor. With complex I deficiency and a disturbed redox balance, this reaction seems unlikely. The other reaction involves the transamination of glutamic acid and oxaloacetate into α-ketoglutarate and aspartic acid. The needed oxaloacetate is normally produced from malate via Mdh1 (producing

NADH in the process). This enzyme also has reduced expression in the knockout group likely due to disturbed redox balance and the enzyme's need for NAD+ as a co-factor (Johnson et al. 2020). Consequently, cytosolic oxaloacetate levels could be lower, which would influence transamination of glutamic acid to α-ketoglutarate. α-Ketoglutarate can move into the mitochondrial matrix via the α-KG/malate exchanger (Slc25a11). This transporter catalyses the movement of α-ketoglutarate into the mitochondrial matrix in exchange for the movement of malate into the cytosol. The expression of Slc25a11 was found to be slightly up regulated in the knockout group. This would contribute to the already accumulating malate in the cytosol.

Complex I plays an important role in the OXPHOS system. It reduces NADH and moves protons over the IMM. Its dysfunction not only disrupts the redox balance, but also the proton gradient of the IMM. Complex II oxidizes FADH2 and passes the electrons to co-enzyme Q10 but does not move protons over the IMM as it is not a transmembrane protein complex like the rest of the OXPHOS complexes. It also plays a part in the TCA cycle. Fumarate was indicated as more abundant in the knockout group (Table 5-5). Fumarate is part of the TCA cycle and is formed from the conversion of succinate via succinate dehydrogenase (also known as complex II) and FADH2 as a co-factor (Martínez-Reyes & Chandel, 2020). It is possible that with the stand-still of the TCA cycle due to the disturbed redox balance, that fumarate is also accumulating as fumarate is converted to malic acid. It has been investigated in previous studies that with complex I dysfunction, complex II is up regulated to maintain the function of the OXPHOS system and ATP production (Esteitie et al, 2005). It is possible that fumarate is higher in abundance to accommodate the upregulated complex II activity.

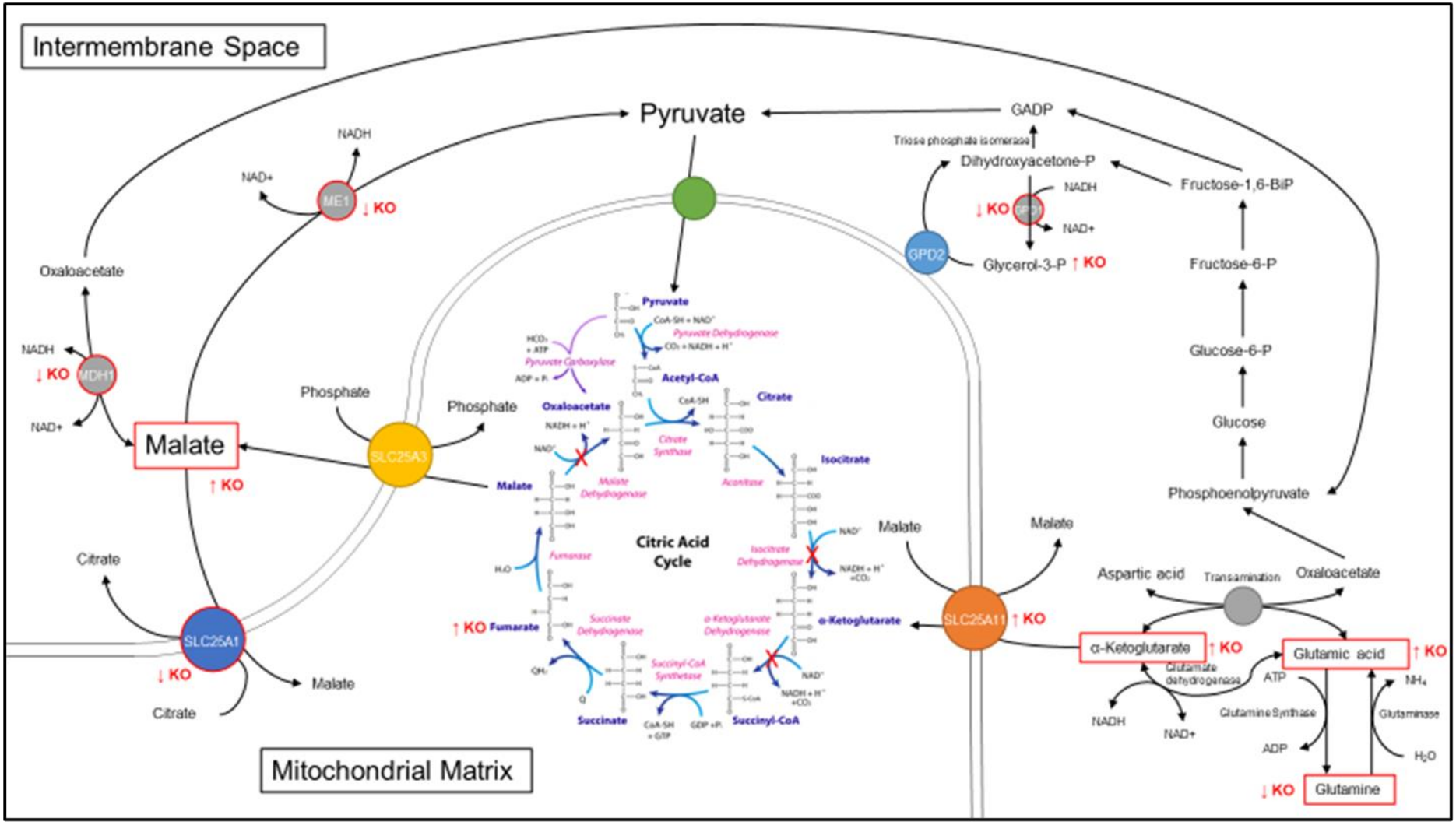

Figure 6-1: Summary of integrated transcriptomic- and metabolomics analysis of the Liver

6.6 Indicated Differences from Statistical Analysis of Heart Data

Most of the mitochondrial transporters and metabolite shuttles in the heart of the knockout mice were comparable to WT mice, except for glutamate carrier 1 (Slc25a22) which had reduced expression in the knockout mice (Table 5-3) (summarised in Figure 6-2). This solute carrier is responsible for moving glutamate into the mitochondrial matrix. This movement is usually in collaboration with the uniport of a proton with glutamate or the antiport of a hydroxyl group (Fiermonte et al. 2022). Since glutamate transport is driven by the proton gradient, it stands to reason that the expression of SLC25A22 is lowered to limit the strain on the already compromised proton gradient in the heart muscle (which is highly dependent on ATP). Moreover, glutamate in the mitochondrial matrix is converted into α-ketoglutarate and ammonia via the enzyme glutamate dehydrogenase. As mentioned above, this enzyme depends on NAD+ (Palmieri, 2004), which is in shortage when complex I is defective. The reduced expression of Slc25a22 then also limited NAD+ usage as well as the accumulation of glutamate in the mitochondrial matrix.

Because of the reduced expression of Slc25a22, one can assume that glutamate will not enter the mitochondrial matrix and start to accumulate in the IMS. The expression of the Slc25a22 gene is mainly controlled by miR-184 (Morita et al., 2013). miRNAs are single stranded 19-23 nucleotide RNAs that can bind to mRNA with a complementary sequence to cause cleavage, degradation or inhibit translation (Gusic & Prokisch, 2020). It is possible to assume that with the effects of complex I dysfunction, there is an increase of miR-184, which causes the reduced expression of Scl25a22. Unfortunately, glutamate was not found to be significantly different between the KO and WT groups when the statistical metabolic analysis was done on the heart tissue results. This could be indicative of glutamate catabolism into other metabolic intermediates. Cytoplasmic glutamate has various functions, one of them being to donate amino groups to form alanine from pyruvate during the first step of branched chain amino acid metabolism. The three branched chain amino acids (isoleucine, leucine and valine) were indicated via statistical analysis as more abundant in the knockout group (Table 5-6). Branched chain amino acid (BCAA) accumulation is not an uncommon occurrence with complex I dysfunction. Many of the steps in the metabolic pathway of BCAAs entail dehydrogenase reactions, which require NAD+ as a co-factor (Terburgh et al. 2021).

Methionine was also found to be more abundant in the knockout group (Table 5-7). Methionine plays a role in the one-carbon cycle (Esterhuizen et al., 2017), where methionine is a substrate for S-adenosyl-methionine (SAM) synthetase (Ducker & Rabinowitz, 2017), along with ATP and H2O. ATP acts as a triphosphate donor to form a sulfonium ion (Lu & Markham, 2002). When considering Leigh syndrome, one of the main bioenergetic symptoms of this disease is a diminished production of ATP (Lake et al., 2015). It is possible that methionine is accumulating in the knockout group due to the reduced production of ATP and considering ATP is required along with methionine to participate in the reaction of SAM synthetase.

One of the most prevalent symptoms in Leigh syndrome is the presentation of cardiomyopathy, which is the weakening of the heart muscle. This ultimately leads to the heart not being able to pump blood effectively (Baldo & Valarinho, 2020). Many have correlated this phenomenon with the specific physiological function of the heart muscle, the high energy requirements of the heart and the diminished production of ATP with Leigh syndrome (Bakare et al., 2021). Phenylalanine was found to be increased in abundance in the knockout group (Table 5-7). Increased levels of phenylalanine have been implicated as a precursor for heart failure is previous studies and may have various origins associated with heart failure as described in Delles et al., 2017. In short, increased levels of phenylalanine with heart failure can be attributed to altered protein metabolism, impaired uptake and utilisation of amino acids, depletion of tetrahydrobiopterin (a co-factor for phenylalanine hydroxylase for the conversion of phenylalanine to tyrosine) and an increased production of catecholamines of which phenylalanine and tyrosine are precursors (Delles el al., 2017).

Malic enzyme 1 was found to be down regulated in the knockout group (Table 5-3). As previously described, Me1 is present in the cytoplasm and is responsible for the reversible conversion of malate into pyruvate. This reaction requires either NADH or NAD+ as a co-factor, depending on the direction of the reaction (Hsieh et al. 2019). It is possible to attribute the down regulation of Me1 to the disturbed redox balance associated with Leigh syndrome (Legault et al. 2015) to attempt to spare the already limited NAD+ from further depletion.

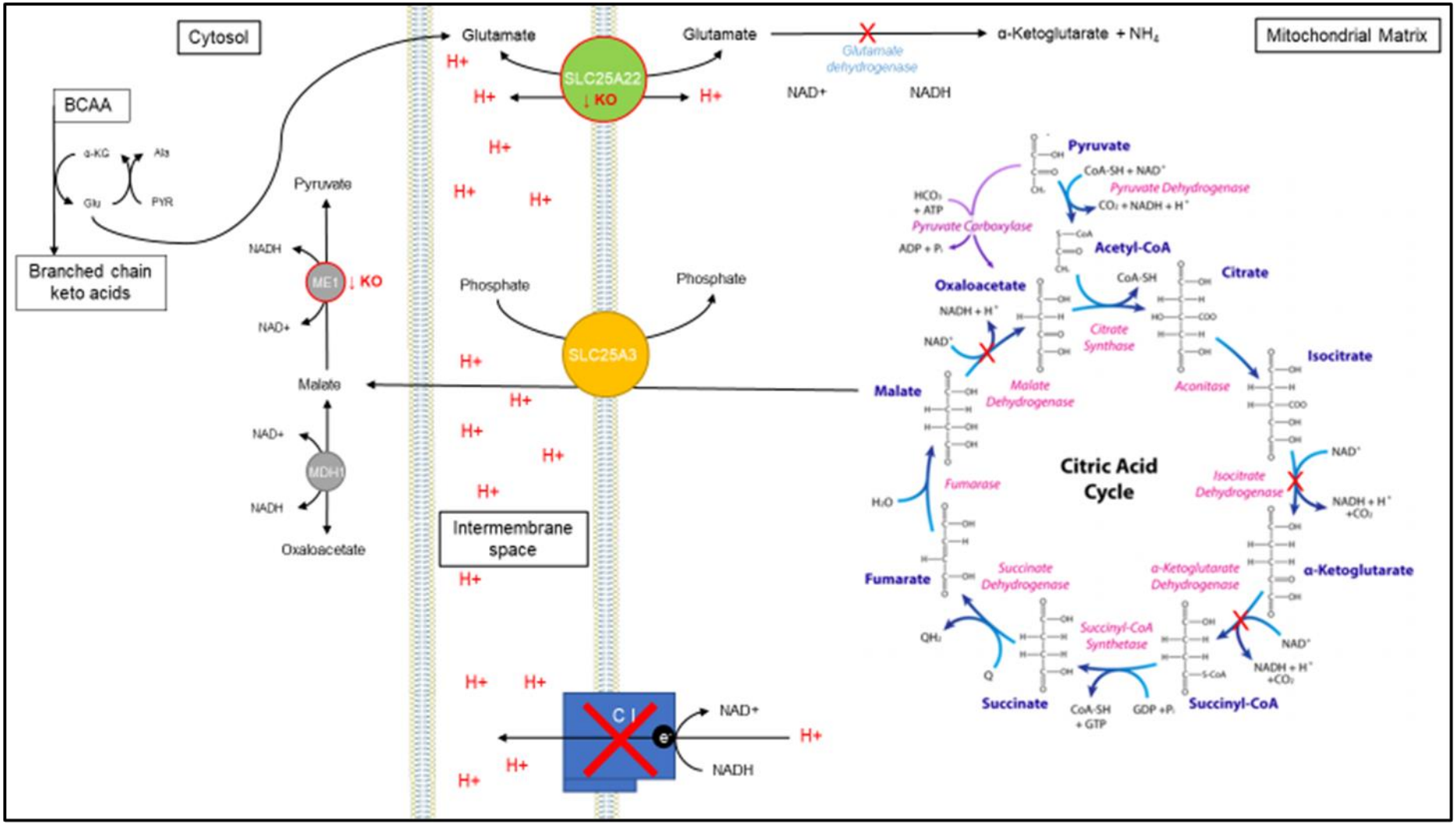

Figure 6-2: Summary of integrated transcriptomic- and metabolomic analysis of the Heart

6.7 Indicated Differences from Statistical Analysis of Brain Data

Statistical analysis indicated that malic enzyme 3 (Me3) was expressed more in the knockout group (Table 5-4). Me3 is one of the three isomers of the enzyme responsible for the reversible conversion of malate to pyruvate. Me3 is located inside the mitochondrial matrix and is dependent on NADP+ or NADPH as a co-factor. It is mainly distributed in the brain, muscle, and heart tissues (Hsieh et al. 2019). Slc25a3 was also expressed more in the knockout group along with Me3. Slc25a3 moves malate from the mitochondrial matrix into the cytosol and inorganic phosphate into the mitochondrial matrix (Runswick et al., 1987). The upregulation of these two proteins could be indicative of the alternative energy producing pathways when complex I is deficient (Bakare et al. 2021). Pyruvate will start to accumulate in the mitochondrial matrix due to the TCA cycle not working. The upregulated Me3 will then convert the accumulating pyruvate into malate. Malate won't enter the TCA cycle either due to malate dehydrogenase's shortage in co-factor (NAD+) (McElroy et al. 2020). Malate will then be moved out of the mitochondrial matrix via upregulated SLC25A3. Malate can then there be converted into oxaloacetate via MDH1. Oxaloacetate was found to be more abundant in the knockout group (Figure 5-10), thus adding more evidence to this possible outcome (Figure 6-3).

Unlike in the heart, the glutamate carrier 1 (Gc1, Slc25a22) was found to be over-expressed in the brain of knockout mice (Table 5-3). GC1 functions by moving glutamate into the mitochondrial matrix. This is coupled with the co-transport of protons (H+) into the mitochondrial matrix or the anti-port of hydroxyl groups into the IMS. Previous studies have shown that when the mitochondria of astrocytes have an increase uptake of glutamate, the microenvironment of the mitochondrial matrix seems to acidify (Azarias et al. 2011). This is likely due to the co-transport of protons with glutamate into the mitochondrial matrix. The lower pH of the mitochondrial matrix can lead to a possible increase in the NAD+ levels (Schaefer et al. 2017). This normally would lead to the activation of sirtuins, but for this study, we hypothesize that this is a futile attempt to replenish the NAD+ shortage included by the deficiency of complex I. Another possible outcome for the increased expression of Slc25a22 is to maintain the cytosolic pool of glutamate in the astrocytes. Glutamate is the principal excitatory neurotransmitter in the brain. Glutamate is mostly present in low concentrations to avoid overexcitation of neurons, which can lead to pathological conditions or even cell death (Shen, 2013). Leigh

syndrome causes astrocytes to cease important neurological functions such as the recycling of glutamine and potassium as neurotransmitters (Lake et al. 2015). There are various metabolic pathways present in the mitochondrial matrix that are supplied via various transporters to produce glutamate in said compartment. Synthesized glutamate can then be transported to the IMS via Slc25a22 (Yoo et al., 2020) where it can function as a neurotransmitter. Most neurological symptoms associated with Leigh syndrome is in response to the dysfunction of the OXPHOS system and diminished ATP production (Baldo & Valarinho, 2020). When considering the transport mechanism of Slc25a22, it is also possible that the symport of glutamate and a proton over the IMM (Taylor, 2017) to the cytosol can replenish the proton gradient for ATP synthesis via ATP synthase (Figure 6-3).

Previous studies done on the Ndufs4 knockout mouse model indicated that certain areas of the brain are more affected and are more lesion prone than the cortex. When these areas are examined individually, very significant changes in the metabolism are observed. With this study, the brain was considered as a whole, instead of the specific areas. The affected areas are smaller in area when compared to the very larger and unaffected areas. This leads to the possible conclusion that the larger and unaffected areas could have diluted the effect of mitochondrial dysfunction on the brain when analysed together with the affected areas. This could be the possible reason as to why not many metabolites were indicated as significant by the t-test and the effect size (Terburgh et al. 2021)

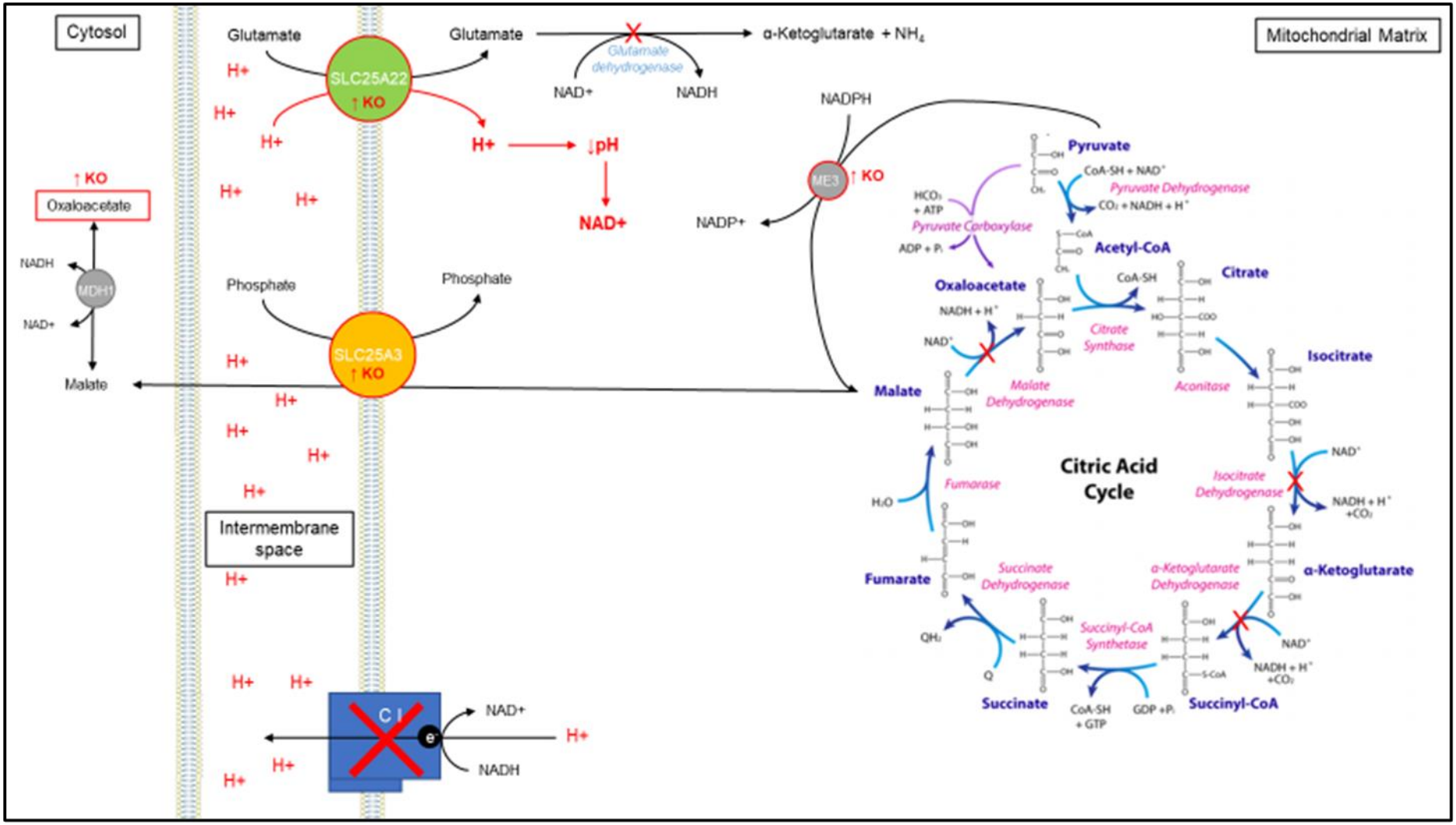

Figure 6-3: Summary of integrated transcriptomic- and metabolomic analysis of the Brain

CHAPTER 7 – CONCLUSIONS

7.1 The Main Aim of the Study

Complex I deficiency and/or dysfunction is one of the most prevalent mitochondrial diseases. With complex I being the largest complex of the OXPHOS system and having a dual genetic origin, a large variety of mutations in both the nDNA and mtDNA can cause mitochondrial dysfunction. This leads to the large heterogeneity of complex I deficiency. Complex I oxidises NADH to NAD^+ and leads to an increase in ROS formation and redox imbalance. During the oxidation of NADH to NAD^+, protons are moved over the IMM that ultimately contributes to the electrochemical gradient that drives ATP synthesis (Schmiedel et al., 2003). As was previously indicated, the SLC25 gene family are responsible for moving most molecules and ions over the impermeable IMM. These carrier proteins can function in synchronization to form shuttle systems that can move reducing equivalents over the IMM, such as malate that can shuttle electrons of NADH in the cytosol to NAD^+ in the mitochondrial matrix (Korla et al., 2015)

The main aim of this study was to investigate if any adaptive responses occur in these shuttle systems to restore the redox imbalance brought on by complex I deficiency and/or dysfunction. There appear to be some adaptive responses in the shuttle systems that occur with a complex I dysfunction, but these adaptive responses seem to be occurring due to the presence of the disease, instead of an attempt to counter act the effects of mitochondria dysfunction. Changes in metabolite abundance was present with specific enzymes involved in the transport of said metabolites, or metabolites that serve as substrate for regulated enzymes or metabolites that occur as the product of an enzyme. Differential expression of enzymes can have different outcomes for the metabolites involved with said enzymes. When an enzyme had reduced expression, substrates would accumulate, and products would be in shortage. Most enzymes with differential expression seem to require NAD^+ as a co-factor. This can be due to gene regulating signalling pathways that are activated by effects of complex I dysfunction.

7.1.1 Objective 1 - Breeding, genotyping and acquisition of Ndufs4-/- and control mice samples (brain, liver and heart)

Breeding of mice was deemed successful after the completion of sufficient sample collection. Each mouse was genotyped, and results was correlated with the physical appearance and was thus also successfully completed. Samples collection was also completed successfully. This objective was thus completed successfully.

7.1.2 Objective 2 – Targeted Transcriptomics of the selected Mitochondrial Transporters and involved enzymes in both Ndufs4$^{-/-}$ and control mice

Transcriptomic analysis was executed via RNA sequencing. The results of the sequencing not only included the selected genes of the SLC25 gene family, but the entire mouse transcriptome. This objective was successfully completed.

7.1.3 Objective 3 – Metabolic Analysis and comparison of the selected shuttles' involved metabolites in both the Ndufs4$^{-/-}$ and control mice

Metabolic analysis was done for both the knockout group and the control group on both GC- an LC-platforms. While some tissue types had more notable changes between the experimental group and the control group, other tissues (such as the brain) did not have much change when comparing the two groups. Possible reasons were discussed in sections 6-5 to 6-7; thus, this objective was completed successfully.

7.1.4 Objective 4 – Integrative interpretation of transcriptomic and metabolic data

When both the transcriptomic data and metabolomic data was compared, correlations could be made where one set of results would confirm the other set of results. Integrating the data led to a better understanding of the effect of a complex I deficiency. This objective was completed successfully.

7.2 Limitations and Strengths

When considering the mice model selected for this study, a possible limitation is the time consumption of mouse breeding, sample collection and sample storage. Breeding of mice did not ever give a guaranteed outcome for the desired genotype and gender combination. The process of tissue collection may have caused some variation due to the long and tedious process of mice dissection after euthanasia. The storage capacity for the collected samples is limited in duration due to the instability of RNA. Possible strengths include that the observed symptoms, changes, and conclusions of the mouse model is comparable to humans.

Transcriptomic work entails RNA isolation, quantification, and quality checks. These are all necessary to ensure the isolated RNA is a true representation of the gene expression. A possible limitation is the instability of RNA molecules and the ever-present RNase enzymes that degrade RNA. One of the strengths regarding the transcriptomics is the experimental approach. Sequencing was chosen due to the availability of AmpliSeq™ ready-to-use panels that targeted the entire genome of mice. Conventional transcriptomic analysis entailed q-PCR which is limited to the genes of which primer pairs are available. Moreover, errors and variance are severely low when the preparation is done with the Ion Chef™ Instrument, which is a fully automated process. Platforms such as the Personal Genome Machine (PGM) require cumbersome and extensive hands-on time with both the library- and template preparation and can cause errors and inconclusive results due to human- an/or pipetting errors. The Ion Chef™ makes both the library and template preparation much more efficient, reproducible, and uniform (Morgensen et al. 2015).

Another possible weakness of this study is that the conclusions of metabolite concentrations are not specific to the involved compartments of the cell and mitochondria. Speculations and supporting literature aided in the conclusions of the metabolic analysis. Brain data might have indicated more changes if specific brain regions were considered. As discussed previously, smaller areas of the brain seem to be more affected than the larger areas of the brain, thus the effect of complex I is diluted to the extent where very few differences were observed.

7.3 Future Prospects

With this study's transcriptomic analysis, only two experimental groups were used, the knockout mice group and the wildtype mice group and all participants were male. A possible expansion of this study could be to add a second experimental group of heterozygous mice to evaluate if any gene regulation is present with the one mutated allele of *Ndufs4*. The inclusion of female mice could also provide information of gene regulation in combination with estrogen and progesterone. It might also be worth considering larger group sizes for transcriptomic analysis.

This study only focused on three tissue types indicated by literature to be affected by complex I deficiency. Other tissues can be included in future studies to investigate if any changes are observed on gene and metabolic level with complex I dysfunction. These could include kidneys and spleen.

Another possible consideration for future studies is the consideration to move away from a mouse model to a more sustainable, more affordable, and less time-consuming round worm model, such as *Caenorhabditis elegans* (*C. elegans*). Most of the genes responsible for mitochondrial diseases have orthologues in *C. elegans*. The reproduction cycle of these round worms is also considerably shorter than the mouse reproduction cycle.

A future prospect in terms of metabolic analysis is isotope tracing to determine in which compartments certain metabolites are accumulating. This study was limited to the shuttle systems, solute carriers and the enzymes involved with these shuttle systems. Thus, possible alternative energy production pathways might not be elucidated due to them not being involved in these shuttles. Thus, the full mechanisms of higher and lower abundances could be further explained. A similar study was done by Arnold et al. in 2022 where they did an investigation on the non-canonical TCA cycle. To further elucidate and confirm the changes of gene expression, protein level testing could be performed on the specific proteins involved in the chosen shuttles of this study.

BIBLIOGRAPHY

Aquila, I., Marino, F., Cianflone, E., Marlotta, P., Torella, M., Mollace, V., Indolfi, C., Nadal-Ginard, B., Torella, D. 2018. The use and abuse of Cre-Lox recombination to identify adult cardiomyocyte renewal rate and origin. Pharmalogical Research. 127:116-128.

Aretz, I., Jakubke,C., Osman, C. 2019. Power to the daughters – mitochondria and mtDNA transmission during cell division. Biological Chemistry. 401(5):533-546.

Aranda, P. S., LaJoie, D. M., Jorcyk, C. L. 2012. Bleach gel: A simple agarose gel for analysing RNA quality. Electrophoresis. 33:366-369.

Arnold, P. K., Jackson, B. T., Paras, K. I., Brunner, J. S., Hart, M. L. Newsom, O. J., Alibeckoff, S. P., Endress, J., Drill, E., Sullivan, L. B., Finley, L. W. S. 2022. A non-canonical tricarboxylic acid cycle underlies cellular identity. Nature. 603:477-481.

Austin, C. P., Batty, J. F., Bradley, A., Bucan, M., Capecchi, M., Collins, F. S., Dove, W. F., Duyk, G., Dymecki, S., Eppig, J. T., Griender, F. B., Heintz, N., Hicks, G., Insel, T.R., Joyner, A., Koller, B. H., Lloyd, K. C. K., Mugnuson, T., Moore, M. W., Nagy, A., Pollock, J. D., Roses, A. D., Sands, A. T., Seed, B., Skarnes, W. C., Snoddy, J., Soriano, P., Steward, D. J., Steward, F., Stillman, B., Varmus, H., Varticovski, L., Verma, I. M., Vogt, T. F., Von Melcher, H., Witkwski, J., Woychik, R. P., Wurst, W., Yancopoulos, G. D., Young, S. G., Zambrowicz, B. 2004. The Knockout Mouse Project. Nature Genetics. 36(9):921-924.

Azarias, G., Perreten, H., Lengacher, S., Poburko, D., Demaurex, N., Magistretti, P. J., Chatton, J. 2011. Glutamate Transport Decreases Mitochondrial pH and Modulates Oxidative Metabolism in Astrocytes. The Journal of Neuroscience. 31(10): 3550-3559.

Bakare, A. B., Dean, J., Chen, Q., Thorat, V., Huang, Y., LaFramboise, T., Lesnefsky, E. J., Iyer, S. 2021. Evaluating the Bioenergetics Health Index Ratio in Leigh Syndrome Fibroblasts to Understand Disease Severity. International Journal of Molecular Sciences. 22:10344.

Baldo, M. S., Valarinho, L., 2020. Molecular basis of Leigh Syndrome: a current look. Orphanel Journal of Rare Diseases. 15(13):77-90.

Bouillaud, F., Alves-Guerra, M., Ricquier, D. 2016. UCP's, at the interface between bioenergetics and metabolism. Biochimica et Biophysica Acta: Molecular cell research. 1863(10):2443-2456.

Bender, T., Martinou, J. 2016. The mitochondrial pyruvate carrier in health and disease: To carry or not to carry. Biochimica et Biophysica Acta. 1863(10):2436-2442.

Birkenmeier, E. H., Hoppe, P. C., Lyfrod, K. A., Gwynn, B. 1992. Tissue- and Cell-specific expression of human sn-glycerol-3-phosphate dehydrogenase in transgenic mice. Nucleic Acids Reseasch. 20(11):2819-2825.

Broadhurst, D., Goodacre, R., Reinke, S. N., Kuligowski, J., Wilson, I. D., Lewis, M. R., Dunn, W. B. 2018. Guidelines and consideration for the use of system suitability and quality control samples in mass spectrometry assays applied in untargeted clinical metabolomic studies. Metabolomics. 14(6):72.

Broeks, M. H., Shamseldin, H. E., Alhashen, A., Hashem, M., Abdulwahab, F., Alshedi, T., Alobaid, I., Zwartkruis, F., Westland, D., Fuchs, S., Verhoeven-Duif, N. M., Hans, J. J. M., Alkuraya, F. S. 2019. MDH1 deficiency is a metabolic disorder of the malate-aspartate shuttle associated with early onset severe encephalopathy. Human Genetics. 138:1247-1257.

Cambiaghi, A., Ferrario, M., Masseroli, M. 2017. Analysis of Metabolomic data: tools, current strategies and future challenges for omics data integration. Briefings in Bioinformatics. 18(3):498-510.

Cajka, T., Hajšlová, J. 2007. Gas Chromatography-Time-of-Flight Mass Spectrometry in Food Analysis. LCGC Europe. 20(1):25-31.

Catalina-Rodriguez, O., Kolukula, V. K., Tomita, Y., Preet, A., Palmieri, F., Wellstein, A., Byers, S., Giaccia, A. J., Glasgow, E., Albanese, C., Avantaggiati, M. L. 2012 The mitochondrial citrate transporters, CIC, is essential for mitochondrial homeostasis. Oncotarget. 3(10):1220-1235.

Chandel, N. S. 2010. Mitochondrial Complex III: An essential component of universal oxygen sensing machinery? Respiratory Physiology & Neurobiology. 174(3):175-181.

Colombini, M. 2016. The VDAC channel: Molecular basis of selectivity. Biochimica et Biophysica Acta. 1863(10):2498-2502.

Crichton, P. G., Lee, Y., Kenji, E. R. S. 2017. The molecular features of UCP1 support a conventional mitochondrial carrier-like mechanism. Biochimie. 134:35-50.

Curthoys, N. P., Watford, M. 1995. Regulation of glutaminase activity and glutamine metabolism. Annual Review of Nutrition. 15:133-159.

De Haas, R., Das, D., Garanto, A., Renekma, H. G., Greupink, R., Van Den Broek, R., Pretijy, J., Collin, R. W. J., Willems, P., Beyrath, J., Heerschap, A., Russel, F. G., Smeitink, J. A. 2017. Therapeutic effects of mitochondrial ROS-redox modulator KH176 in mammalian model of Leigh Disease. Scientific Reports. 7(11733).

De Livera, M., Olshansky, M., Speed, T. P. 2013. Statistical Analysis of Metabolomics Data. Methods in Molecular Biology. 2013(1055):291-307.

Di Donna, L., Taverna, D., Mazzotti, F., Benabdelkamel, H., Attya, M., Napoli., A., Sindona, G. 2013. Comprehensive assay of flavanones in citrus juices and beverages by UHPLC-MS/MS and derivatization chemistry. Food Chemistry. 141(13): 2328-2333.

Delles, C., Rankin, N. J., Boachie, C., McConnachi, A., Ford, I., Kangas, A., Soininen, P., Trompet,S., Mooijaart, S. P., Jukema, J. W., Zannad, F., Ala-Korpela, M., Salomaa, V., Havulinna, A. S., Welsh, P., Würtz, P., Sattar, N. 2017. Nuclear magnetic resonance-based metabolomics identifies phenylalanine as a novel predictor of incident heart failure hospitalisation: results from PROSPER and FINRISK 1997. European Journal of Heart Failure. 20:663-673.

Dölken, L., Ruzsics, Z., Rädle, B., Friedel, C. C., Zimmer, R., Mages, J., Hoffman, R., Dickinson, P., Forster, T., Ghazal, P., Koszinowski, U. H. 2010. High-resolution gene expression profiling for simultaneos kinetic parameter analysis of RNA synthesis and decay. RNA. 14(9):1959-1972.

Ducker. G. S., Rabinowitz, J. D. 2017. One-Carbon Metabolism in Health and Disease. Cell Metabolism. 25:27-42.

Dunn, W. B., Wilson, I. D., Nicholls, A. W., Broadhurst, D. 2012. The importance of experimental design and QC samples in large-scale and MS-driven untargeted metabolomic studies of humans. Bioanalysis. 4:2249-2264.

El-Hattab, A. W., Scaglia, F. 2016. Mitochondrial Cytopathies. Cell Calcium. 60(3):199-206.

Esteitie, N., Hinttala, R., Wibom, R., Nilsson, H., Hance, N., Naess, K., Fahnehjelm, K. T., Von Döbeln, U., Majamaa, K., Larsson, N. 2005. Secondary Metabolomic effects of complex I deficiency. Annals of Neurology. 58(4):544-552.

Esterhuizen, K., Van Der Westhuizen, F. H., Louw, R. 2017. Metabolomics of mitochondrial disease. Mitochondrion. 35(2017), 97-110.

Fabre, A., Colotte, M.m Luis, A., Tuffer, S., Bonnet, J. 2014. An efficient method for long-term room temperature storage of RNA. European Journal of Human Genetics. 22:379-385.

Fassbinder-Orth, C. A. 2014. Methods for quantifying gene expression in Ecoimmunology: From qPCR to RNA-Seq. Integrative and Comparative Biology. 54(3):396-406.

Fernandez-Vizarra, E., Zeviani, M., 2015. Nuclear gene mutations as the cause of mitochondrial complex III deficiency. Frontiers in Genetics. 134(6):1-11.

Ferramosca, A., Zara, V. 2013. Biogenesis of mitochondrial carrier proteins: Molecular mechanisms of import into the mitochondria. Biochimica et Biophysica Acta: Molecular cell research. 1833(3):494-502.

Fiermonte,G., Palmieri, L., Todisco, S., Agrimi, G., Palmieri, F., Walker, J, E. 2002. Identification of the Mitochondrial Glutamate Transporter. The Journal of Biological Chemistry. 277(22):19289-19294.

Finisterer, F. (2008) Leigh and Leigh-like Syndrome in Children and Adults. Pediatric Neurology 39(4):223-235.

Fortana, R., Torre, S. D., 2015. The Deep Correlation between Energy Metabolism and Reproduction: A View on the Effects of Nutrition for Women Fertility. Nutrients 8(2):87.

Frane, A. V. 2015. Planned Hypothesis tests are not necessarily exempt from multiplicity adjustments. Journal of Research Practice. 11(1):Article P2.

Fu, J., Allen, W. 2019. A method to estimate the age of bloodstains using quantitative PCR. Forensic Science International: Genetics. 39(2019):103-108.

Fullerton, M., McFarland, R., Taylor, R. W., Alston, C. L. 2020. The genetic basis of isolated mitochondrial complex II deficiency. Molecular Genetics and Metabolism. 131:53-65.

Giacomello, M., Pyakurel, A., Glytsou, C., Scorrano, L. 2020. The cell biology of mitochondrial membrane dynamics. Nature Reviews: Molecular Cell Biology. 21(4):204-224.

Green, M. R., Sambrook, J. 2019. Polymerase Chain Reaction. Cold Spring Harbor Laboratory Press. 219(6): top095109

Gnoni, G. V., Priore, P., Geelen, M. J. H., Siculella, L. (2009). The Mitochondrial Citrate Carrier: Metabolic role and Regulation of its Activity and expression. IUBMB Life 61(10): 987-994.

Gonzalez-Hunt, C.P., Rooney, J.P., Ryde, I.T., Anbalagan, C., Joglekar, R., Meyer, J.N. 2016. PCR-based analysis of mitochondrial DNA copy number, mitochondrial DNA damage, and nuclear DNA damage. Current Protocols in Toxicology. 67(20):1-25.

Gstraunthaler, G., Seppi, T., Pfaller, W., 1999. Impact of culture conditions, culture media volumes, and glucose content on metabolic properties of renal epithelial cell cultures. Cellular Physiology and Biochemistry. 9(3):150-172.

Gusic, M., Prokisch, H. ncRNAs: New Players in Mitochondrial Health and Disease. Frontiers in Genetics. 11(95):1-27.

Ha, H., Kim, K., Yeom, Y., Lee, J., Han, P. Chronic restraint stress massively alters the expression of genes important for lipid metabolism and detoxification in Liver. Toixcology Letters. 146(1):49-63.

Haitina, T., Lindblom, J., Renström, T., Fredriksson, R. 2006. Fourteen novel human members of mitochondrial solute carrier family 25 (SLC25) widely expressed in the central nervous system. Genomics 88:779-790.

Hall, B., Limaye, A., Kulkarni, A. B. 2009. Overview: Generation of Gene Knockout Mice. Current Protocols in Cell Biology. 2009;Chapter 19:Unit19.12.17.

Hanse, E. A., Ruan, C., Kachman, M., Wang, D., Lowman. X. H., Kelekar, A. 2017. Cytosolic malate dehydrogenase activity helps support glycolysis in actively proliferating cells and cancer. Oncogene. 36:3915-3924.

Hashemipetroudi, S, H., Nematzadeh, G., Ahmadian, G., Yamchi, A., Kuhlmann, M. 2018. Assessment of DNA Contamination in RNA samples based on Ribosomal DNA. Journal of Visualized Experiments. 131:55451

Hediger, M. A., Romero, M. F., Peng, J., Rolfs, A., Takanaga, H., Bruford, E. A. 2004. The ABCs of solute carriers: physiological, pathological and therapeutic implications of human membrane transport proteins. European Journal of Physiology. 447:465-468.

Hsieh, J., Shih, W., Kuo, Y., Liu, G., Hung, H. 2019. Functional Roles of Metabolic Inetmediates in Regulating the Human Mitochondrial NAD(P)+ Dependent Malic Enzyme. Scientific Reports. 9:9081.

Hernandez, A., Garcia-Jimenez, C., Santisteban, P., Obregon, M.J. 1993. Regulation of malic-enzyme-gene expression by cAMP and retinoic acid in differentiating brown adipocytes. European Journal of Biochemistry. 215:285-290.

Huizing, M., Ruitenbeek, W., Van Den Heuvel, L. P., Dolce, V., Iacobazzi, V., Smeitink, J. A. M., Palmieri, F., Trijbels, J. M. F. 1998. Human Mitochondrial Transmembrane Metabolite Carriers: Tissue Distribution and its Implication for Mitochondrial Disorders. Journal of Bioenergetics and Biomembranes. 30(3):277-283.

Inak, G., Rybak-Wolf, A., Lisowski, P., Pentimalli, T. M., Jüttner, R., Glazar, P., Uppal, K., Bottani, E., Brunetti, D., Secker, C., Zink, A., Meierhofer, D., Henke, M. T., Dey, M., Cipasari, U., Mlody, B., Hahn, T., Berruezo-Llacuna, M., Karaiskos, N., Di Virgilio, M., Mayr, J. A., Wortmann, S. B., Priller, J., Gotthardt, M., Jones, D, P., Mayatepek, E., Stenzel, W., Diecke, S., Kühn, R., Wanker, E. E., Rajewsky, N., Schuelke, M., Prigione,

A. 2021. Defective metabolic reprogramming impairs early neuronal morphogenesis in neural cultures and an organoid model of Leigh syndrome. Nature Communications. 12:1929.

Indiveri, C., Kramers, R., Palmieri, F. 1987. Reconstitution of the malate-aspartate shuttle from mitochondria. Journal of Biological Chemistry. 262(33):15979-15983.

Jones, J., Stenerson, K. 2021. The Use of Derivatization Reagents of GC. https://www.sigmaaldrich.com/ZA/en/technical-documents/technical-article/analytical-chemistry/gas-chromatography/the-use-of-derivatization Date of access: 18 Sep. 2021. (Jones & Stenerson, 2021)

Infantion, V., Iacobazzi, V., De Santis, F., Mastrapasqua, M., Palmieri, F. 2007. Transcription of the mitochondrial citrate carrier gene: Role of SREBP-1, upregulation by insulin and downregulation by PUFA. Biochemical and Biophysical Research Communications. 356(1):249-254.

Johnson, S. C., Kayser, E. B., Bornstein, R., Stokes, J., Bitto, A., Park, K. Y., Pan, A., Sun, G., Raftery, D., Kaeberlein, M., Sedensky, M. M., Morgan, P. G., 2020. Regional Metabolic signature in the Ndufs4(KO) mouse brain implicate defective glutamate/α-ketoglutarate in mitochondrial disease. Molecular Genetics and Metabolism. 130:118-132.

Joshi, M., Eagan, J., Desai, N. K., Newton, S. A., Towne, M. C., Marinakis, N. S., Esteves, K. M., De Ferranti, S., Bennett, M. J., McIntyre, A., Beggs, A. H., Berry, G. T., Agrawal, P. B. 2014. A compound heterozygous mutation in GPD1 causes hepatomegaly, steatohepatits and hypertriglyceridemia. European Journal of Human Genetics. 2014(22):1229-1232.

Kang, H. 2013. The prevention and handling of the missing data. Korean Journal of Anesthesiology. 64(5):402-406.

Kaplan, R. S., Mayor, J. A., Wood, D. O. (1993) The Mitochondrial Tricarboxylate Transport Protein. The Journal of Biological Chemistry. 268(18):13682-13690.

Knapp, D.R. 1979. Handbook of Analytical Derivatization Reactions. 1st ed. New York: John Wiley & Sons

Kolisek, M., Beck, A., Fleig, A., Penner, R. 2005. Cyclic ADP-Ribose and Hydrogen Peroxide Synergize with ADP_Ribose in the Activation of TRPM2 Channels. Molecular Cell. 18:61-69.

Konstantinidis, I., Sætrom, P., Mjelle, R., Nedoluzhko, A. V., Robledo, D., Fernandes, J. M. O. 2020. Major gene expression changes in epigentic remodelling in Nile tilapia muscle after just one generation of domestication. Epigenetics. 15(10):1052-1067.

Korla, K., Vadlakonda, L., Mitra, C. K. (2015) Kinetic stimulation of the malate-aspartate and citrate-pyruvate shuttles in association the Krebs cycle. Journal of Biomolecular Structure and Dynamics. 33(11):2390-2403.

Kruse, S. E., Watt, W. C., Marcinek, D. J., Kapur, R. P., Schenkman, K. A., Palmiter, R. D. 2008. Mice with Mitochondrial Complex I Deficiency Develop a Fetal Encephalomyopathy. Cell Metabolism. 7(4):312-320.

Kuang, J., Yan, X., Genders, A. J., Granata, C., Bishop, D. J. 2018. An overview of technical considerations when using qualitative real-time PCR analysis of gene expression in human exercise research. PLoS ONE. 13(5):e0196438.

Kumar, M., Khan, M. S., Zubair, M., Sehgal, S., Jaithliya, T., Tiwari, A. (2018). Liquid Chromatography – Mass Spectroscopy. European Journal of Biomedical and Pharmaceutical Sciences. 5(5):941-947.

Kunji, E. R. S., King, M. S., Ruprecht, J. J. 2020. The SLC25 Carrier Family: Important Transport Proteins in Mitochondrial Physiology and Pathology. Physiology. 35(5):302-327.

Lake, N. J., Bird, M. J., Isohanni, P., Paetau, A. 2015. Leigh Syndrome: Neuropathology and Pathogenesis. Journal of Neuropathology and Experimental Neurology. 74(6):482-492.

Lake, N. J., Comptom, A. G., Rahman, S., Thorburn, D. R. 2015, Leigh syndrome: One disorder, more than 75 monogenic causes. Annals of Neurology. 79(2):190-203

Lakens, D. 2013. Calculating and reporting effect sizes to facilitate cumulative science a practical primer for t-tests and ANOVAs. Frontiers in Psychology. 4(863):1-12.

Lamichhane, S., Sen, P., Dickens, A. M., Hyötyläinen, T., Orešič, M. 2018. An Overview of Metabolomics Data Analysis: Current Tools and Future Perspectives. Comprehensive Analytical Chemistry. 82:387-413.

Legault, J. T., Striimatter, L., Tardif, J., Rohit, S., Tremblay-Vaillancourt, V., Aubut, C., Broucher, G., Clish, C. B., Cyr, D., Daneault, C., Waters, P. J., Vachon, L., Morin, C., Laprise, C., Rioux, J. D., Mootha, V. K., Des Rosiers, C. 2015. A Metabolic Signature trough a Monogenic Form of Leigh Syndrome. Cell Reports. 13:981-989.

Li, J., Batcha, A. M. N., Grüning, B., Mansmann, U. R. 2015. An NGS workflow blueprint for DNA sequencing data and its application in individualized molecular oncology. Cancer Informatics. 14(Suppl 5):87-107.

Lorenzo, M., Fabregat, I., & Benito, M. (1989). Hormonal regulation of malic enzyme expression in primary cultures of foetal brown adipocytes. Biochemical and Biophysical Research Communications. 163(1):341–347.

Lou, D. I., Hussmann, J. A., McBee, R. M., Acevedo, A., Andino, R., Press, W. H., & Sawyer, S. L. (2013). High-throughput DNA sequencing errors are reduced by orders of magnitude using circle sequencing. Proceedings of the National Academy of Sciences of the United States of America, 110(49), 19872–19877.

Lu, Z. J., Markham, G. D. 2002. Enzymatic properties of S-Adenosylmethionine Synthetase from the Archaeon Methanococcus jannaschii. The Journal of Biological Chemistry. 277(19):16624-16631.

Lu, M., Zhou, L., Stanley, W. E., Cabrera, M. E., Saidel, G. M., Yu, X. 2008. The role of the Malate-Aspartate Shuttle on the Metabolic Response to Myocardial Ischemia. Journal of Theoretical Biology. 25(2):466-475.

Lunetti, P., Cappello, A. R., Marsano, R. M., Pierri, C. L., Carrisi, C., Martello, E., Caggese, C., Dolce, V., Capobianco, L. 2013. Mitochondrial glutamate carrier from Drosophila melangaster: Biochemical, evolution and modeling studies. Biochimica et Biophysica Acta: Bioenergetics. 1827(10):1245-1255.

Martinez-Reyes, I., Chandel, N. S. 2020. Mitochondrial TCA cycle metabolites control physiology and disease. Nature Communications. 11:102.

Mattman, A., Sirrs, S., Mezei, M. M., Salvarinova-Zivkovic, R., Alfadhel, M., Lillquist, Y. Mitochondrial disease clinical manifestations: An overview. BC Medical Journal. 53(4):183-187.

McElroy, G. S., Reczeck, C. R., Reyfman, P. A., Mithal, D. S., Horbinski, C. M., Chandel, N. S. 2020. NAD+ Regeneration Rescues Lifespan, but Not Ataxia, in a Mouse Model of Brain Mitochondrial Complex I Dysfunction. Cell Metabolism. 32:301-308.

McLellan, M. A., Rosenthal, N. A., Pinto, A. R. 2017. Cre-loxP-mediated Recombination: General Principles and Experimental Considerations. Current Protocols in Mouse Biology. 7:1-12.

McKenna, M. C., Tildon, J. T., Stevenson, J. H., Huang, X., Kingwell, K. G. 1995. Regulation of Mitochondrial and Cytosolic Malic Enzymes from Cultured Rat Brain Astrocytes. Neurochemical Research. 20:1491-1501.

Menya, J., Gonzalez-Manchon, C., Parrilla, R., Ayuso, M. S. 1995. Molecular cloning, sequencing and expression of cDNA encoding a human liver NAD-dependent α-glycerol-3-phosphate dehydrogenase. Biochimica et Biophysica Acta. 1262:91-94.

Mikhed, Y., Görlach, A., Knaus, U. G., Diaber, A. 2015. Redox regulation of genome stability by effects on gene expression, epigenetic pathways and DNA damage/repair. Redox Biology 5:275-289.

Miller, H. C., Louw, R., Mereis, M., Venter, G., Boshoff, J. D., Mienie, L., Van Reenen, M., Venter, M., Lindeque, J. Z., Domínquez-Martínez, A., Quintana. A., Van Der Westhuizen, F. H. 2021. Metallothionein 1 overexpression does not protect against mitochondrial disease pathology in Ndufs4 knockout mice. Molecular Neurobiology. 58:243-262.

Morgenson, J., Van Tintelen, J. P., Fokstuen, S., Elliot, P., Van Langen, I. M., Meder, B., Richard, P., Syrris, P., Caforio, A. L. P., Adler, Y., Anastasakis, A., Gimeno, J, R., Klingel, K., Linhart, A., Imazio, M., Pinto, Y., Newbery, R., Schmidtke, J., Charron, P. 2015. The current role of next-generation DNA sequencing in routine care of patients with hereditary cardiovascular conditions: a viewpoint paper of the European Society

of Cardiology working group on myocardial and pericardial diseases and members of the European Society of Human Genetics. European Heart Journal. 36(22):1367-1370.

Morita, S., Horii, T., Kimura, M., Hatada, I. 2013. MiR-184 regulates insulin secretion through repression of Scl25a22. PeerJ. 1:e162.

Mráček, T., Drahota, Z., Houštěk, J. 2013. The function of the mitochondrial glycerol-3-phosphate dehydrogenase in mammalian tissues. Biochimica et Biophysica Acta – Bioenergetics. 1827(3):401-410.

Monné, M., Miniero, D. V., Bisaccia, F., Fiermonte, G. 2013. The mitochondrial oxoglutarate carrier: from identification to mechanism. Ournam for Bioenergetics and Biomembranes. 45(2):1-13.

Palmieri, F. 2004. The mitochondrial transporter family (SLC25): Physiological and Pathological Implications. European Journal of Physiology. 447(5):689-709.

Palmieri, F. 2013. The mitochondrial transporter family SLC25: Identification, properties and physiopathology. Molecular aspects of medicine. 34:465-484.

Palmieri, F., Monné, M. 2016. Discoveries, metabolic roles and disease of mitochondrial carriers: A review. Biochimica et Biophysica Acta. 2016:2362-2378.

Palmieri, F., Pierri, C. L. 2010. Structure and function of mitochondrial carriers – Role of the transmembrane helix P and G residues in the gating and transport mechanism. FEBS Letters. 584:1931-1939.

Pang, Z., Chong, J., Zhou, G., Anderson de Lima Morais, D., Chang, L., Barrette, M., Gaunthier, C., Jacques, P, E., Li, S., Xia, J. 2021. MetaboAnalyst 5.0: narrowing the gap between raw spectra and functional insights. Nucleic Acids Research. 49(W1):W388-W396.

Pereira, R., Oliveira, J., Sousa, M. 2020. Bioinformatics and Computational Tools for Next-Generation Sequencing Analysis in Clinical Genetics. Journal of Clinical Medicine. 9(1):132.

Ralston, A. Shaw, K. 2008. Gene expression regulates cell differentiation. Nature Education. 1(1):127.

Roger, A. J., Munoz-Gomez, S. A., Kamikawa, R. 2017. The origin and Diversification of Mitochondria. Current Biology. 27(21):R1177-R1192.

Romero, I. G., Pai, A. A., Tung, J., Gilad, Y. 2014. RNA-seq: impact of RNA degradation on transcript quantification. BMC Biology. 12(42).

Rothberg, J. M., Hinz, W., Rearick, T. M., Schultz, J., Mileski, W., Davey, M., Leamon, J. H., Johnson, K., Milgrew, M. J., Edwards, M., Hoon, J., Simons, J. F., Marran, D., Myers, J. W., Davidson, J. F., Branting, A., Nobile, J. R., Puc, B. P., Light, D., Clark, T. A., Huber, M., Branciforte, J. T., Stoner, I. B., Cawley, S. E., Lyons, M., Fu, Y., Homer, N., Sedova, M., Miao, X., Reed, B., Sabina, J., Feierstein, E., Schorn, M., Alanjary, M., Dimalanta, E., Dressman, D., Kasinskas, R., Sokolsky, T., Fidanza, J. A., Namsaraev, E., McKernan, K. J., Williams, A., Roth, G. T., Bustillo, J. 2011. An integrated semiconductor device enabling non-optical genome sequencing. Nature. 475(2011):348-352.

Runswick, M. J., Powell, J. P., Nyren, P., Walker, J. E. (1987) Sequence of the bovine mitochondrial phosphate carrier protein: structural relationship to ADP/ATP translocase and the brown fat mitochondria uncoupling protein. The EMBO Journal. 6(5):1367-1387.

Runswick, M. J., Walker, J. E., Bisaccia, F., Iacobazzi, V., Palmieri, F. (1990) Sequence of the bovine 2-oxoglutarate/malate carrier protein: Structural reationship to other mitochondrial transport proteins. Biochemistry 29(50):11033-11040.

Sato, M., Sato, K. 2013. Maternal inheritance of mitochondrial DNA by diverse mechanisms to eliminate paternal mitochondrial DNA. Biochimica et Biophysica Acta. 1833(8):1979-1984.

Sato, T., Yoshida, Y., Morita, A., Mori, N., Miura, S. 2016. Glycerol-3-phosphate dehydrogenase 1 deficiency induces compensatory amino acid metabolism during fasting in mice. Metabolism. 65(11):1646-1656.

Sauve, A. A. 2007. NAD+ and Vitamin B3: From Metabolism to Therapies. The Journal of Pharmacology and Experimental Therapeutics. 324(3):883-893.

Schaefer, P. M., Hilpert, D., Niederschweiberer, M., Neuhauser, L., Kalinina, S., Calzia, E., Rueck, A., Von Einem, B., Arnim, C. A. F. 2017. Mitochondrial matrix pH decisive factor in neurometabolic imaging. Neurophotonics. 4(4):045004

Schmiedel, S., Jackson, S., Schafer, J., Reichmann, H. 2003. Mitochondrial Cytopathies. Journal of Neurology. 250:267-277.

Shen, J. 2013. Modeling the glutamate-glutamine neurotransmitter cycle. Frontiers in Neuroenergetics. 5:1-13.

Shen, W., Wei, Y., Dauk, M., Tan, Y., Taylor, D. C., Selvaraj, G., Zou, J. 2006. The involvement of a Glycerol-3-phospahte dehydrogenase in modulating the NADH/NAD+ ratio provides evidence of a mitochondrial glycerol-3-phosphate shuttle in Arabidopsis. The plant cell. 18:422-441

Shokere, L. A., Holden, M. J., Jenkins, G. R. 2009. Comparison of fluorometric and spectrophotometric DNA quantification for real-time quantitative PCR of degrade DNA. Food Control. 20(4):391-401.

Sings, A., Fernandez-Vizarra, E. 2018. Assembly of mammalian oxidative phosphorylation complexes I-V and supercomplexes. Essays in Biochemistry. 62(3):255-270.

Staib-Lasarzik, I., Kriege, O., Timaru-Kast, R., Pieter, D., Werner, C., Eneglhard, K., Thal, S. C. 2014. Anesthesia for Euthanasia Influences mRNA Expression in Healthy Mice and after Traumatic Brain Injury. Journal of Neurotrauma. 31(19):1664-1671.

Tang, J. X., Tompson, K., Taylor, R. W., Oláhová, M. 2020. Mitochondrial OXPHOS Biogenesis: Co-Regulation of Protein Synthesis, Import and Assembly Pathways. International Journal of Molecular Science. 21(11):3820.

Taylor, E. B. (2017). Functional Properties of the Mitochondrial Carrier System. Trends in Cell Biology. 27(9):633-644.

Terburgh, K., Coetzer, J., Lindeque, J. Z., Van Der Westhuizen, F. H., Louw, R. 2021, Aberrant BCAA and glutamate metabolism linked to reginal neurodegeneration on a mouse model of Leigh syndrome. BBA – Molecular Basis of Disease. 1867(5):166082.

Terburgh, K., Lindeque, Z., Mason, S., Van Der Westhuizen, F. H., Louw, R. 2019. Metabolomics of Ndusf4-/- skeletal muscle: Adaptive convage at the ubiquinone cycle. BBA-Molecular basis of Disease. 2019, 98-106.

Valsecchi, F., Monge, C., Forkink, M., de Groof, A.J., Benard, G., Rossignol, R., Swarts, H.G., van Emst-de Vries, S.E., Rodenburg, R.J. & Calvaruso, M.A. 2012. Metabolic consequences of NDUFS4 gene deletion in immortalized mouse embryonic fibroblasts. Biochimica et Biophysica Acta (BBA)-Bioenergetics, 1817(10):1925-1936.

Van den Berg, A., Hoefsloot, H. C. J., Westerhuis, J. A., Smilde, A. G., Van der Werf, M. J. 2006. Centering, scaling and transforming: Improving the biological information content of metabolomics data. BMC Genomics. 7:142.

Vermeulen, J., De Preter, K., Lefever, S., Nuytens, J., De Vloed, F., Derevaux, S., Hellemans, J., Speleman, F., Vandesompele, J. 2011. Measurable impact of RNA quality on gene expression results from quantitative PCR. Nucleic Acids Research. 39(9):e63.

Venter, L. 2017. Application of metabolomics to identify functional metabolic changes associated with Hilitotis midae growth. Potchefstroom: North-West University. (Thesis – PhD)

Venter, L., Loots, D., Mienie, L. J., Janse van Rensburg, P., Mason, S., Vosloo, A., Lindeque, J. Z. 2018. Uncovering the metabolic response of abalone (Haliotis midae) to environmental hypoxia through metabolomics. Metabolomics. 14(49).

Venter, L., Lindeque, Z., Jansen van Rensburg, P., Van Der Westhuizen, F., Smuts, I., Louw, R. 2015. Untargeted urine metabolomics reveals a biosignature for muscle respiratory chain deficiencies. Metabolomics. 11:111-121.

Wal, P., Kumar, B., Bhandari, A., Raj, A. K., Wal, A. (2010). Bioanaltical Method Devolopment - Determination of Drugs in Biological Fluids. Journal of Pharmaceutical Science and Technology. 2(10):333-347.

Wieczorek, D., Delauriere, L., Schagat, T. 2021. Methods of RNA Quality Assessment. https://worldwide.promega.com/resources/pubhub/methods-of-rna-quality-assessment/#introduction Date of access: 03 Nov. 2021.

Williams, N. C., O'Neill, L. A. J. 2018. A role for the Krebs Cycle Intermediate Citrate in Metabolic Reprogramming in Innate Immunity and Inflammation. Frontiers in Immunology. 9:1-11.

Wilson, K., Walker, J. 2010. Principles and Techniques of Biochemistry and Molecular Biology. 7th ed. New York. Cambridge University Press.

Xiao, D., Zeng, L. Yao, K., Kong, X., Wu, G., Yin, Y., 2016. The glutamine-alpha-ketoglutarate (AKG) metabolism and its nutritional implications. Amino Acids. 48:2067-2080.

Ylikallio, E., Tyynismaa, H., Tsutsui, H., Ide, T., Suomalainen, A. 2010. High mitochondrial DNA copy number has detrimental effects in mice. Human Molecular Genetics. 19(13):2695-2705.

Yoo, H. C., Yu, Y. C., Sung, Y., Han, J. M. 2020. Glutamine reliance in cell metabolism. Experimental and Molecular Medicine. 52:1496-1516.

Zhang, K., Zuo, Y. 2005. Pitfalls and solution for simultaneous determination of estrone and 17-ethinylestradiol by gas chromatography–mass spectrometry after derivatization with N,O-bis(trimethylsilyl)trifluoroacetamide. Analytica Chimica Acta. 554(1-2):190-196.

Zhao, R., Jiang, S., Zhang, L., Yu, Z. 2019. Mitochondrial electron transport chain, ROS generation and uncoupling. International Journal of Molecular Science. 44():3-15.

Zorova, L. D., Popkov, V. A., Plotnikov, E. Y., Silachev, D. N., Pevzner, I. B., Jankauskas, S. S., Babenko, V. A., Zorov, S. D., Balakireva, A. V., Juhaszova, M., Sollot, S. J., Zorov, D. B. 2018. Mitochondrial Membrane Potential. Analytical Biochemistry. 552:50-59.

ANNEXURE A – GENOTYPING RESULTS

D.O.B = Date of Birth
= Number assigned to each mouse by the vivarium for identification purposes
♂/♀ = gender of each mouse
Purity = the A260/A280 ration obtained from the NanoDrop One to indicate the purity of the isolated DNA
ng/µl = the concentration value of the isolated DNA obtained from the NanoDrop One
Water added = nuclease free water added to each sample after PCR amplification to dilute DNA to 25 ng/µl
Genotype = genotype identified after imaging the 1% agarose gel
Collection date = Date on which mouse was euthanized. Not all mice would have a collection date as not all mice were euthanized.

D.O.B	#	♂/♀	Purity	ng/µl	Water added	Genotype	Collection date
21.10.2019	1	♂	1,66	195,7	39,14	WT	Not collected
21.10.2019	2	♂	1,78	89,1	17,82	WT	Not collected
21.10.2019	3	♂	1,65	202,5	40,5	HT	Not collected
21.10.2019	4	♂	1,82	147,9	29,58	WT	Not collected
21.10.2019	5	♂	1,74	126,6	25,32	HT	Not collected
21.10.2019	6	♂	1,6	252,5	50,5	KO	11.12.2019
21.10.2019	7	♂	1,74	106,6	21,32	HT	Not collected
21.10.2019	8	♂	1,81	91,4	18,28	HT	Not collected
21.10.2019	9	♀	1,7	264	52,8	WT	Not collected
21.10.2019	10	♀	1,78	102,3	20,46	KO	11.12.2019
21.10.2019	11	♀	1,78	124,2	24,84	WT	Not collected
21.10.2019	12	♀	1,83	126,9	25,38	HT	Not collected
20.12.2019	13	♂	1,77	226,2	40,24	WT	06.02.2020
20.12.2019	14	♂	1,85	284,7	51,94	WT	05.02.2020
20.12.2019	15	♂	1,85	323,7	59,74	KO	04.02.2020
20.12.2019	16	♂	1,85	273,6	49,72	HT	Not collected
20.12.2019	17	♂	1,79	480,5	91,1	HT	Not collected
20.12.2019	18	♀	1,85	309,6	56,92	WT	07.02.2020
20.12.2019	19	♀	1,72	486	92,2	KO	07.02.2020
20.12.2019	20	♀	1,79	245,8	44,16	KO	07.02.2020
13.01.2020	21	♂	1,68	285,9	52,18	HT	Not collected
13.01.2020	22	♂	1,62	415	78	HT	Not collected
13.01.2020	23	♂	1,75	208,8	36,76	HT	Not collected
13.01.2020	24	♂	1,76	267,1	48,42	HT	Not collected
13.01.2020	25	♂	1,75	275,1	50,02	HT	Not collected
13.01.2020	26	♀	1,8	187	32,4	WT	03.03.2020
13.01.2020	27	♀	1,69	254,6	45,92	WT	03.03.2020
13.01.2020	28	♀	1,77	287,9	52,18	HT	Not collected

13.01.2020	29	♀	1,71	354,3	65,68	HT	Not collected
13.01.2020	30	♀	1,76	91,16	91,16	HT	Not collected
10.03.2020	31	♂	1,78	100,4	15,1	KO	10.03.2020
10.03.2020	32	♂	1,83	126,7	20,3	KO	10.03.2020
10.03.2020	33	♀	1,84	176	30,3	HT	Not collected
10.03.2020	34	♂	1,84	113,1	17,6	HT	Not collected
10.03.2020	35	♂	1,83	132,5	21,6	HT	Not collected
10.03.2020	36	♂	1,79	87,1	12,4	KO	10.03.2020
10.03.2020	37	♀	1,83	129,1	20,8	WT	Not collected
10.03.2020	38	♀	1,83	79,1	10,8	WT	Not collected
10.03.2020	39	♂	1,84	121,2	19,2	WT	10.03.2020
24.03.2020	40	♂	1,79	109,9	17	KO	12.05.2020
24.03.2020	41	♀	1,78	46,6	4,3	HT	Not collected
24.03.2020	42	♀	1,8	70,5	9,1	HT	Not collected
24.03.2020	43	♂	1,82	74,7	9,9,	HT	Not collected
24.03.2020	44	♂	1,8	115,6	18,1	WT	12.05.2020
24.03.2020	45	♂	1,74	54,2	5,8	KO	12.05.2020
24.03.2020	46	♀	1,8	90,9	13,2	HT	Not collected
24.03.2020	47	♀	1,8	117,5	18,5	HT	Not collected
24.03.2020	48	♀	1,83	121,8	19,4	WT	Not collected
24.03.2020	49	♀	1,71	45,3	4,1	WT	Not collected
24.03.2020	50	♀	1,83	128,8	20,8	HT	Not collected
24.03.2020	51	♀	1,77	54,2	5,8	KO	12.05.2020
24.03.2020	52	♀	1,75	61,3	7,3	Sample Lost	Not collected
21.04.2020	53	♀	1,85	173,3	29,66	HT	Not collected
21.04.2020	54	♀	1,83	127,5	20,5	HT	Not collected
21.04.2020	55	♀	1,84	160,6	27,15	HT	Not collected
21.04.2020	56	♀	1,8	161,9	27,38	HT	Not collected
21.04.2020	57	♂	1,84	148	24,6	HT	15.06.2020
21.04.2020	58	♂	1,85	149,6	24,92	HT	15.06.2020
21.04.2020	59	♀	1,84	148	24,6	HT	15.06.2020
21.04.2020	60	♀	1,83	89,7	12,94	KO	15.06.2020
21.04.2020	61	♂	1,85	185,3	32,06	WT	30.06.2020
21.04.2020	62	♂	1,84	148,9	24,78	WT	29.06.2020
21.04.2020	63	♀	1,82	98	14,6	HT	Not collected
21.04.2020	64	♂	1,85	152,8	25,56	WT	01.06.2020
02.06.2020	65	♂	1,85	204,6	35,9	HT	21.07.2020
02.06.2020	66	♀	1,85	160,9	27,18	HT	Not collected
02.06.2020	67	♀	1,85	260,5	47,1	HT	Not collected
02.06.2020	68	♀	1,73	359,7	66,94	HT	Not collected
02.06.2020	69	♂	1,82	206,4	36,28	KO	20.07.2020
02.06.2020	70	♀	1,76	262,1	47,42	HT	Not collected
02.06.2020	71	♀	1,83	172,7	92,54	HT	Not collected
02.06.2020	72	♀	1,83	254,6	45,92	WT	23.07.2020

02.06.2020	73	♀	1,83	204,3	35,86	HT	Not collected
17.07.2020	75	♂	1,53	119,9	18,98	HT	03.09.2020
17.07.2020	76	♂	1,7	59,2	6,84	KO	02.02.2020
17.07.2020	77	♂	1,7	115,7	18,14	WT	01.09.2020
17.07.2020	78	♂	1,57	120,9	19,18	HT	03.09.2020
17.07.2020	79	♀	1,78	106,4	16,28	HT	Not collected
17.07.2020	80	♀	1,75	71,9	9,38	HT	Not collected
17.07.2020	81	♀	1,74	69,7	8,94	HT	Not collected
17.07.2020	82	♀	1,64	195,4	34,08	HT	Not collected
17.07.2020	83	♀	1,79	83,8	11,96	HT	Not collected
17.07.2020	84	♀	1,67	134,3	21,86	WT	31.08.2020
17.07.2020	85	♀	1,79	88,2	12,64	WT	31.08.2020
17.07.2020	86	♂	1,78	90,8	13,16	KO	02.09.2020
17.07.2020	87	♂	1,8	87,4	12,48	WT	01.09.2020
17.07.2020	88	♂	1,81	44,5	3,9	WT	01.09.2020
17.07.2020	89	♂	1,8	299,5	54,9	HT	03.09.2020
17.07.2020	90	♂	1,74	127,2	20,44	KO	02.09.2020
17.07.2020	91	♂	1,81	174,8	30,56	HT	03.09.2020
17.07.2020	92	♀	1,81	179	30,8	HT	Not collected
17.07.2020	93	♀	1,82	144,5	23,9	HT	Not collected
17.07.2020	94	♀	1,82	174,7	29,94	HT	Not collected
17.07.2020	95	♀	1,81	135,2	22,04	HT	Not collected
17.07.2020	96	♀	1,75	189,4	32,88	KO	Not collected
17.07.2020	97	♀	1,83	62,9	7,58	WT	31.08.2020
27.07.2020	1	♂	1,75	30,8	1,16	WT	14.09.2020
27.07.2020	2	♂	1,73	45,9	4,18	HT	14.09.2020
27.07.2020	3	♂	1,81	144,1	23,82	KO	14.09.2020
27.07.2020	4	♂	1,65	43,5	3,7	WT	14.09.2020
27.07.2020	5	♀	1,79	65,3	8,06	HT	Not collected
27.07.2020	6	♀	1,73	17,5	9,3	HT	Not collected
27.07.2020	7	♀	1,82	111,9	17,38	HT	Not collected
10.09.2020	8	♂	1,76	138,2	22,64	KO	16.10.2020
10.09.2020	9	♂	1,84	151,7	25,34	HT	Not collected
10.09.2020	10	♀	1,83	93	13,6	WT	16.10.2020
10.09.2020	11	♀	1,79	118	18,6	HT	Not collected
10.09.2020	12	♀	1,83	186,9	32,38	WT	16.10.2020
10.09.2020	13	♀	1,77	268,3	48,66	KO	16.10.2020
01.10.2020	14	♂	1,8	191,3	33,26	HT	Not collected
01.10.2020	15	♂	1,86	471,6	89,32	HT	Not collected
01.10.2020	16	♀	1,82	234,1	41,82	WT	Not collected
01.10.2020	17	♀	1,81	136	22,2	WT	Not collected
01.10.2020	18	♀	1,81	199,1	34,84	HT	Not collected
22.09.2020	19	♀	1,86	264,8	47,85	HT	Not collected
22.09.2020	20	♂	1,84	268,8	48,75	HT	Not collected

22.09.2020	21	♂	1,84	24,17	43,33	WT	11.11.2020
22.09.2020	22	♂	1,71	46,1	4,22	KO	11.11.2020
22.09.2020	23	♀	1,81	124,7	19,94	HT	Not collected
22.09.2020	24	♀	1,84	189,5	23,9	KO	11.11.200
22.09.2020	25	♀	1,74	254,1	45,83	HT	Not collected
22.09.2020	26	♀	1,83	206,9	36,37	HT	Not collected
22.09.2020	27	♀	1,85	220,2	39,03	KO	11.11.2020
22.09.2020	28	♀	1,84	291	53,19	WT	11.11.2020
22.09.2020	29	♂	1,82	92,7	13,53	HT	Not collected
22.09.2020	30	♀	1,8	61,7	7,34	KO	11.11.2020
22.09.2020	31	♀	1,83	273,5	49,7	HT	Not collected
22.09.2020	32	♀	1,8	149,3	27,83	HT	Not collected
22.09.2020	33	♀	1,85	201,1	35,22	WT	11.11.2020
22.09.2020	34	♀	1,89	136,8	22,36	HT	Not collected
22.09.2020	35	♀	1,84	115,5	18,1	HT	Not collected
29.10.2020	36	♂	1,82	157,09	26,42	WT	17.12.2020
29.10.2020	37	♂	1,77	49	4,08	KO	17.12.2020
29.10.2020	38	♂	1,77	127,64	20,53	KO	17.12.2020
29.10.2020	39	♀	1,79	221,87	39,37	WT	17.12.2020
29.10.2020	40	♀	1,85	166,97	28,39	KO	17.12.2020
29.10.2020	41	♀	1,84	85,18	12,04	HT	Not collected
29.10.2020	42	♀	1,78	55,36	6,07	WT	17.12.2020
29.10.2020	43	♂	1,81	151,84	25,37	KO	17.12.2020
29.10.2020	44	♂	1,84	91,7	13,34	KO	17.12.2020
29.10.2020	45	♂	1,82	194,33	33,87	KO	17.12.2020
29.10.2020	46	♂	1,76	190,24	33,05	HT	Not collected
29.10.2020	47	♂	1,79	221,66	39,33	HT	Not collected
29.10.2020	48	♂	1,76	122,92	19,58	HT	Not collected
29.10.2020	49	♀	1,81	136,41	22,28	WT	17.12.2020
29.10.2020	50	♀	1,81	89,94	12,99	HT	Not collected
29.10.2020	51	♀	1,82	178,75	30,75	HT	Not collected

ANNEXURE B – RNA QUANTIFICATION (NANODROP RESULTS)

Date of RNA isolation	Tissue	Sample #		ng/µl		A260/A280		A260/A230	
16.09.2020	Liver	1	WT	120,40	121,10	2,0	2,0	1,6	1,6
16.09.2020	Liver	4	WT	159,40	159,70	2,0	2,0	1,9	1,9
16.09.2020	Liver	39	WT	72,00	71,40	2,0	2,0	1,7	1,7
16.09.2020	Liver	44	WT	89,90	89,60	2,0	2,0	1,1	1,1
16.09.2020	Liver	61	WT	112,30	112,60	2,0	2,0	2,0	2,0
16.09.2020	Liver	64	WT	25,20	25,60	2,0	2,0	1,6	1,6
16.09.2020	Liver	77	WT	56,40	56,60	2,0	2,0	1,8	1,8
16.09.2020	Liver	87	WT	136,60	136,20	2,0	2,0	2,0	2,0
16.09.2020	Liver	88	WT	138,00	140,00	2,0	2,0	2,0	2,0
16.09.2020	Liver	31	KO	115,10	114,30	2,0	2,0	1,8	1,8
16.09.2020	Liver	32	KO	140,70	140,90	2,0	2,1	1,9	1,9
16.09.2020	Liver	36	KO	175,10	176,20	2,0	2,1	2,0	2,0
16.09.2020	Liver	40	KO	93,00	93,90	2,1	2,1	0,2	0,2
16.09.2020	Liver	45	KO	155,70	156,70	2,0	2,0	2,0	2,0
16.09.2020	Liver	62	KO	121,60	122,60	2,0	2,0	1,9	1,9
16.09.2020	Liver	69	KO	22,60	22,50	2,0	2,0	1,2	1,1
16.09.2020	Liver	76	KO	28,00	27,80	2,0	2,0	0,8	0,7
16.09.2020	Liver	86	KO	71,40	71,10	2,0	1,9	1,6	1,6
16.09.2020	Liver	90	KO	193,80	195,00	2,0	2,0	1,8	1,8
19.09.2020	Liver	1	WT	59,70	60,50	2,0	2,0	1,0	1,0
19.09.2020	Liver	31	KO	54,10	52,70	2,9	2,0	2,0	1,8
19.09.2020	Liver	32	KO	64,90	64,10	2,0	2,0	1,4	1,4
19.09.2020	Liver	36	KO	37,00	36,20	2,0	2,0	0,4	0,4
29.09.2020	Liver	44	WT	39,93	39,98	1,8	1,8	1,2	1,2
29.09.2020	Liver	61	WT	149,52	149,20	2,0	2,0	1,6	1,6
29.09.2020	Liver	87	WT	49,31	49,37	1,9	1,9	0,7	0,7
29.09.2020	Liver	88	WT	149,44	148,16	2,0	2,0	1,4	1,4
29.09.2020	Liver	36	KO	136,86	136,79	1,9	1,9	1,4	1,4
29.09.2020	Liver	40	KO	76,31	75,78	2,0	2,0	0,8	0,8
29.09.2020	Liver	76	KO	87,63	88,17	1,9	1,9	1,5	1,5
29.09.2020	Liver	86	KO	71,95	71,06	1,9	1,9	1,5	1,5
28.09.2020	Heart	1	WT	2,98	2,90	1,3	1,5	0,3	0,3
28.09.2020	Heart	4	WT	4,31	4,20	1,6	1,4	0,1	0,1
28.09.2020	Heart	44	WT	5,20	5,46	1,5	1,7	0,5	0,5
28.09.2020	Heart	61	WT	1,97	1,30	1,1	2,8	0,1	0,1
28.09.2020	Heart	64	WT	2,45	2,84	1,5	2,2	0,6	0,7
28.09.2020	Heart	77	WT	1,21	1,45	2,3	2,6	0,2	0,3
28.09.2020	Heart	87	WT	4,34	4,59	2,0	2,0	0,8	0,8
28.09.2020	Heart	88	WT	2,58	4,08	2,3	1,7	0,4	0,4

28.09.2020	Heart	31	KO	4,05	7,44	1,8	1,9	0,3	0,3
28.09.2020	Heart	32	KO	3,51	6,23	1,4	2,2	0,1	0,1
28.09.2020	Heart	36	KO	3,49	3,25	1,4	2,4	0,1	0,1
28.09.2020	Heart	40	KO	4,55	4,18	1,5	1,4	0,4	0,4
28.09.2020	Heart	45	KO	2,43	1,18	1,3	2,0	0,1	0,1
28.09.2020	Heart	62	KO	11,21	10,98	2,0	2,2	0,2	0,2
28.09.2020	Heart	76	KO	3,14	2,96	2,1	2,1	0,1	0,1
28.09.2020	Heart	86	KO	5,87	6,05	2,0	2,0	0,4	0,4
11.11.2020	Heart	1	WT	19,22	18,89	1,7	1,7	1,2	1,2
11.11.2020	Heart	39	WT	24,86	24,80	1,8	1,9	1,6	1,5
11.11.2020	Heart	44	WT	29,37	30,03	1,9	1,8	1,2	1,1
11.11.2020	Heart	61	WT	43,28	43,89	1,9	1,9	1,9	1,9
11.11.2020	Heart	64	WT	9,56	9,72	1,6	1,7	1,2	1,1
11.11.2020	Heart	77	WT	22,33	22,20	1,8	1,8	1,2	1,2
11.11.2020	Heart	87	WT	17,26	17,42	1,9	1,8	1,2	1,1
11.11.2020	Heart	88	WT	40,31	40,60	1,9	1,9	1,7	1,7
11.11.2020	Heart	31	KO	13,78	14,00	1,7	1,7	1,1	1,1
11.11.2020	Heart	32	KO	7,30	7,71	1,5	1,5	1,0	0,9
11.11.2020	Heart	36	KO	3,26	2,92	1,4	1,5	0,1	0,1
11.11.2020	Heart	40	KO	16,55	16,88	1,8	1,8	1,3	1,1
11.11.2020	Heart	45	KO	309,92	311,16	2,0	2,0	1,4	1,4
11.11.2020	Heart	62	KO	16,67	16,99	1,8	1,7	1,5	1,5
11.11.2020	Heart	76	KO	26,02	26,11	1,9	1,8	1,5	1,5
11.11.2020	Heart	86	KO	22,40	22,51	1,8	1,9	0,5	0,5
13.11.2020	Heart	64	WT	30,60	29,90	1,8	1,9	1,2	1,2
13.11.2020	Heart	32	KO	31,00	31,40	1,9	1,8	1,3	1,3
13.11.2020	Heart	36	KO	34,50	34,50	1,9	1,9	1,6	1,6
13.11.2020	Heart	45	KO	131,80	133,00	2,0	2,0	1,5	1,5
18.11.2020	Heart	1	WT	14,50	13,96	1,9	1,8	1,3	1,3
18.11.2020	Heart	39	WT	22,96	22,16	1,9	1,9	0,7	0,6
18.11.2020	Heart	44	WT	13,86	14,10	1,8	1,9	0,4	0,4
18.11.2020	Heart	77	WT	26,23	26,11	1,9	1,9	1,3	1,4
18.11.2020	Heart	87	WT	25,85	25,52	2,0	2,0	1,2	1,2
18.11.2020	Heart	31	KO	17,91	17,80	1,9	1,9	0,7	0,7
18.11.2020	Heart	40	KO	15,70	15,65	1,8	2,0	0,4	0,4
18.11.2020	Heart	62	KO	15,82	16,04	2,1	2,0	0,1	0,1
18.11.2020	Heart	76	KO	28,74	28,88	2,0	2,0	0,3	0,3
18.11.2020	Heart	86	KO	23,37	23,17	1,9	2,0	1,1	1,1
26.11.2020	Heart	40	KO	7,43	6,93	1,6	1,6	1,2	1,1
26.11.2020	Heart	62	KO	8,54	8,47	1,6	1,7	0,2	0,2
26.11.2020	Heart	69	KO	11,71	10,94	1,8	1,8	0,9	0,8
26.11.2020	Heart	90	KO	18,62	18,75	1,9	1,9	1,1	1,1
30.11.2020	Brain	31C	KO	9,26	9,06	1,8	1,9	1,0	1,1
30.11.2020	Brain	31F	KO	37,45	37,38	2,0	2,0	1,4	1,4

30.11.2020	Brain	39C	WT	15,37	14,76	1,8	1,9	1,3	1,2
30.11.2020	Brain	39F	WT	19,55	19,50	1,9	2,0	1,3	1,3
30.11.2020	Brain	32C	KO	19,82	19,74	1,9	1,9	1,2	1,2
30.11.2020	Brain	32F	KO	24,26	24,80	1,9	1,9	1,6	1,6
30.11.2020	Brain	44C	WT	6,24	6,13	1,6	1,6	1,0	1,0
30.11.2020	Brain	44F	WT	29,01	28,91	2,0	2,0	1,6	1,6
01.12.2020	Brain	36F	KO	4,04	3,65	2,4	2,2	0,0	0,0
01.12.2020	Brain	36C	KO	16,15	16,24	2,0	2,1	0,9	0,9
01.12.2020	Brain	64C	WT	11,70	11,63	1,9	2,0	0,7	0,7
01.12.2020	Brain	64F	WT	20,48	20,27	1,9	2,0	1,0	1,0
01.12.2020	Brain	61C	WT	17,56	17,65	2,0	1,9	1,0	1,1
01.12.2020	Brain	61F	WT	4,22	4,64	2,3	2,3	0,3	0,3
03.01.2020	Brain	40C	KO	15,74	13,57	1,8	1,9	1,2	1,1
03.01.2020	Brain	40F	KO	5,70	5,97	1,7	1,9	0,5	0,6
03.01.2020	Brain	77F	WT	5,72	5,67	1,7	1,7	0,3	0,3
03.01.2020	Brain	77C	WT	42,92	42,20	1,9	1,9	1,5	1,5
04.01.2020	Brain	62C	KO	12,49	12,66	1,7	1,8	1,1	1,1
04.01.2020	Brain	62F	KO	6,55	6,92	1,5	1,5	0,9	0,9
04.01.2020	Brain	69C	KO	6,44	5,98	1,5	1,6	0,1	0,1
04.01.2020	Brain	69F	KO	9,43	9,22	1,7	1,7	1,3	1,2
04.01.2020	Brain	87C	WT	17,64	18,02	1,8	1,8	1,4	1,5
04.01.2020	Brain	87F	WT	5,39	6,14	1,6	1,8	0,9	0,9
07.12.2020	Brain	76C	KO	17,48	17,71	1,9	2,0	1,0	1,1
07.12.2020	Brain	76F	KO	20,33	19,88	1,9	1,9	1,3	1,3
07.12.2020	Brain	86C	KO	26,67	25,86	2,0	2,0	0,9	0,9
07.12.2020	Brain	86F	KO	28,87	28,51	2,0	2,0	1,4	1,3
07.12.2020	Brain	88C	WT	24,28	23,89	2,0	2,0	1,2	1,2
07.12.2020	Brain	88F	WT	19,06	18,62	2,0	2,1	1,2	1,2
09.12.2020	Brain	21C	WT	16,63	16,61	1,8	1,7	0,4	0,4
09.12.2020	Brain	21F	WT	23,58	22,87	1,8	1,8	1,1	1,2
10.12.2020	Brain	3C	KO	11,44	13,23	1,7	1,6	1,4	1,1
10.12.2020	Brain	3F	KO	8,43	9,67	1,9	1,8	1,2	1,1
10.12.2020	Brain	8C	KO	6,08	6,06	1,7	1,9	0,6	0,6
10.12.2020	Brain	8F	KO	19,05	19,02	1,9	2,0	1,5	1,5
10.12.2020	Brain	4C	KO	46,57	46,44	2,0	2,0	1,7	1,8
10.12.2020	Brain	4F	WT	24,10	24,28	2,0	2,0	1,2	1,2

ANNEXURE C – RNA QUANTIFICATION (QUIBIT)

Sample name (Mouse #, Tissue abbr., Date of RNA isolation)	Assay Conc.	Units	Stock Conc.	Units	Assay Type	Sample Vol (µL)	Dilution Factor
#90L1 16/09/2020	>6.0	µg/ml	Not detected	ng/µl	RNA BR	1	200
#88L1 16/09/2020	>6.0	µg/ml	Not detected	ng/µl	RNA BR	1	200
#87L1 16/09/2020	6	µg/ml	120	ng/µl	RNA BR	1	200
#86.2L1 16/09/2020	2,48	µg/ml	49,6	ng/µl	RNA BR	1	200
#86.1L1 16/09/2020	3,18	µg/ml	63,6	ng/µl	RNA BR	1	200
#77L1 16/09/2020	2,32	µg/ml	46,4	ng/µl	RNA BR	1	200
#76L1 16/09/2020	1,15	µg/ml	23	ng/µl	RNA BR	1	200
#69L1 16/09/2020	0,962	µg/ml	19,24	ng/µl	RNA BR	1	200
#64L1 16/09/2020	1,02	µg/ml	20,4	ng/µl	RNA BR	1	200
#62L1 16/09/2020	5	µg/ml	100	ng/µl	RNA BR	1	200
#61L1 16/09/2020	4,71	µg/ml	94,2	ng/µl	RNA BR	1	200
#45L1 16/09/2020	6	µg/ml	120	ng/µl	RNA BR	1	200
#44L1 16/09/2020	3,89	µg/ml	77,8	ng/µl	RNA BR	1	200
#40L1 16/09/2020	4,01	µg/ml	80,2	ng/µl	RNA BR	1	200
#39L1 16/09/2020	3,07	µg/ml	61,4	ng/µl	RNA BR	1	200
#36L1 16/09/2020	>6.0	µg/ml	Not detected	ng/µl	RNA BR	1	200
#32L1 16/09/2020	>6.0	µg/ml	Not detected	ng/µl	RNA BR	1	200
#31L1 16/09/2020	5,1	µg/ml	102	ng/µl	RNA BR	1	200
#4L1 16/09/2020	>6.0	µg/ml	Not detected	ng/µl	RNA BR	1	200
#1L1 19/09/2020	1,01	µg/ml	40,4	ng/µl	RNA BR	1	200

#4L1 16/09/2020	2,98	µg/ml	119,2	ng/µl	RNA BR	1	200
#31L1 19/09/2020	0,946	µg/ml	37,84	ng/µl	RNA BR	1	200
#32L1 19/09/2020	1,17	µg/ml	46,8	ng/µl	RNA BR	1	200
#36L1 19/09/2020	0,708	µg/ml	28,32	ng/µl	RNA BR	1	200
#40L1 16/09/2020	1,81	µg/ml	72,4	ng/µl	RNA BR	1	200
#44L1 16/09/2020	1,08	µg/ml	43,2	ng/µl	RNA BR	1	200
#45L1 16/09/2020	3,23	µg/ml	129,2	ng/µl	RNA BR	1	200
#61L1 16/09/2020	2,56	µg/ml	102,4	ng/µl	RNA BR	1	200
#62L1 16/09/2020	2,47	µg/ml	98,8	ng/µl	RNA BR	1	200
#64L1 16/09/2020	0,479	µg/ml	19,16	ng/µl	RNA BR	1	200
#76L1 16/09/2020	0,502	µg/ml	20,08	ng/µl	RNA BR	1	200
#77L1 16/09/2020	1,09	µg/ml	43,6	ng/µl	RNA BR	1	200
#86.2L1 16/09/20	0,937	µg/ml	37,48	ng/µl	RNA BR	1	200
#87L1 16/09/2020	2,65	µg/ml	106	ng/µl	RNA BR	1	200
#88L1 16/09/2020	2,87	µg/ml	114,8	ng/µl	RNA BR	1	200
#36L1 29/09/2020	5	µg/ml	Not detected	µg/mL	RNA BR	1	200
#86L1 29/09/2020	1,82	µg/ml	364	µg/mL	RNA BR	1	200
#76L1 29/09/2020	2,24	µg/ml	448	µg/mL	RNA BR	1	200
#40L1 29/09/2020	2,15	µg/ml	430	µg/mL	RNA BR	1	200
#88L1 29/09/2020	1,87	µg/ml	374	µg/mL	RNA BR	1	200
#87L1 29/09/2020	1,3	µg/ml	260	µg/mL	RNA BR	1	200
#61L1 29/09/2020	4,4	µg/ml	880	µg/mL	RNA BR	1	200
#44L1 29/09/2020	1,02	µg/ml	204	µg/mL	RNA BR	1	200
#36H1 28/09/2020	0,108	µg/ml	21,6	µg/mL	RNA BR	1	200

#32H1 28/09/2020	0,082	µg/ml	16,4	µg/mL	RNA BR	1	200
#4H1 28/09/2020	0,121	µg/ml	24,2	µg/mL	RNA BR	1	200
#1H1 28/09/2020	0,075	µg/ml	15	µg/mL	RNA BR	1	200
#40H1 28/09/2020	0,142	µg/ml	28,4	µg/mL	RNA BR	1	200
#31H1 28/09/2020	0,497	µg/ml	99,4	µg/mL	RNA BR	1	200
#64H1 28/09/2020	0,083	µg/ml	16,6	µg/mL	RNA BR	1	200
#61H1 28/09/2020	<0.050	µg/ml	10	µg/mL	RNA BR	1	200
1	0,34	µg/ml	6,88	ng/µl	RNA BR	1	200
39	0,98	µg/ml	19,64	ng/µl	RNA BR	1	200
44	0,97	µg/ml	19,48	ng/µl	RNA BR	1	200
61	1,66	µg/ml	33,2	ng/µl	RNA BR	1	200
64-2	1,24	µg/ml	24,8	ng/µl	RNA BR	1	200
77	0,46	µg/ml	9,12	ng/µl	RNA BR	1	200
87	0,27	µg/ml	5,46	ng/µl	RNA BR	1	200
88	1,25	µg/ml	25	ng/µl	RNA BR	1	200
31	0,12	µg/ml	2,36	ng/µl	RNA BR	1	200
32-2	1,19	µg/ml	23,8	ng/µl	RNA BR	1	200
36-2	1,30	µg/ml	26	ng/µl	RNA BR	1	200
40	0,41	µg/ml	8,12	ng/µl	RNA BR	1	200
45-2	#N/A	µg/ml	#N/A	ng/µl	RNA BR	1	200
62	0,27	µg/ml	5,3	ng/µl	RNA BR	1	200
76	0,97	µg/ml	19,34	ng/µl	RNA BR	1	200
86	0,59	µg/ml	11,84	ng/µl	RNA BR	1	200
1-3 H	0,45	µg/ml	90	µg/ml	RNA BR	1	200

39-3 H	0,572	µg/ml	114,4	µg/ml	RNA BR	1	200
44-3 H	0,289	µg/ml	57,8	µg/ml	RNA BR	1	200
77-3 H	0,578	µg/ml	115,6	µg/ml	RNA BR	1	200
87-3 H	0,704	µg/ml	140,8	µg/ml	RNA BR	1	200
31-3 H	0,559	µg/ml	111,8	µg/ml	RNA BR	1	200
40-3 H	0,517	µg/ml	103,4	µg/ml	RNA BR	1	200
62-3 H	0,534	µg/ml	106,8	µg/ml	RNA BR	1	200
76-3 H	0,741	µg/ml	148,2	µg/ml	RNA BR	1	200
86-3 H	0,582	µg/ml	116,4	µg/ml	RNA BR	1	200
69 H	0,362	µg/ml	72,4	µg/ml	RNA BR	1	200
90 H	0,562	µg/ml	112,4	µg/ml	RNA BR	1	200
21F	207	ng/ml	4,14	ng/µL	dsDNA HS	10	20
90F	7,26	ng/ml	0,145	ng/µL	dsDNA HS	10	20
90C	27,8	ng/ml	0,556	ng/µL	dsDNA HS	10	20
45C	31,7	ng/ml	0,634	ng/µL	dsDNA HS	10	20
45F	148	ng/ml	2,96	ng/µL	dsDNA HS	10	20
1C	38,5	ng/ml	0,77	ng/µL	dsDNA HS	10	20
1F	168	ng/ml	3,36	ng/µL	dsDNA HS	10	20
88C	92,2	ng/ml	1,84	ng/µL	dsDNA HS	10	20
88F	127	ng/ml	2,54	ng/µL	dsDNA HS	10	20
86C	189	ng/ml	3,78	ng/µL	dsDNA HS	10	20
86F	202	ng/ml	4,04	ng/µL	dsDNA HS	10	20
76C	118	ng/ml	2,36	ng/µL	dsDNA HS	10	20
76F	115	ng/ml	2,3	ng/µL	dsDNA HS	10	20

4F	67,2	ng/ml	2,69	ng/µL	dsDNA HS	5	40
4C	171	ng/ml	6,84	ng/µL	dsDNA HS	5	40
8F	48,7	ng/ml	1,95	ng/µL	dsDNA HS	5	40
8C	<0,50	ng/ml	Not detected		dsDNA HS	5	40
3F	6,05	ng/ml	0,242	ng/µL	dsDNA HS	5	40
3C	17,2	ng/ml	0,688	ng/µL	dsDNA HS	5	40
4F	443,00	ng/ml	17,7	ng/µL	RNA	5	40
4C	830,00	ng/ml	33,2	ng/µL	RNA	5	40
8F	325,00	ng/ml	13	ng/µL	RNA	5	40
8C	69,80	ng/ml	2,79	ng/µL	RNA	5	40
3F	144,00	ng/ml	5,76	ng/µL	RNA	5	40
3C	192,00	ng/ml	7,68	ng/µL	RNA	5	40
4F	4,59	µg/ml	184	ng/µL	RNA BR	5	40
4C	>6,0	µg/ml	Not detected	ng/µL	RNA BR	5	40
8F	3,4	µg/ml	136	ng/µL	RNA BR	5	40
8C	0,761	µg/ml	30,4	ng/µL	RNA BR	5	40
3F	1,56	µg/ml	62,4	ng/µL	RNA BR	5	40
3C	2,08	µg/ml	83,2	ng/µL	RNA BR	5	40

ANNEXURE D – SASBMB 2022 CONFERENCE PARTICIPATION

The outcome of this study was presented at the SASBMB 2022 conference. Below is the confirming email for registration to present at this conference.

SASBMB 2022: Poster Acceptance Notice and Guidelines
1 message

Kerry Firmani <KerryF@turnersconferences.co.za> Wed, Jan 5, 2022 at 11:47 AM
To: "daneelnel123@gmail.com" <daneelnel123@gmail.com>

SASBMB 2022
BIOCHEMISTRY MATTERS
originally SASBMB 2020

Dear Daneel Nel,

Thank you for your submission for the SASBMB 2022 Conference. Your submission details are as follows:

Submission ID: 126

Submission Title: Investigating the adaptive mitochondrial shuttles and metabolic reprogramming of transporters in complex I (Ndufs4) knockout mice.

We are pleased to inform you that your submission has been accepted as a **POSTER PRESENTATION**.